Molecular Insights into the Ubiquitin Transfer Mechanism of RING-in-between-RING Ubiquitin ligases.

Katja K. Dove

A dissertation submitted

in partial fulfillment of the

requirements for the degree of

Doctor of Philosophy

University of Washington

2016

Reading Committee:

Rachel E. Klevit, Chair

Dana L. Miller

Rich G. Gardner

Program Authorized to Offer Degree:

Department of Biochemistry

University of Washington

Abstract

Molecular Insights into the Ubiquitin Transfer Mechanism of
RING-in-between-RING Ubiquitin ligases

Katja K. Dove

Chair of Supervisory Committee:
Professor Rachel E. Klevit
Department of Biochemistry

Ubiquitination is a posttranslational modification that regulates virtually every aspect of cellular function in eukaryotes including cell cycle progression, endocytosis, cell signaling, transcription, translation, DNA damage and even autophagy. Substrate modification with ubiquitin (Ub) requires the coordination of two types of enzymes: Ub-conjugating enzymes (E2s) and Ub ligases (E3s). While E3s are generally thought to bind substrates, substrate ubiquitination can be performed by either an E2 or an E3, depending on the type of E3. There are three classes of eukaryotic E3s: the RING (Really Interesting New Gene) E3s, do not contain an active site. They bind E2~Ub and activate Ub transfer directly onto a substrate. RBR (RING-in-between-RING) and HECT (Homologous to E6AP C-Terminus) E3s contain an active site Cys residue to which Ub is transferred from the E2~Ub to generate a covalent E3~Ub thioester that transfers Ub to a substrate.

It was only six years ago that a landmark study discovered that RBR E3 are indeed not RING-type Es3 as had been assumed for many years. In 2011, when I began my studies, very little was known about how RBR E3s function. In fact, RBR E3s were originally termed RING-type E3s based on their primary sequence analysis of the two domains: RING1 (binds E2) and

RING2 (contains active site). Based on structural work by other groups, we know today that RING2 does not contain a typical RING fold whereas RING1 domains are structurally similar to canonical RINGs.

Nevertheless, in my graduate work I demonstrate that RING1 domains perform opposing functions to canonical RING E3s: instead of promoting *closed* E2~Ub conformations, RING1s actively favor *open* E2~Ub conformations. This strategy ensures that the transfer of Ub proceeds via the active site Cys on RING2 and therefore that the type of product generated is determined by the RBR E3 and not by the E2 (as done in the context of canonical RING domains). That RBR RING1 domains have opposing functions to canonical RING domains can be explained functionally, yet a structural explanation for this observation is not immediately apparent. I found that a two-residue extension of the second Zn^{2+}-loop - unique to RING1 domains - is largely responsible for promoting open E2~Ubs.

Three years ago, an initial study proposed that the RBR E3 HHARI is able to bind to neddylated cullins (N8-CUL) which are RING-type E3s; and that this interaction results in activation of the normally auto-inhibited HHARI. The biological significance of this complex formation was perplexing. In conjunction with others, my work shows that two types of E3s, the RBR E3 HHARI and the RING E3 N8-CUL-1, work together with their respective E2s to coordinately ubiquitinate a common substrate and that this plays an essential role in a developmental pathway in *C. elegans*.

This work was based on the combination of structural, biochemical and organismal studies that led to a deeper understanding of how RBR E3s work.

Table of Contents

Chapter I: Introduction

What is ubiquitination?

Ubiquitination, sometimes also referred to as ubiquitylation (both are interchangeable), is a posttranslational modification by which substrates are covalently modified with a small 76-residue protein called *ubiquitin* (Ub). Although it is most famous for its role in intracellular protein quality control by signaling for proteasome-dependent degradation of target proteins, Ub modification of substrates also signals for non-degradative processes such as change of cellular localization, effects on enzymatic activity or protein-protein interactions [1]. As a result, ubiquitination regulates virtually every aspect of cellular function in eukaryotes including cell cycle progression, endocytosis.

Important historical events

Prior to the discovery that proteins are degraded via the ubiquitin-proteasome system, two major false assumptions slowed down the development of the ubiquitin field. First, it was assumed for a long time that intracellular proteins were long-lived and second, protein degradation was believed to be restricted to non-energy dependent pathways such as the lysosome (intracellular) and digestive enzymes (extracellular). These assumptions were held until late 1970s/early 1980s despite two earlier studies showing that proteins were continuously turned over [2] and that intracellular protein degradation was an energy dependent process [3]. In 1978, fractionation of reticulocyte lysate *Ciechanover et al*. found that a small polypeptide of roughly 9kDa is required for energy-dependent proteolysis, and it was named AFP-1 (active principle of fraction 1). Two years later, *Wilkinson et al*. showed that AFP-1 was ubiquitin and

that it was covalently conjugated to other proteins. In 1975, Goldstein *at al*. originally discovered ubiquitin as part of a study of lymphocyte differentiation. In 1977, *Busch et al.* discovered a polypeptide containing one C-terminus (C-term), but two N-termini (N-term). This was the first finding that Ub can be covalently linked to another protein. Interestingly, this Ub-modified protein was Histone 2A and the non-degradative function of its modification with only a single Ub is still studied today.

Two additional important discoveries were made by *Hershko et al*. in 1980: 1) multiple Ubs can be conjugated to one substrate and 2) Ub conjugation is reversible (deubiqitination). Within the next few years, three scientists: Ciechanover, Hershko and Rose isolated and characterized three enzymes - E1, E2 and E3 - needed in sequential steps to conjugate Ub to substrates. This was the foundation of the ubiquitin field, which rapidly grew into a diverse field encompassing most of eukaryotic biology that it is today. As a result, in 2004 Aaron Ciechanover, Avram Hershko and Irwin Rose received the Nobel Prize in Chemistry.

The Ubiquitin Code

The discovery of the ubiquitin system arose from early studies centered on the desire to understand protein degradation. It is therefore no surprise that today ubiquitin is well known as a degradative signal. However, its actual role as a signaling molecule is much more intricate and we are only now beginning to understand its vast complexity.

It is astonishing that substrate modification with one small protein can result in such diverse signaling capacity. An explanation for how this high degree of versatility is achieved can be found in the ubiquitin code. Ub is covalently attached to substrates via the carboxyl group of its C-term and typically a side chain amino group of a substrate lysine (Lys), generating a stable

isopeptide bond (Fig. 1, [4-6]). The attachment of a single Ub (mono-Ub) to a substrate can, for example, can affect its activity or cellular location [7, 8]. However, Ub itself contains seven Lys residues allowing for one Ub molecule to act as a substrate for another Ub molecule and thereby the possibility for Ub chain formation (Fig. 1A). Depending on which of the seven Lys residues (K6, K11, K27, K29, K33, K48 or K63) is used to connect the Ub moieties within a chain, the three dimensional topology of the polymers differs and with that the signal that is conveyed. For example, the two best understood types of chain linkages thus far, K48- and K63-linked chains, differ greatly in their three-dimensional topology. Whereas K48-linked chains are more compact due to intramolecular interactions, K63-linked chains adopt a more linear conformation (Fig. 1B, [9]). As a result, this allows Ub-binding proteins to distinguish among different chain linkages and therefore the signal conveyed through each chain type differs: K48-linked chains signal for proteasomal degradation and K63-linked chains act to recruit DNA damage repair proteins [4, 10]. Since Ub contains seven Lys at least seven different types of homogenous Ub chains can be formed. Although more studies are required to uncover biological function of other chain types, much knowledge has been gained over the past several years. K6-linked chains are thought to be involved in mitochondrial quality control, K11-linked chains regulate the cell cycle and the hypoxic response, K27-linked chains contribute to the DNA damage response and innate immunity, K29-linked chains have been shown to inhibit Wnt signaling, and K33-linked chains have recently been associated with post-Golgi trafficking [11-18]. The complexity of the ubiquitin code is further increased by the possibility of mixed and branched chain formation which have both been suggested to act as an unconventional signal in proteasomal degradation [19, 20]. Furthermore, Ub can also be covalently linked to non-Lys residues such as Ser, Thr, Cys and the amino group of the N-terminus (N-term) [21-23]. Covalent linkages of the C-term of

one Ub molecule with the N-term of another Ub molecule leads to the formation of linear Ub chains which play a crucial role in NFκB signaling pathways [24-26].

Lastly, to add more layer of complexity to the *ubiquitin code*, Ub itself can be post-translationally modified, for example, by phosphorylation or acetylation [11, 27-30]. Altogether, the *ubiquitin code* provides our cells with a large toolbox of ubiquitin signals to coordinate complex networks of moving parts that underlie the basic functions of life.

The Ubiquitination Cascade

Protein ubiquitination is accomplished in three steps, catalyzed by three distinct enzymes: a Ub-activating enzyme (E1), a Ub-conjugating enzyme (E2), and a Ub ligase (E3). First, the E1 activates the C-term of Ub in an ATP-dependent manner and covalently links it to its own active site Cys. The activated Ub is then transferred onto an E2 active site cysteine (Cys) via a transthiolation reactions to generate a E2~Ub ("~" denotes a thioester bond). The E2~Ub then coordinates with an E3 and its substrate to facilitate substrate ubiquitination (Fig 2).
There are three major classes of eukaryotic Ub ligases, each utilizing distinct Ub-transfer mechanisms. The largest class, the RING (Really Interesting New Gene) E3s, do not contain an active site; instead they bind the substrate and the E2~Ub and Ub *directly* transferred onto a substrate by the E2~Ub. In contrast, RBR (RING-in-between-RING) and HECT (Homologous to E6AP C-Terminus) E3s contain an active site Cys residue to which Ub is initially transferred from the E2~Ub to generate a covalent E3~Ub thioester. Finally, the E3~Ub binds its substrate and catalyzes its ubiquitination through an aminolysis reaction (transfer to Lys).

In all cases known to date, it is the enzyme (E2 or E3) that carries out the *final* aminolysis reaction that determines the type of Ub modification on a given substrate. In the case of RING-type E3s it is the E2 that directly modifies substrates with Ub and therefore it is the E2 that determines whether poly-Ub chains are built as well as the type of chain linkage. For example, the E2 Ube2k possesses intrinsic ability to build K48-linked Ub chains, whereas the E2 pair Ubc13/MMS2 are known to form K63-linked chains [31]. As a result, RING-type E3s that are able to bind various E2s could modify each substrate with different ubiquitin signals, depending on which E2 was used. On the contrary, in the case of E3 ligases that utilize an E3~Ub intermediate, such as RBR-and HECT-type E3s, the E3 controls the final Ub product formation.

As a result, the E3 must overwrite the intrinsic preference of the E2. For example, when the E2 Ube2k is paired with HOIL-1L/HOIP, RBR E3s known to build linear Ub chains, the final products are linear chains as dictated by the E3 and not K48-linked chains as would be the case if the E2 determined product formation [32]. In such reactions the E2~Ub acts as a supplier of Ub for the E3, but must not modify substrates directly.

E1 - Ubiquitin-activating Enzymes

While there are over >40 E2s and >600 E3s there are only two genes encoding for E1s in the mammalian genomes [33-35]. The human E1 is a monomeric ~115kDa protein that activates Ub in several steps: First, the C-term of Ub is adenylated in an ATP-dependent manner followed by the formation of a thioester bond between the C-term of Ub and the active site Cys of the E1 (E1~Ub). Next, the E1~Ub binds a second Ub and catalyzes the adenylation of its C-term, generating a ternary Ub^{AMP}:E1~Ub complex in which one Ub is covalently linked to the active site Cys and one adenylated Ub (Ub^{AMP}) is non-covalently bound. Finally, an E2 is recruited to

the ternary complex and the Ub on the active site of the E1 is transferred onto the active site Cys of the E2 via a transthiolation reaction, generating a E2~Ub [36].

E2 - Ubiquitin-conjugating Enzymes

E2s share a common fold of its 150-residues core of: the UBC domain. In addition, some E2s may contain extra insertions/extensions often found at either N-term or C-term. However, structurally most E2s are restricted to the UBC fold and given the structurally similarities it is remarkably how diverse the function of E2s can be. Many E2s are able to form specific Ub-chains: K48-linked chains (Cdc34 and Ube2k), K63-linked chains (Ubc13/Mms2) and K11-linked chains (Ube2s) while others such as UbcH5a/b/c are quite promiscuous in their ability to build various chains [37-40]. Yet other E2s, such as Ube2w which is unable to form poly-Ub chains and as a result modify substrates with only mono-Ub [41]. Furthermore, some E2s have evolved to specifically modify non-canonical residues on substrates. For example, Ube2w ligates Ub almost exclusively to the N-term amino group of substrates whereas the yeast ortholog of Ube2j2 has been shown to ubiquitinate Ser and Thr residues [23, 42, 43]. The diverse range of functions among the E2s provides a large repertoire of possibilities for substrate ubiquitination.

Most E2s are able to transfer Ub either onto Cys residues (transthiolation) when bound to RBR- and HECT-type E3 or Lys residues (aminolysis) when bound to RING-type E3s. The E2 UbcH7 is unique in that it can only perform transthiolation reactions and is therefore a dedicated E2 for RBR- and HECT-type E3s [44].

E3 - Ubiquitin Ligases

The largest class of E3s are the RING-types which contain a RING/Ubox-domain defined by a characteristic cross-brace fold to bind the E2~Ub (Fig. 3, top). Like a scaffold, RING E3s

bind both the E2~Ub and substrate simultaneously to coordinate Ub transfer from the E2~Ub *directly* onto a substrate amino group, usually a Lys side chain. Moreover, RING-type E3s activate the E2~Ub to transfer Ub onto Lys residues (an aminolysis reaction) by promoting closed conformations of the E2~Ub [45-49]. A central feature of the E2~Ub activation by RING-type E3s is a conserved basic residue (Lys/Arg), also referred to as the "linchpin" residue, that contacts both the E2 and the Ub of closed E2~Ub states [48].

HECT-type E3s bind the E2~Ub via a conserved HECT domain that is structurally distinct from a RING domain (Fig. 3, bottom). More importantly, HECT-type E3s contain a conserved active site Cys residue required for the formation of an obligatory E3~Ub prior to Ub transfer onto a substrate Lys. This mechanism requires two types of chemical reactions: 1) a transthiolation reaction that transfers Ub from the E2~Ub to the E3 active site Cys to generate a reactive E3~Ub species and 2) a subsequent aminolysis reaction to transfer the C-term of Ub from the active site Cys of the E3 to a substrate Lys to form a stable isopeptide bond. Unlike RING-type E3 ligases that induce closed E2~Ub conformations, available data on HECT ligases suggest that they do not need a closed E2~Ub for activity [44, 50].

The third class of E3s, the RBR E3s, was discovered more recently when HHARI (human homologue of Ariadne) and Parkin were shown to function via a RING/HECT-hybrid mechanism [44]. Despite containing an E2-binding RING domain, RBR E3 require a E3~Ub thioester intermediate similar to HECT-type E3s (Fig. 3, middle). The functional importance of an active site Cys for catalytic activity has since been confirmed for other RBR E3s including HOIP, HOIL-1L, TRIAD1, and RNF144 [51-54]. Although RBR E3s are a small class with only a dozen members in the human genome, RBR E3s regulate several essential cellular pathways. The most well known RBR E3 is Parkin for which mutations have been linked to autosomal-

recessive juvenile Parkinson's disease [55, 56]. The RBR E3s HOIP and HOIL-1L are unique as they are the only enzymes know to date to be able to generate linear Ub chains, which are important in the regulation of the NF-κB signaling pathway [24-26, 32]. HHARI and TRIAD1 belong to the Ariadne family of RBR E3s which is defined by a C-term auto-inhibitory Ariadne domain [57]. HHARI and its homologues in *Drosophila* and *C. elegans* have been implicated in processes including regulation of translation via the translation initiation factor 4EHP, cellular proliferation, and developmental processes [58-61].

RBR E3s are defined by a characteristic RBR domain that can be subdivided into three separate domains each of which coordinates two Zn^{2+} ions: RING1, in-between RING (IBR), and RING2. A RBR domain can be found at any position relative to other domains within an RBR E3, but its subdomains RING1-IBR-RING2 always appear in order: N-term to C-term (Fig. 4). RING1 is the E2-binding domain and RING2 harbors the active site Cys that when mutated to an Alanine (Ala) renders RBRs inactive [44, 52, 53, 62-64]. While RING1 domains adopt folds similar to canonical RING-type E3s, RING2 domains do not resemble canonical RING domains, either structurally or functionally [57, 65-68]. This domain was originally named "RING2" based on primary sequence analysis and although it is misleading attempts to change it have failed so far [69]. The structure of the IBR domain adopts a fold similar to RING2, but its function remains unknown [57, 65-68].

Another common feature of RBR E3s is that they exist in auto-inhibited states characterized by low levels of activity. Structures of auto-inhibited states for HHARI and Parkin reveal two common features that define the auto-inhibited states[54, 57, 65-67, 70]. First, the active site Cys on RING2 is partially buried by another domain (Ariadne in the case of HHARI and RING0 in the case of Parkin). Second, very large distances separate RING1, which is the

E2-binding domain, and RING2, which contains the active site Cys (Fig. 7A). These two features imply that RBR E3s must undergo major rearrangements to form active enzymes. Regardless of the specific mechanism by which RBR E3s are activated, the E2-binding RING1 domain and the active-site-containing RING2 domain must come together for transfer of Ub from the E2~Ub onto the E3 active site. Although there are no structures of other auto-inhibited RBR E3s available, biochemical evidence suggests that other RBRs also occupy auto-inhibited states. Two independent studies showed that full-length HOIP exhibits auto-inhibition similar to Parkin and HHARI, but HOIP is mainly inhibited by the UBA domain located at the N-term [53]. In addition, the release of auto-inhibition varies among the RBR E3s. While Parkin can be activated by binding to phosphorylated-Ub, HOIP has been shown to exhibit increased ability to form linear chains in the presence of its partner HOIL-1[29, 53, 54, 70-72]. The RBR RNF144 is one of the smallest members as it only contains one additional domain (a transmembrane domain) in addition to its eponymous RBR domain. Yet, despite lacking a domain that could perform an auto-inhibitory role, RNF144 has been shown to activated through dimerization via its transmembrane domain [62]. Finally, the two Ariadne family members, HHARI and TRIAD1, have been shown to be activated through complex formation with neddylated-Cullin E3s [51, 73]. Whether there are additional mechanisms that can activate any of the RBR E3s remains to be seen.

Understanding RBR E3 ligases ubiquitin transfer mechanism

Until a few years ago RBR E3s were thought to be RING-type E3s based on primary sequence alignment. However, in 2011 a hallmark study revealed that RBR E3s contain an active site Cys located in RING2 through which an obligatory E3~Ub has to be formed prior to

substrate ubiquitination [44]. Thereafter RBR E3s were termed RING/HECT-hybrids. This surprising finding completely change how the field continued to study important enzymes such as Parkin and HOIP/HOIL-1L.

As mentioned above, canonical RING-type E3s activate E2~Ub conjugates by promoting closed states of E2~Ubs. These states display increased reactivity towards the amino groups of Lys residues. A signature of closed E2~Ub states are non-covalent interactions between a surface on the E2 formed by the "cross-over" helix (also known as helix-2) and the hydrophobic patch or "I44 surface" of Ub. Mutations of residues within the E2:Ub interface abrogate activation by RING-type E3s [45-49]. Paradoxically, despite their close structural resemblance to canonical RING domains, HHARI RING1 does not activate the E2~Ub for Ub transfer by aminolysis [44]. Furthermore, mutations of the E2 cross-over helix significantly decrease *in vitro* Ub transfer activity with canonical RING-type E3s, yet the same mutations do not affect Ub transfer activity of the RBR E3 HHARI [48]. These observations imply that at least HHARI RING1 is mechanistically distinct from its canonical RING relatives.

RBR E3s such as Parkin, HOIP, and HHARI display activity with a variety of different E2s; in particular they are all active with two well-characterized human E2s, UbcH5 and UbcH7 [44, 52, 53]. While most E2s, including UbcH5, are able to perform both transthiolation reactions and aminolysis reactions, UbcH7 solely performs transthiolation reactions [44]. This suggests that UbcH7 can function with HECT-type and RBR-type E3s, but not with RING-type E3s. Notably, *C. elegans* orthologs of HHARI and UbcH7 act together in pharyngeal development, suggesting that UbcH7 is a biologically relevant E2 for HHARI [60, 74]. But HHARI, Parkin, and HOIP are also known to work with E2s that are able to transfer Ub directly to (Lys) amino groups [44, 52, 53, 55, 75, 76]. Importantly, HOIP specifically generates linear

Ub chains regardless of the chain linkage preference of the E2 with which it works [32]. This suggests a dichotomy in the determining factor for product formation: in the case of RING-type E3s, the identity of the E2 determines the type of product while in RBR E3s, the E3 determines the type of product.

This lead to one central question of my thesis project:

How do RBR E3s ensure that transfer of Ub occurs via the E3 active cite Cys to maintain control of product formation?

Chapters II and III of this thesis address this question specifically. Chapter II contains my first manuscript titled *"Molecular Insights into RBR E3 ligase Ubiquitin Transfer Mechanisms"*. Here I show that, despite structural similarity to canonical RINGs that promote closed E2~Ub states, RING1 domains of HHARI and RNF144 disfavor closed E2~Ub. This feature has two consequences: it ensures that Ub transfer occurs through the E3 active site by reducing UbcH5~Ub reactivity towards Lys residues and it reveals the hydrophobic patch of Ub. I identified a Ub binding site on RING2 important for recruitment of RING1-bound E2~Ub. Mutations in either Ub or HHARI RING2 that ablate Ub binding also inhibit ligase activity, consistent with RING2 recruitment being a critical for Ub transfer mechanism by RBR E3s. Finally, I demonstrate that the mechanism defined here is utilized by a variety of RBR E3 ligases.

Chapter III of my thesis addresses how RBR RING1 domains disrupt closed E2~Ubs. Here I uncover how HHARI RING1 specifically promotes open UbcH7~Ub states. By mutagenesis and NMR I reveal that an extension of the second Zn^{2+}-loop (Zn^{2+}-loop II) is mainly

responsible for the disruption of closed UbcH7~Ub states. Furthermore, a new crystal structure of full-length HHARI in complex with UbcH7~Ub confirms that UbcH7~Ub is in its open state when bound to RING1. A structure-based model shows that the extension of Zn^{2+}-loop II of HHARI contacts UbcH7 in a position that would conflict with Ub of a closed E2~Ub. The structure also confirms that RING1 binding to an E2~Ub does not release HHARI form its auto-inhibited state. Pertinent to its activation through binding to neddylated-Cullins, I confirm by solution NMR that HHARI is able to bind to free Nedd8 and to free Ub via its UBA-Like domain. Additional crystallographic evidence and mutational analysis further define details of the interacting surfaces between HHARI and Ub/NEDD8.

Chapters II and III are centered on mechanistic details regarding Ub transfer from the E2~Ub onto the active site Cys located on RING2 for RBRs in general. In contrast, Chapter IV specifically focuses on substrate ubiquitination by the RBR HHARI. Initially, this project originated by the desire to investigate the biological role of the unique E2 UBCH7. UBCH7 is highly conserved in *C. elegans* and its homolog, UBC-18, is implicated in developmental processes via its cooperation with the RBR E3 ARI-1 (homolog to human HHARI) [74]. In human cell culture, UBCH7 has been shown to regulate S-phase transition of the cell cycle [77]. Yet, to date it is mainly the multi-subunit RING-type E3s known as Cullin-RING Ligases (CRL) that are associated regulation of the cell cycle [78]. Since UbcH7 is not able to function with RING-type E3s, it is unclear how it can perform its role during the cell. To deepen our understanding of the biological role of UbcH7, a member of the Miller Lab at the University of Washington, Hilary Kemp, conducted an RNAi screen to identify genes that interact genetically with *ubc-18* in *C. elegans*. This screen revealed that the *C. elegans* ortholog of the conserved E2 *CDC34*, *ubc-3*, acts with *ubc-18* in pharyngeal development. *CDC34* is considered a dedicated

E2 for Skp/Cullin/Fbox (SCF)-type E3s, a sub-class of CRLs. We further uncovered synthetic genetic relationships between *ubc-18* and other components of SCF-type RING E3s. As UBC-18, just like its human homology UBCH7, is incapable of working with RING-type E3s and UBC-3 is a dedicated E2 for CRL E3s, these two E2s cannot be functionally redundant. Our data support a model in which UBC-18 and UBC-3 work either in parallel or coordinately. Recent studies in mammalian cell culture suggested that Ariadne family members of RBRs (HHARI and TRIAD1) and CRL E3 complexes can work together [73]. We show that the E2/E3 pairs UBC-18/ARI-1 and UBC-3/CUL-1 work cooperatively to ubiquitinate the Skp1-like protein SUP-36. Our work provides the first biological evidence for the existence of cross talk between two different types of E3s, RING-and RBR-type E3s, and their respective, dedicated E2s in an organism. This work was combined into manuscript titled: *"Two functionally distinct E2/E3 pairs coordinate ubiquitination of a common substrate in C. elegans development"* (currently under revision).

Each of the three main chapters (II, III & IV) contains full versions of each manuscript to allow for each chapter to stand alone. In addition, Chapter I (Introduction) and V (Concluding Remarks) are also designed to be read and understood as independent entities. Therefore, this work as a whole might contain some redundancies.

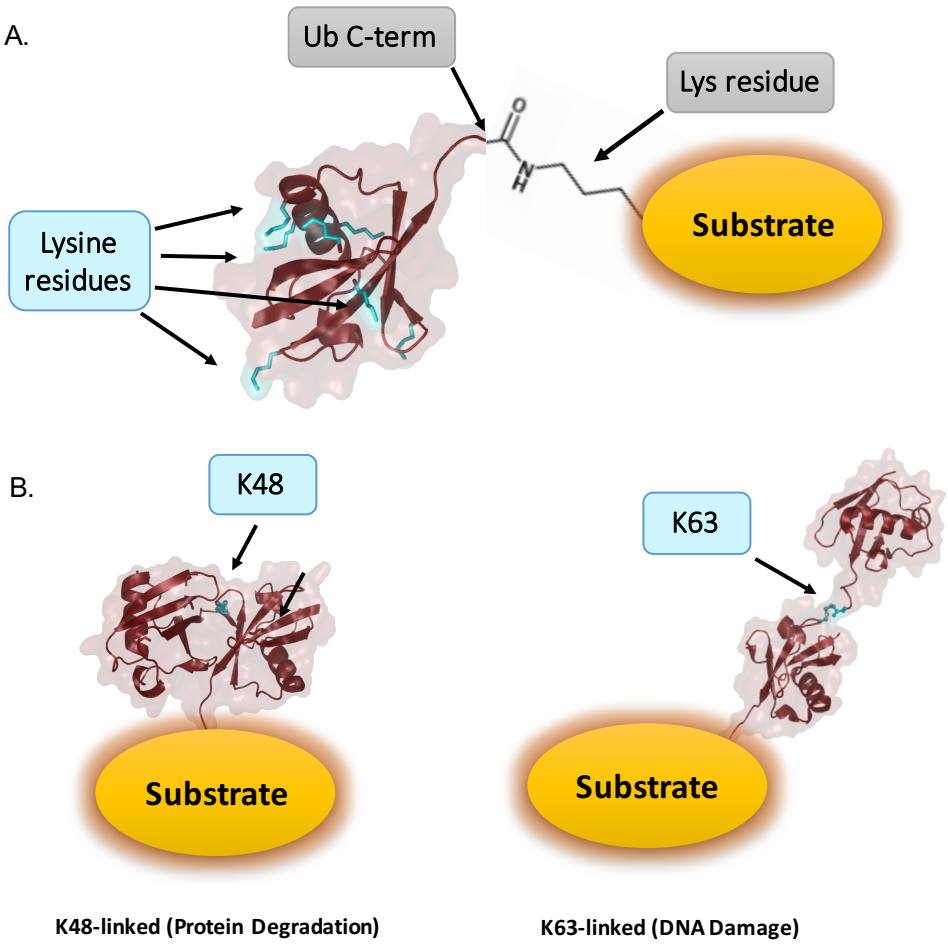

(adapted from an original figure generated by Dr. Peter Brzovic)

Figure 1. The ubiquitin code. a) Cartoon and surface representation of a Ub structure (pdb 1ubq) with its seven Lys residues highlighted as blue sticks. Ub is covalently attached to substrates via the carboxyl group of its C-terminus (C-term) and typically the side chain of a substrate Lys, generating a stable isopeptide bond. b) Ub chains can be built by using any of the seven Ub Lys residues (K6, K11, K27, K29, K33, K48 or K63), but the three dimensional topology of each polymeric chain differs. For example, K48-linked chains are more compact due to intramolecular interactions (left), whereas K63-linked chains adopt a more linear conformation (right). This allows Ub-binding proteins to distinguish among different chain linkages and therefore the signal conveyed through each chain type varies: K48-linked chains signal for proteasomal degradation and K63-linked chains act to recruit DNA damage repair proteins [4, 10].

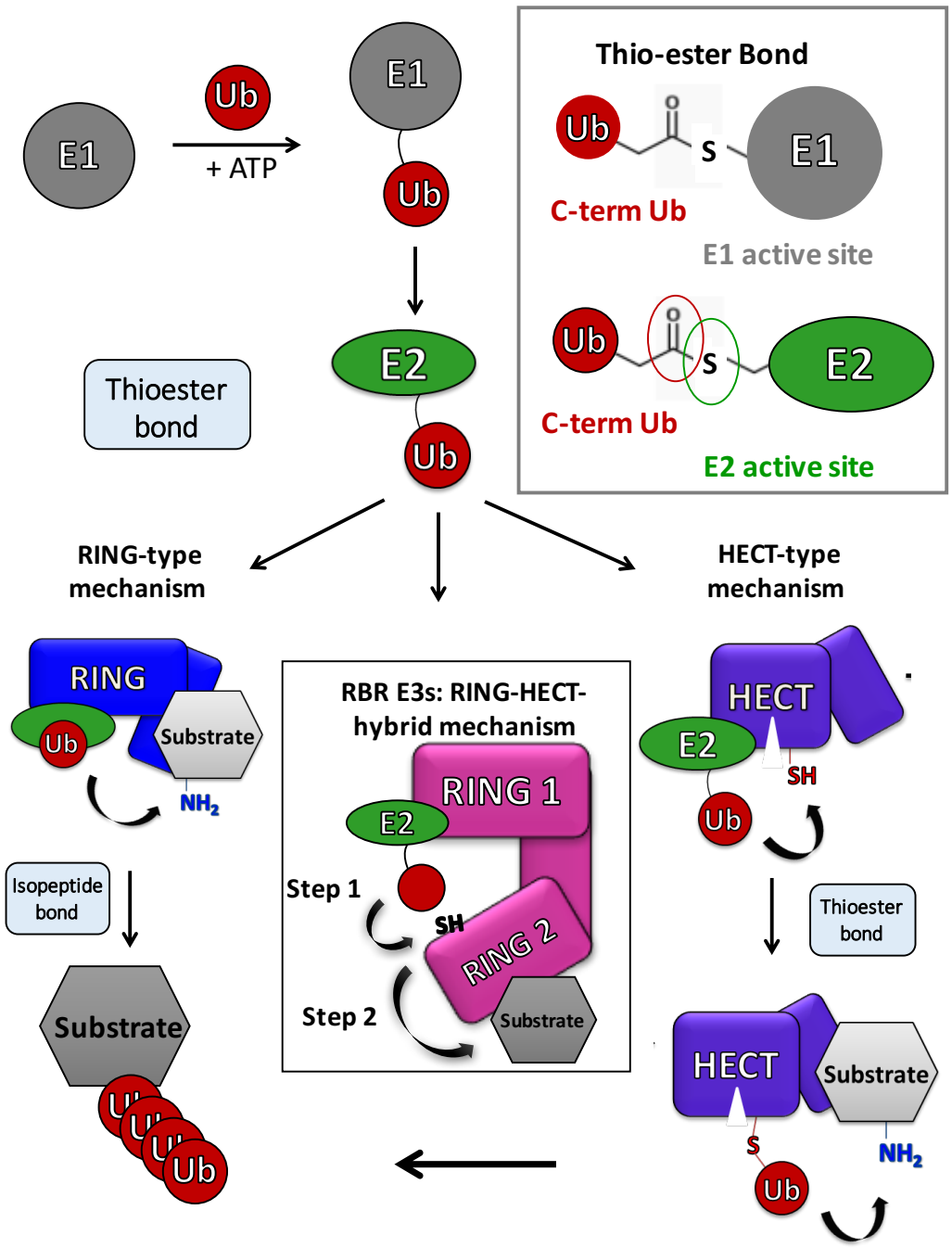

Figure 2. The ubiquitination cascade. Substrate modification with Ub requires a cascade of three enzymes: The E1 activates the C-term of Ub in an ATP-dependent manner and transfers it to its own active site Cys, generating a E1~Ub thioester. Ub is then transferred onto an E2 via a transthiolation reaction. Substrate ubiquitination occurs through a third enzyme, the E3 ubiquitin ligase. There are three major classes of eukaryotic E3s: RING-type E3s (left), HECT-type E3 (right) and RBR-type E3s (middle box). While E2~Ub directly ubiquitinate substrates when bound to RING-E3s, reactions catalyzed by HECT-type E3s require an obligatory E3~Ub intermediate. RBR E3s are considered RING/HECT hybrids, because they contain an E2-binding RING-domain (while HECT E3s bind the E2 via a structurally distinct HECT domain), yet Ub must be transferred through an active site Cys, similar to HECT-type E3s [44].

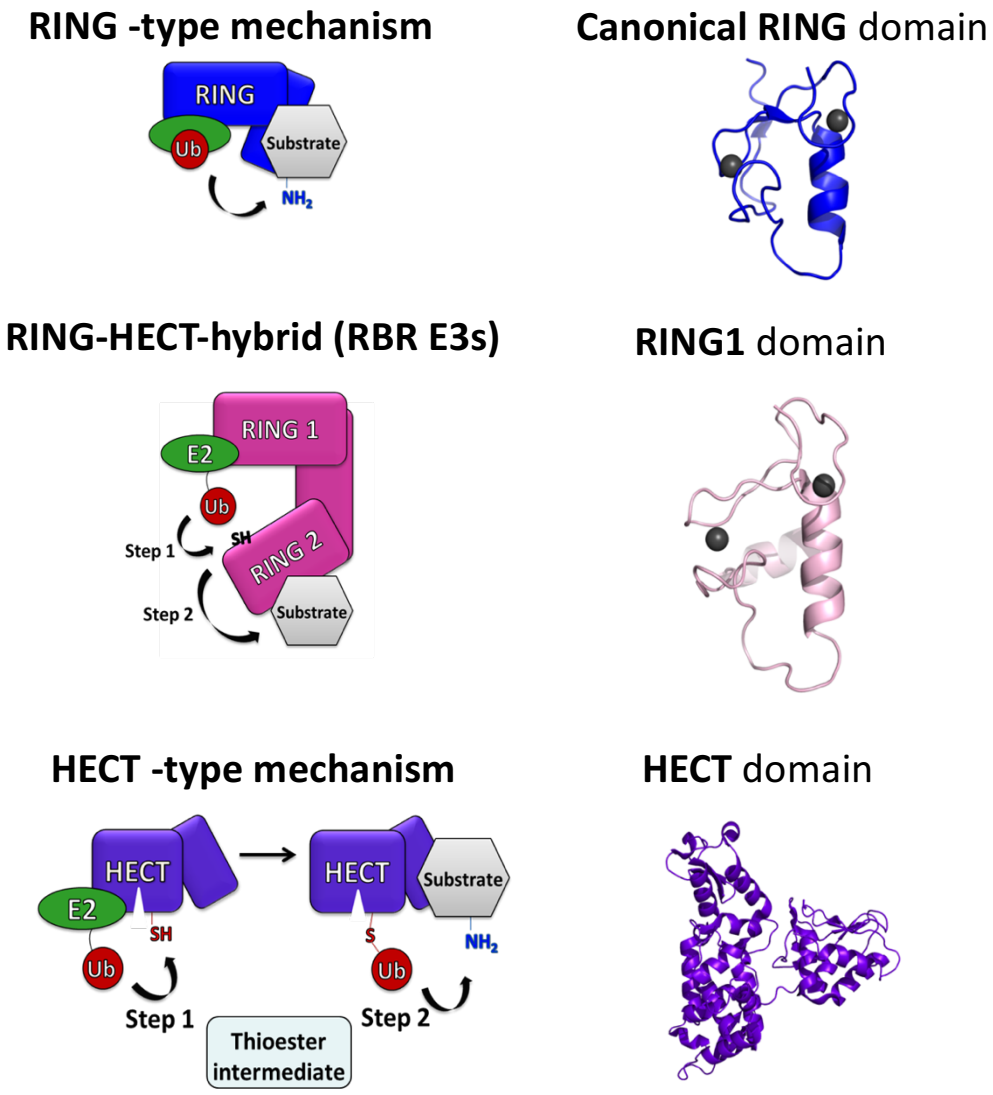

Figure 3. RING and HECT domains. *Top panel*. RING-E3s bind E2s via a conserved RING-domain defined by a characteristic cross-brace fold that coordinates two Zinc ions. A ribbon diagram of a structure of the BRCA1 RING domain [79]is shown. *Middle panel.* RBR E3s contain an E2-binding RING1 domain. The structure of RING1 is highly similar to canonical RING domains as exemplified by a ribbon diagram of HHARI RING1[57]. *Bottom panel*. The E2-binding domain of HECT E3s is structurally distinct from RING domains. A ribbon diagram of the Rsp5 HECT domain of Rsp5 is shown as an example [80].

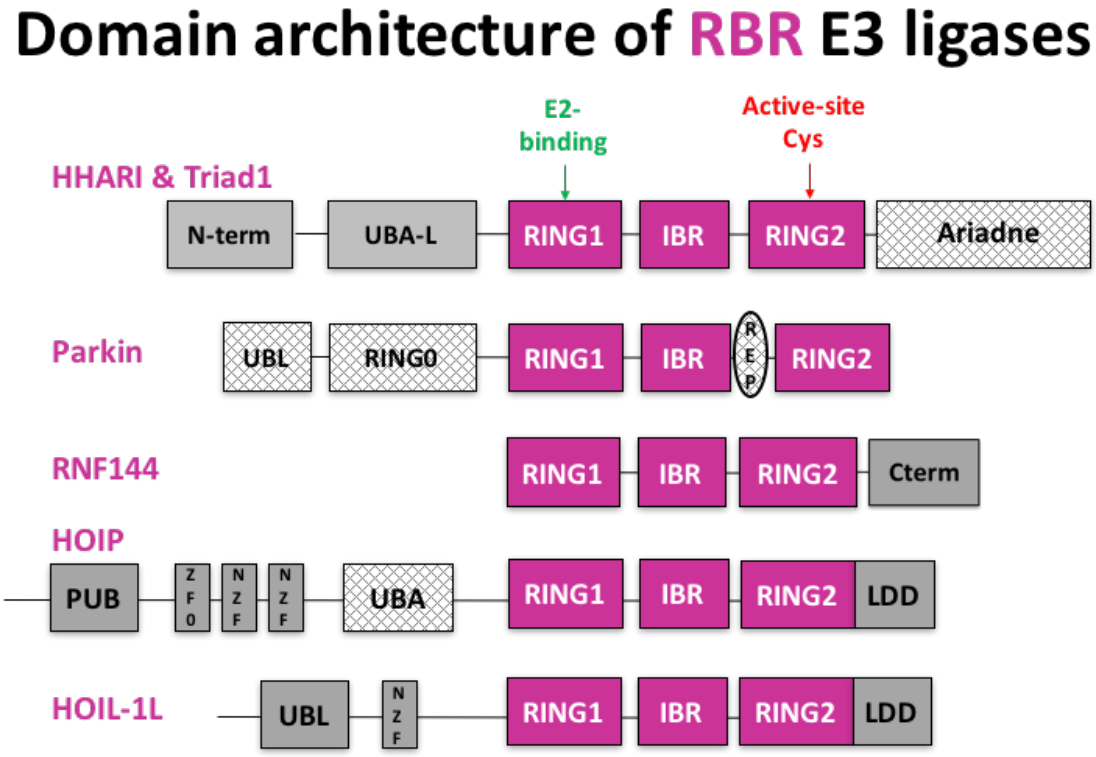

Figure 4. RBR domain architecture. All RBR E3s contain a RBR domain (pink boxes) comprised of RING1, IBR and RING2, but the position of the RBR domain and the occurrence of additional domains within each RBR varies (grey boxes). RING1 binds the E2 while RING2 (which does not resemble a RING domain structurally) contains the active site Cys RING2. Another common feature among RBR E3 is they require activation, often through the movement of auto-inhibitory domains (that occlude the active site Cys in the three-dimensional structure) in the case of HHARI, Triad1, Parkin and HOIP (hatched boxes) or dimerization through the C-term as has been shown for RNF144 [51, 57, 62, 65-67].

References

1. Schnell JD, Hicke L (2003) Non-traditional functions of ubiquitin and ubiquitin-binding proteins. *J Biol Chem* **278**: 35857-60

2. Schoenheimer R (1942) The Dynamic State of Body Constituents. *Harvard University Press, Cambridge, MA*

3. Simpson M (1953) The release of labeled amino acids from the proteins of rat liver slices. *J Biol Chem*

4. Hershko A, Ciechanover A (1998) The ubiquitin system. *Annu Rev Biochem* **67**: 425-79

5. Varshavsky A (1997) The ubiquitin system. *Trends Biochem Sci* **22**: 383-7

6. Pickart CM, Eddins MJ (2004) Ubiquitin: structures, functions, mechanisms. *Biochim Biophys Acta* **1695**: 55-72

7. van Delft S, Govers R, Strous GJ, Verkleij AJ, van Bergen en Henegouwen PM (1997) Epidermal growth factor induces ubiquitination of Eps15. *J Biol Chem* **272**: 14013-6

8. Jura N, Scotto-Lavino E, Sobczyk A, Bar-Sagi D (2006) Differential modification of Ras proteins by ubiquitination. *Mol Cell* **21**: 679-87

9. Komander D, Reyes-Turcu F, Licchesi JD, Odenwaelder P, Wilkinson KD, Barford D (2009) Molecular discrimination of structurally equivalent Lys 63-linked and linear polyubiquitin chains. *EMBO Rep* **10**: 466-73

10. Spence J, Sadis S, Haas AL, Finley D (1995) A ubiquitin mutant with specific defects in DNA repair and multiubiquitination. *Mol Cell Biol* **15**: 1265-73

11. Ordureau A, Sarraf SA, Duda DM, Heo JM, Jedrychowski MP, Sviderskiy VO, Olszewski JL, Koerber JT, Xie T, Beausoleil SA*, et al.* (2014) Quantitative proteomics reveal a feedforward mechanism for mitochondrial PARKIN translocation and ubiquitin chain synthesis. *Mol Cell* **56**: 360-75

12. Matsumoto ML, Wickliffe KE, Dong KC, Yu C, Bosanac I, Bustos D, Phu L, Kirkpatrick DS, Hymowitz SG, Rape M*, et al.* (2010) K11-linked polyubiquitination in cell cycle control revealed by a K11 linkage-specific antibody. *Mol Cell* **39**: 477-84

13. Bremm A, Freund SM, Komander D (2010) Lys11-linked ubiquitin chains adopt compact conformations and are preferentially hydrolyzed by the deubiquitinase Cezanne. *Nat Struct Mol Biol* **17**: 939-47

14. Moniz S, Bandarra D, Biddlestone J, Campbell KJ, Komander D, Bremm A, Rocha S (2015) Cezanne regulates E2F1-dependent HIF2alpha expression. *J Cell Sci* **128**: 3082-93

15. Gatti M, Pinato S, Maiolica A, Rocchio F, Prato MG, Aebersold R, Penengo L (2015) RNF168 promotes noncanonical K27 ubiquitination to signal DNA damage. *Cell Rep* **10**: 226-38

16. Wang Q, Liu X, Cui Y, Tang Y, Chen W, Li S, Yu H, Pan Y, Wang C (2014) The E3 ubiquitin ligase AMFR and INSIG1 bridge the activation of TBK1 kinase by modifying the adaptor STING. *Immunity* **41**: 919-33

17. Fei C, Li Z, Li C, Chen Y, Chen Z, He X, Mao L, Wang X, Zeng R, Li L (2013) Smurf1-mediated Lys29-linked nonproteolytic polyubiquitination of axin negatively regulates Wnt/beta-catenin signaling. *Mol Cell Biol* **33**: 4095-105

18. Yuan WC, Lee YR, Lin SY, Chang LY, Tan YP, Hung CC, Kuo JC, Liu CH, Lin MY, Xu M*, et al.* (2014) K33-Linked Polyubiquitination of Coronin 7 by Cul3-KLHL20 Ubiquitin E3 Ligase Regulates Protein Trafficking. *Mol Cell* **54**: 586-600

19. Meyer HJ, Rape M (2014) Enhanced protein degradation by branched ubiquitin chains. *Cell* **157**: 910-21

20. Xu P, Duong DM, Seyfried NT, Cheng D, Xie Y, Robert J, Rush J, Hochstrasser M, Finley D, Peng J (2009) Quantitative proteomics reveals the function of unconventional ubiquitin chains in proteasomal degradation. *Cell* **137**: 133-45

21. Vosper JM, McDowell GS, Hindley CJ, Fiore-Heriche CS, Kucerova R, Horan I, Philpott A (2009) Ubiquitylation on canonical and non-canonical sites targets the transcription factor neurogenin for ubiquitin-mediated proteolysis. *J Biol Chem* **284**: 15458-68

22. Tait SW, de Vries E, Maas C, Keller AM, D'Santos CS, Borst J (2007) Apoptosis induction by Bid requires unconventional ubiquitination and degradation of its N-terminal fragment. *J Cell Biol* **179**: 1453-66

23. Weber A, Cohen I, Popp O, Dittmar G, Reiss Y, Sommer T, Ravid T, Jarosch E (2016) Sequential Poly-ubiquitylation by Specialized Conjugating Enzymes Expands the Versatility of a Quality Control Ubiquitin Ligase. *Mol Cell* **63**: 827-39

24. Tokunaga F, Nakagawa T, Nakahara M, Saeki Y, Taniguchi M, Sakata S, Tanaka K, Nakano H, Iwai K (2011) SHARPIN is a component of the NF-kappaB-activating linear ubiquitin chain assembly complex. *Nature* **471**: 633-6

25. Ikeda F, Deribe YL, Skanland SS, Stieglitz B, Grabbe C, Franz-Wachtel M, van Wijk SJ, Goswami P, Nagy V, Terzic J*, et al.* (2011) SHARPIN forms a linear ubiquitin ligase complex regulating NF-kappaB activity and apoptosis. *Nature* **471**: 637-41

26. Gerlach B, Cordier SM, Schmukle AC, Emmerich CH, Rieser E, Haas TL, Webb AI, Rickard JA, Anderton H, Wong WW*, et al.* (2011) Linear ubiquitination prevents inflammation and regulates immune signalling. *Nature* **471**: 591-6

27. Ohtake F, Saeki Y, Sakamoto K, Ohtake K, Nishikawa H, Tsuchiya H, Ohta T, Tanaka K, Kanno J (2015) Ubiquitin acetylation inhibits polyubiquitin chain elongation. *EMBO Rep* **16**: 192-201

28. Kane LA, Lazarou M, Fogel AI, Li Y, Yamano K, Sarraf SA, Banerjee S, Youle RJ (2014) PINK1 phosphorylates ubiquitin to activate Parkin E3 ubiquitin ligase activity. *J Cell Biol* **205**: 143-53

29. Kazlauskaite A, Kondapalli C, Gourlay R, Campbell DG, Ritorto MS, Hofmann K, Alessi DR, Knebel A, Trost M, Muqit MM (2014) Parkin is activated by PINK1-dependent phosphorylation of ubiquitin at Ser65. *Biochem J* **460**: 127-39

30. Koyano F, Okatsu K, Kosako H, Tamura Y, Go E, Kimura M, Kimura Y, Tsuchiya H, Yoshihara H, Hirokawa T*, et al.* (2014) Ubiquitin is phosphorylated by PINK1 to activate parkin. *Nature* **510**: 162-6

31. Hofmann RM, Pickart CM (2001) In vitro assembly and recognition of Lys-63 polyubiquitin chains. *J Biol Chem* **276**: 27936-43

32. Kirisako T, Kamei K, Murata S, Kato M, Fukumoto H, Kanie M, Sano S, Tokunaga F, Tanaka K, Iwai K (2006) A ubiquitin ligase complex assembles linear polyubiquitin chains. *EMBO J* **25**: 4877-87

33. Schulman BA, Harper JW (2009) Ubiquitin-like protein activation by E1 enzymes: the apex for downstream signalling pathways. *Nat Rev Mol Cell Biol* **10**: 319-31

34. Ye Y, Rape M (2009) Building ubiquitin chains: E2 enzymes at work. *Nat Rev Mol Cell Biol* **10**: 755-64

35. Li W, Bengtson MH, Ulbrich A, Matsuda A, Reddy VA, Orth A, Chanda SK, Batalov S, Joazeiro CA (2008) Genome-wide and functional annotation of human E3 ubiquitin ligases identifies MULAN, a mitochondrial E3 that regulates the organelle's dynamics and signaling. *PLoS One* **3**: e1487

36. Haas AL, Warms JV, Hershko A, Rose IA (1982) Ubiquitin-activating enzyme. Mechanism and role in protein-ubiquitin conjugation. *J Biol Chem* **257**: 2543-8

37. Feldman RM, Correll CC, Kaplan KB, Deshaies RJ (1997) A complex of Cdc4p, Skp1p, and Cdc53p/cullin catalyzes ubiquitination of the phosphorylated CDK inhibitor Sic1p. *Cell* **91**: 221-30

38. Williamson A, Wickliffe KE, Mellone BG, Song L, Karpen GH, Rape M (2009) Identification of a physiological E2 module for the human anaphase-promoting complex. *Proc Natl Acad Sci U S A* **106**: 18213-8

39. Deng L, Wang C, Spencer E, Yang L, Braun A, You J, Slaughter C, Pickart C, Chen ZJ (2000) Activation of the IkappaB kinase complex by TRAF6 requires a dimeric ubiquitin-conjugating enzyme complex and a unique polyubiquitin chain. *Cell* **103**: 351-61

40. Kirkpatrick DS, Hathaway NA, Hanna J, Elsasser S, Rush J, Finley D, King RW, Gygi SP (2006) Quantitative analysis of in vitro ubiquitinated cyclin B1 reveals complex chain topology. *Nat Cell Biol* **8**: 700-10

41. Christensen DE, Brzovic PS, Klevit RE (2007) E2-BRCA1 RING interactions dictate synthesis of mono- or specific polyubiquitin chain linkages. *Nat Struct Mol Biol* **14**: 941-8

42. Scaglione KM, Basrur V, Ashraf NS, Konen JR, Elenitoba-Johnson KS, Todi SV, Paulson HL (2013) The ubiquitin-conjugating enzyme (E2) Ube2w ubiquitinates the N terminus of substrates. *J Biol Chem* **288**: 18784-8

43. Tatham MH, Plechanovova A, Jaffray EG, Salmen H, Hay RT (2013) Ube2W conjugates ubiquitin to alpha-amino groups of protein N-termini. *Biochem J* **453**: 137-45

44. Wenzel DM, Lissounov A, Brzovic PS, Klevit RE (2011) UBCH7 reactivity profile reveals parkin and HHARI to be RING/HECT hybrids. *Nature* **474**: 105-8

45. Branigan E, Plechanovova A, Jaffray EG, Naismith JH, Hay RT (2015) Structural basis for the RING-catalyzed synthesis of K63-linked ubiquitin chains. *Nat Struct Mol Biol* **22**: 597-602

46. Plechanovova A, Jaffray EG, Tatham MH, Naismith JH, Hay RT (2012) Structure of a RING E3 ligase and ubiquitin-loaded E2 primed for catalysis. *Nature* **489**: 115-20

47. Saha A, Lewis S, Kleiger G, Kuhlman B, Deshaies RJ (2011) Essential role for ubiquitin-ubiquitin-conjugating enzyme interaction in ubiquitin discharge from Cdc34 to substrate. *Mol Cell* **42**: 75-83

48. Pruneda JN, Littlefield PJ, Soss SE, Nordquist KA, Chazin WJ, Brzovic PS, Klevit RE (2012) Structure of an E3:E2~Ub complex reveals an allosteric mechanism shared among RING/U-box ligases. *Mol Cell* **47**: 933-42

49. Dou H, Buetow L, Sibbet GJ, Cameron K, Huang DT (2012) BIRC7-E2 ubiquitin conjugate structure reveals the mechanism of ubiquitin transfer by a RING dimer. *Nat Struct Mol Biol* **19**: 876-83

50. Kamadurai HB, Souphron J, Scott DC, Duda DM, Miller DJ, Stringer D, Piper RC, Schulman BA (2009) Insights into ubiquitin transfer cascades from a structure of a UbcH5B approximately ubiquitin-HECT(NEDD4L) complex. *Mol Cell* **36**: 1095-102

51. Kelsall IR, Duda DM, Olszewski JL, Hofmann K, Knebel A, Langevin F, Wood N, Wightman M, Schulman BA, Alpi AF (2013) TRIAD1 and HHARI bind to and are activated by distinct neddylated Cullin-RING ligase complexes. *EMBO J* **32**: 2848-60

52. Smit JJ, Monteferrario D, Noordermeer SM, van Dijk WJ, van der Reijden BA, Sixma TK (2012) The E3 ligase HOIP specifies linear ubiquitin chain assembly through its RING-IBR-RING domain and the unique LDD extension. *EMBO J* **31**: 3833-44

53. Stieglitz B, Morris-Davies AC, Koliopoulos MG, Christodoulou E, Rittinger K (2012) LUBAC synthesizes linear ubiquitin chains via a thioester intermediate. *EMBO Rep* **13**: 840-6

54. Sauve V, Lilov A, Seirafi M, Vranas M, Rasool S, Kozlov G, Sprules T, Wang J, Trempe JF, Gehring K (2015) A Ubl/ubiquitin switch in the activation of Parkin. *EMBO J* **34**: 2492-505

55. Haddad DM, Vilain S, Vos M, Esposito G, Matta S, Kalscheuer VM, Craessaerts K, Leyssen M, Nascimento RM, Vianna-Morgante AM*, et al.* (2013) Mutations in the intellectual disability gene Ube2a cause neuronal dysfunction and impair parkin-dependent mitophagy. *Mol Cell* **50**: 831-43

56. Kitada T, Asakawa S, Hattori N, Matsumine H, Yamamura Y, Minoshima S, Yokochi M, Mizuno Y, Shimizu N (1998) Mutations in the parkin gene cause autosomal recessive juvenile parkinsonism. *Nature* **392**: 605-8

57. Duda DM, Olszewski JL, Schuermann JP, Kurinov I, Miller DJ, Nourse A, Alpi AF, Schulman BA (2013) Structure of HHARI, a RING-IBR-RING ubiquitin ligase: autoinhibition of an Ariadne-family E3 and insights into ligation mechanism. *Structure* **21**: 1030-41

58. Aguilera M, Oliveros M, Martinez-Padron M, Barbas JA, Ferrus A (2000) Ariadne-1: a vital Drosophila gene is required in development and defines a new conserved family of ring-finger proteins. *Genetics* **155**: 1231-44

59. Tan NG, Ardley HC, Scott GB, Rose SA, Markham AF, Robinson PA (2003) Human homologue of ariadne promotes the ubiquitylation of translation initiation factor 4E homologous protein, 4EHP. *FEBS Lett* **554**: 501-4

60. Qiu X, Fay DS (2006) ARI-1, an RBR family ubiquitin-ligase, functions with UBC-18 to regulate pharyngeal development in C. elegans. *Dev Biol* **291**: 239-52

61. Elmehdawi F, Wheway G, Szymanska K, Adams M, High AS, Johnson CA, Robinson PA (2013) Human Homolog of Drosophila Ariadne (HHARI) is a marker of cellular proliferation associated with nuclear bodies. *Exp Cell Res* **319**: 161-72

62. Ho SR, Mahanic CS, Lee YJ, Lin WC (2014) RNF144A, an E3 ubiquitin ligase for DNA-PKcs, promotes apoptosis during DNA damage. *Proc Natl Acad Sci U S A* **111**: E2646-55

63. Lazarou M, Narendra DP, Jin SM, Tekle E, Banerjee S, Youle RJ (2013) PINK1 drives Parkin self-association and HECT-like E3 activity upstream of mitochondrial binding. *J Cell Biol* **200**: 163-72

64. Zheng X, Hunter T (2013) Parkin mitochondrial translocation is achieved through a novel catalytic activity coupled mechanism. *Cell Res* **23**: 886-97

65. Trempe JF, Sauve V, Grenier K, Seirafi M, Tang MY, Menade M, Al-Abdul-Wahid S, Krett J, Wong K, Kozlov G*, et al.* (2013) Structure of parkin reveals mechanisms for ubiquitin ligase activation. *Science* **340**: 1451-5

66. Wauer T, Komander D (2013) Structure of the human Parkin ligase domain in an autoinhibited state. *EMBO J* **32**: 2099-112

67. Riley BE, Lougheed JC, Callaway K, Velasquez M, Brecht E, Nguyen L, Shaler T, Walker D, Yang Y, Regnstrom K*, et al.* (2013) Structure and function of Parkin E3 ubiquitin ligase reveals aspects of RING and HECT ligases. *Nat Commun* **4**: 1982

68. Lechtenberg BC, Rajput A, Sanishvili R, Dobaczewska MK, Ware CF, Mace PD, Riedl SJ (2016) Structure of a HOIP/E2~ubiquitin complex reveals RBR E3 ligase mechanism and regulation. *Nature* **529**: 546-50

69. Spratt DE, Walden H, Shaw GS (2014) RBR E3 ubiquitin ligases: new structures, new insights, new questions. *Biochem J* **458**: 421-37

70. Kumar A, Aguirre JD, Condos TE, Martinez-Torres RJ, Chaugule VK, Toth R, Sundaramoorthy R, Mercier P, Knebel A, Spratt DE*, et al.* (2015) Disruption of the autoinhibited state primes the E3 ligase parkin for activation and catalysis. *EMBO J* **34**: 2506-21

71. Wauer T, Simicek M, Schubert A, Komander D (2015) Mechanism of phospho-ubiquitin-induced PARKIN activation. *Nature* **524**: 370-4

72. Kazlauskaite A, Muqit MM (2015) PINK1 and Parkin - mitochondrial interplay between phosphorylation and ubiquitylation in Parkinson's disease. *FEBS J* **282**: 215-23

73. Scott DC, Rhee DY, Duda DM, Kelsall IR, Olszewski JL, Paulo JA, de Jong A, Ovaa H, Alpi AF, Harper JW*, et al.* (2016) Two Distinct Types of E3 Ligases Work in Unison to Regulate Substrate Ubiquitylation. *Cell* **166**: 1198-1214 e24

74. Mani K, Fay DS (2009) A mechanistic basis for the coordinated regulation of pharyngeal morphogenesis in Caenorhabditis elegans by LIN-35/Rb and UBC-18-ARI-1. *PLoS Genet* **5**: e1000510

75. Fiesel FC, Moussaud-Lamodiere EL, Ando M, Springer W (2014) A specific subset of E2 ubiquitin-conjugating enzymes regulate Parkin activation and mitophagy differently. *J Cell Sci* **127**: 3488-504

76. Lim GG, Chew KC, Ng XH, Henry-Basil A, Sim RW, Tan JM, Chai C, Lim KL (2013) Proteasome inhibition promotes Parkin-Ubc13 interaction and lysine 63-linked ubiquitination. *PLoS One* **8**: e73235

77. Whitcomb EA, Taylor A (2009) Ubiquitin control of S phase: a new role for the ubiquitin conjugating enzyme, UbcH7. *Cell Div* **4**: 17

78. Chaugule VK, Walden H (2016) Specificity and disease in the ubiquitin system. *Biochem Soc Trans* **44**: 212-27

79. Brzovic PS, Rajagopal P, Hoyt DW, King MC, Klevit RE (2001) Structure of a BRCA1-BARD1 heterodimeric RING-RING complex. *Nat Struct Biol* **8**: 833-7

80. Kamadurai HB, Qiu Y, Deng A, Harrison JS, Macdonald C, Actis M, Rodrigues P, Miller DJ, Souphron J, Lewis SM*, et al.* (2013) Mechanism of ubiquitin ligation and lysine prioritization by a HECT E3. *Elife* **2**: e00828

Chapter II: Molecular Insights into RBR E3 ligase Ubiquitin Transfer Mechanisms

The following chapter was published in the journal ***EMPO reports***.

> **Dove KK**, Stieglitz B, Duncan ED, Rittinger K, Klevit RE. (2016) Molecular Insights into RBR Ubiquitin Transfer Mechanisms. *EMBO Rep*. 17(8):1221-35. Reproduced with permission from EMBO.

Author contributions

K.K.D., K.R., and R.E.K. conceived the experiments and wrote the manuscript. K.K.D. performed the NMR and biochemical experiments with crucial support by E.D. B.S. performed linear chain building assays with HOIP.

Introduction

Ubiquitin (Ub) is a small protein involved in the regulation of a wide variety of cellular processes. Ub signaling occurs through the covalent attachment of the Ub C-terminus to protein substrates via a trio of enzymes: a Ub-activating enzyme (E1), a Ub-conjugating enzyme (E2), and a Ub ligase (E3). E1s activate the C-terminus of Ub in an ATP-dependent manner and facilitate the transfer of Ub onto the E2 active site cysteine (Cys) via transthiolation to generate an E2~Ub conjugate ("~" denotes a thioester bond). Most E2~Ub conjugates can pair with one or more E3 Ub ligases to facilitate Ub transfer onto a substrate amino group, usually the sidechain of a lysine (Lys). There are three major types of eukaryotic E3 Ub ligases: Really Interesting New Gene (RING)-type E3s (including Ubox E3s), Homologous to E6AP C-Terminus (HECT)-type E3s, and RING-in-between-RING (RBR) E3s.

A majority of E3s are RING-type ligases that use a conserved RING/Ubox-domain defined by a characteristic cross-brace fold to bind the E2~Ub. These E3s bind both the substrate and E2~Ub to facilitate Ub transfer from the E2~Ub directly onto a substrate amino group, usually a lysine sidechain. In addition to this scaffolding role, RING-type E3s activate the E2~Ub to transfer Ub onto Lys residues (an aminolysis reaction) by promoting closed conformations of the E2~Ub [1-5]. A crucial feature of the RING-type activation mechanism is a conserved basic residue (Lys/Arg) that contacts both the E2 and the Ub, referred to as the "linchpin" residue [1]. HECT-type E3s bind the E2~Ub via a conserved HECT domain that is structurally distinct from a RING domain. Importantly, HECT-type E3 ligases contain a conserved Cys residue on which an obligatory E3~Ub intermediate is formed prior to Ub transfer onto a substrate Lys. This mechanism requires two types of chemical reactions: 1) a transthiolation reaction transfers Ub from E2~Ub to the E3 active site Cys to generate a reactive

E3~Ub species and 2) a subsequent aminolysis reaction transfers the C-terminus of Ub from the E3 to a substrate Lys to form a stable isopeptide bond. Unlike the mechanism utilized by RING-type E3 ligases that induce closed E2~Ub conformations, available data on HECT ligases suggest that they do not need a closed E2~Ub for activity [6, 7].

The third class of E3 ligases was discovered more recently when two RBR E3s, HHARI (human homologue of Ariadne) and Parkin, were shown to function via a RING/HECT-hybrid mechanism [6]. Despite containing an eponymous E2-binding RING domain, RBR E3s proceed through an E3~Ub thioester intermediate similar to HECT-type E3s. The functional importance of an active site Cys for catalytic activity has since been confirmed for other RBR E3 ligases including HOIP, HOIL-1L, TRIAD1, and RNF144 [8-11]. Although a small class with only 12-14 members in the human genome, RBR E3s are involved in many essential cellular pathways. The most studied RBR E3 is Parkin for which mutations have been linked to autosomal-recessive juvenile Parkinson's disease [12, 13]. HOIP and HOIL-1L are distinctive for their unique ability to generate linear Ub chains that are crucial regulators of the NF-κB signaling pathway [14-17]. HHARI and TRIAD1 belong to the Ariadne family of RBR E3 ligases defined by their C-terminal auto-inhibitory Ariadne domain. HHARI and its homologues in *Drosophila* and *C. elegans* have been implicated in processes including regulation of translation via the translation initiation factor 4EHP, cellular proliferation, and development [18-21].

RBR E3s are defined by three characteristic domains each of which coordinates two Zn^{2+} ions: RING1, in-between RING (IBR), and RING2. An RBR unit may be found at any position relative to other domains within an RBR E3, but its subdomains RING1-IBR-RING2 always appear in order (N-term to C-term). RING1 is the E2-binding domain and RING2 contains the active site Cys that when mutated to an Alanine (Ala) renders RBRs inactive [6, 8-11, 22, 23].

While RING1 domains adopt structures similar to canonical RING-type E3 ligases, RING2 domains do not resemble canonical RING domains, either structurally or functionally. The IBR domain adopts a structure that is similar to that of RING2, though its function remains elusive. As mentioned above, canonical RING-type E3s activate an E2~Ub conjugate by promoting closed E2~Ub conformations that exhibit increased reactivity towards the amino groups of Lys residues. A signature of closed conformations are non-covalent interactions between a surface on the E2 formed by the "cross-over" helix (also known as helix-2) and the hydrophobic patch or "I44 surface" of Ub. Mutations of residues within the E2:Ub interface abrogate activation by RING-type E3 ligases [1-5]. Paradoxically, HHARI RING1 fails to activate the E2~Ub for Ub transfer by aminolysis despite their close structural resemblance to canonical RING domains [6]. Furthermore, mutations of the E2 cross-over helix that significantly decrease *in vitro* Ub transfer activity with canonical RING-type E3s do not affect Ub transfer activity of the RBR E3 HHARI [1]. These observations imply that HHARI RING1 is mechanistically distinct from its canonical RING relatives in ways yet to be defined.

RBR E3s such as Parkin, HOIP, and HHARI display activity with a variety of E2s; in particular they are all active with two well characterized human E2s, UbcH5 and UbcH7 [6, 8, 9]. While most E2s, including UbcH5, are able to perform both transthiolation reactions and aminolysis reactions, UbcH7 solely performs transthiolation reactions [6]. This suggests that UbcH7 can function with HECT-type and RBR-type E3s, but not with RING-type E3s. Notably, *C.elegans* orthologues of HHARI and UbcH7 act together in pharyngeal development, suggesting that UbcH7 is a biologically relevant E2 for HHARI [20, 24]. But HHARI, Parkin, and HOIP are also known to work with E2s that are able to transfer Ub directly to (Lys) amino groups. Importantly, HOIP specifically generates linear Ub chains regardless of the chain linkage

preference of the E2 with which it works [6, 8, 9, 15, 25-28]. This suggests a dichotomy in the determining factor for product formation: in the case of RING-type E3s, the identity of the E2 determines the type of product while in RBR E3s, the E3 determines the type of product. This leads to the question: How do RBR E3s ensure that transfer of Ub occurs via the E3 active cite Cys to maintain control of product formation?

Here we report the mechanistic strategies used by RBR-type E3s to transfer ubiquitin from the E2 onto the E3. First, we show that RING1 domains of HHARI and RNF144 specifically *inhibit* closed E2~Ub conformations. This strategy ensures that Ub transfer occurs via the RBR active site by preventing off-target Ub transfer events. Second, we identify a weak but functionally important interaction between HHARI RING2 and Ub which serves to recruit RING2 to the RING1:E2~Ub complex. In structures of auto-inhibited RBR E3s, RING1 and RING2 are far from each other and a large domain rearrangement is required to bring the RING2 active site close to the E2~Ub active site bound to RING1 [29-34]. Consistent with this notion, mutations in either Ub or RING2 at the Ub:RING2 interface substantially reduce Ub transfer from E2~Ub to RING2. Finally, we demonstrate that the mechanism defined here is utilized by a variety of RBR E3 ligases, indicating its generality for this important class of enzymes.

Results

RBR E3 ligases do not require closed states of E2~Ub for ubiquitin transfer

In the absence of an E3, UbcH5~Ub is highly dynamic, with the Ub moiety populating mainly open states relative to the E2 [35]. Upon binding a canonical RING/Ubox, UbcH5~Ub is biased towards closed states that are activated for aminolysis reactions which constitute the final step in Ub transfer by RING-type E3s. Closed E2~Ub states bound to RING/Ubox domains have

been visualized in several co-crystal structures and by NMR [1-4]. Mutation of a residue on the cross-over helix of UbcH5 (L104Q) disrupts formation of closed states and dramatically decreases ubiquitination activity with canonical RINGs such as BRCA1/BARD1 (Fig 1A) [1]. Though RBRs contain an E2-binding RING domain (RING1), $UbcH5^{L104Q}$ shows robust activity with $HHARI_{RBR}$, $TRIAD1_{\Delta Ari}$, $Parkin_{RBR}$, and $HOIP_{RBR\text{-}LDD}$ (Fig 1A & EV1; information regarding constructs used in this study is included in Appendix Table S1). This observation indicates that RBR E3s do not require closed E2~Ub conformations for Ub transfer activity. Therefore, we wondered whether RING1s of RBRs are able to induce closed E2~Ub conformations. To address this question, we used an active site Cys-to-Ser E2 mutant to generate a stable oxyester mimic of E2~Ub ("E2-O-Ub"). In a previous study, the NMR spectrum of ^{15}N-UbcH5c-O-^{15}N -Ub exhibited chemical shift perturbations (CSPs) in the presence of a canonical RING/Ubox that are hallmarks of the closed state [1]. We therefore performed similar NMR binding experiments of ^{15}N-UbcH5c-O-^{15}N -Ub with the HHARI RING1 domain (residues 177-270). Comparable to previous observations for canonical RINGs, binding of HHARI RING1 to UbcH5-O-Ub occurs in fast-to-intermediate exchange (peaks shift and broaden), indicating that the interaction is of fairly modest affinity (Fig 1B). CSP analysis of free UbcH5-O-Ub compared to HHARI RING1-bound UbcH5-O-Ub revealed residues that are perturbed upon HHARI RING1 binding: these define a surface composed of residues in helix 1, loops 4, and 7 – those known to be central to binding of UbcH5 by canonical RING-type E3s [2, 3, 36-38]. These results indicate that HHARI RING1 binds UbcH5 in a manner similar to that used by canonical RINGs (Fig 1C). However, CSPs are not observed for most residues of the UbcH5 cross-over helix nor are they are observed for the Ub moiety upon HHARI RING1 binding to UbcH5-O-Ub (Fig 1C). Together, these observations are strong evidence that HHARI RING1 does not promote

UbcH5-O-Ub closed conformations. This finding provides a basis for understanding two previous observations: 1) HHARI RING1 does not enhance UbcH5~Ub reactivity towards free Lys [6] and 2) $HHARI_{RBR}$ exhibits robust activity with the cross-over helix mutant $UbcH5^{L104Q}$ ([1] and Fig 1A).

A highly conserved position in canonical RINGs, called the linchpin residue, is largely responsible for the ability to promote closed E2~Ubs by forming hydrogen bonds to both E2 and Ub [1-4]. In RINGs, the linchpin is most often a basic residue (Arg or Lys) and is occasionally a neutral H-bonding residues such as Asn. HHARI contains an Asp residue in the structurally analogous position to the linchpin, and RBRs in general do not share a common residue that could fulfill the function of a hydrogen-bonding linchpin (Fig 1D). This provides one possible explanation for HHARI RING1's failure to induce closed states of UbcH5~Ub.

HHARI RING1 promotes open E2~Ub conformations

UbcH7 is a specialized E2 that can only perform transthiolation reactions, making it an RBR/HECT-specific E2 [6]. UbcH7 is active *in vitro* with many, if not all, RBR-type E3 ligases. Notably, *C.elegans* orthologs of UbcH7 and HHARI are vital partners *in vivo* [20] prompting us to examine the effects of HHARI RING1 binding on UbcH7~Ub.

Unexpectedly, we discovered that in the absence of an E3, UbcH7-O-Ub populates closed conformations to a considerable extent. NMR CSP analysis of UbcH7-O-Ub compared to free UbcH7 reveals perturbed residues in the cross-over helix of UbcH7 in addition to residues around the active site (Fig 2A). The perturbations identify a surface similar to that seen in closed states of other E2~Ubs [1-4, 35]. To verify this conclusion, we conjugated I44A-Ub to ^{15}N-UbcH7 because Ub^{I44A} disrupts closed states of other E2~Ubs [1-3]. Indeed, residues of the

UbcH7 cross-over helix as exemplified by Q106 and S107 resonate at positions more similar to free UbcH7 than to UbcH7-O-Ub when I44A-Ub is the conjugated species (Fig 2B & Appendix Fig S1). Altogether, these data are consistent with UbcH7~Ub adopting closed conformations in the *absence* of an E3 that require surfaces that include the cross-over helix of UbcH7 and the I44-surface of Ub (Fig 2A&B and Appendix Fig S1).

We next asked what effect HHARI RING1 binding has on UbcH7~Ub. Due to the high affinity of UbcH7 for HHARI RING1 [29], residues affected by complex formation exhibit slow-exchange behavior in ^{1}H-^{15}N-HSQC-type NMR experiments. This property leads to peak intensity loss rather than peak shifting in binding experiments (Fig EV2A). First, the effect of HHARI RING1 binding to unconjugated UbcH7 was analyzed to map the RING1 binding surface. Comparison of peak intensities between the spectrum of free ^{15}N-UbcH7 and of RING1-bound ^{15}N-UbcH7 reveals that the RING1-binding surface on UbcH7 is very similar to that mapped for UbcH5 bound to RING1 (Fig EV2B&C). To simplify analysis of the UbcH7-O-Ub conjugate, either ^{15}N-labeled UbcH7 or ^{15}N-labeled Ub was incorporated into conjugates for HHARI RING1 binding experiments. Turning to the Ub moiety, an overlay of NMR spectra of free UbcH7-O-^{15}N-Ub and RING1-bound UbcH7-O-^{15}N-Ub shows several perturbed Ub resonances, as exemplified in Fig 3A. Notably, a majority of Ub residues (47, 49, 71-74) that are affected by HHARI RING1 binding to UbcH7~Ub are among those identified in a comparison of UbcH7~Ub versus free Ub (Appendix Fig S2). For example, when UbcH7~Ub binds to RING1, the Ub Q49 resonance, which experiences the largest chemical shift upon Ub conjugation to UbcH7, moves back close to its position in the spectrum of free Ub (Fig 3A & Appendix Fig S2). The simplest explanation for this observation is that RING1 binding alters or disrupts contacts between Ub and UbcH7 in UbcH7~Ub. Importantly, chemical shifts for Ub residues within both

RING1-bound UbcH7~Ub and UbcH5~Ub (Fig 1B&3A and Appendix Fig S2) are similar to those seen for *free* Ub. We propose that RING1 promotes open conformations of E2~Ub. We note that while Ub resonances of RING1-bound UbcH7~Ub are similar to those of free Ub, they are not identical, indicating that the environment of the Ub moiety may be affected by its proximity to RING1 in the complex (Fig 3A & Appendix Fig S2).

For additional evidence of disruption of UbcH7~Ub closed conformations by RING1 binding, we used ^{1}H-^{13}C-HSQC type experiments and published assignments to observe and interpret sidechain resonances of ^{13}C-UbcH7 [39]. Sidechain resonances of UbcH7 cross-over helix residues shift upon conjugation to Ub, consistent with closed UbcH7~Ub states (as exemplified in Fig 3B and Appendix Fig S3). Figure 3B compares three spectra: free ^{13}C-UbcH7 (blue) and ^{13}C-UbcH7-O-Ub in the absence (black) and presence of HHARI RING1 (red). Notably, the methyl resonance of the surface-accessible cross-over helix residue Ala110 is significantly perturbed upon conjugation of Ub to UbcH7, as evidenced by the *lack* of a (black) peak on or near the blue peak labeled Ala110 (Fig 3B), indicating that the side chain of Ala110 interacts with Ub. Upon the addition of RING1 (red spectrum), the Ala110-CH_3 peak reappears at the chemical shift observed for Ala110-CH_3 in free ^{13}C-UbcH7 (blue), evidenced by the red peak that overlays the blue Ala110 peak (Fig3B & Appendix Fig S3). These data corroborate the notion that UbcH7~Ub populates closed conformations in the absence of an E3 and that these are disrupted by HHARI RING1 binding.

To test whether disruption of UbcH7~Ub closed state is specific to HHARI RING1, we assessed the effects of binding of other RING domains to UbcH7-O-^{15}N-Ub. Though all domains tested bind to UbcH7, neither the canonical RING heterodimer BRCA1/BARD1 nor the UBox E4BU disrupted the closed conformation of UbcH7~Ub while RNF144 RING1 produced effects

similar to HHARI RING1 upon binding to UbcH7-O-^{15}N-Ub (Fig 3C & Appendix Fig S4). Thus, RBR-type RING1 domains share the ability to discourage closed UbcH7~Ub conformations, making them functionally distinct from canonical RING-type domains despite their structural similarities. Finally, we wondered whether HHARI RING1 can disrupt closed conformations of other E2~Ub species. Ubc13~Ub detectably populates closed conformations in the absence of E3 [35]. Indeed, addition of HHARI RING1 to Ubc13-O-^{15}N-Ub leads to chemical shifts of Ub resonances back towards their positions in free Ub, along the same trajectory as the "open" to "closed" perturbations (Fig EV3). Thus, the ability of HHARI RING1 to disrupt closed E2~Ub states is not limited to UbcH7.

Closed E2~Ubs are associated with increased reactivity towards Lys amino groups [1, 2, 3 , 4-6].Therefore a possible corollary to increased open E2~Ub conformations is an increase in transthiolation (reactivity towards Cys) as this is the relevant nucleophile in the context of RBR-type E3 ligases. However, we did not observe a difference between UbcH7~Ub reactivity towards free Cys in the absence versus presence of HHARI RING1 (Appendix Fig S5). Based on these data, we propose a mechanism in which not only does the RING1 of an RBR fail to *promote* closed E2~Ub states, it actively discriminates *against* them.

RING1 opening of E2~Ub enforces Ub transfer via the RING2 active site Cys

RBR E3s are active with E2s that are also active with canonical RING-type E3s [6, 8, 9, 15, 25-28]. This implies that the E2~Ub must distinguish between its two reaction modes (transthiolation and aminolysis) based on the type of E3 ligase with which it interacts. Open E2~Ub states are minimally reactive towards Lys and require activation for canonical RING-type Ub transfer [1-4]. We wondered whether there would be negative consequences if an RBR

RING1 could also stabilize closed, aminolysis-activated E2~Ubs as seen with canonical RINGs. However, our efforts to generate a HHARI RING1 that activates the E2~Ub for aminolysis by mutating positions known to be critical in canonical RING domains failed. We took an alternative approach to assess the consequence of having aminolysis activity in the context of an RBR E3 by replacing the RING1 domain within the HHARI RING1-IBR-RING2 (WT-RBR-domain) construct with the Ubox domain of E4BU to generate a Ubox-IBR-RING2 (UBR) hybrid (Fig 4A). Ubox domains are E2-binding domains that contain RING-like folds, but do not ligate Zn^{2+} and are therefore more likely to fold successfully within a hybrid construct. Importantly, the Ubox domain of E4BU has been shown to activate UbcH5~Ub for aminolysis via promotion of closed E2~Ub conformations [1].

We posited that an RBR with the ability to activate E2~Ub for aminolysis might circumvent the obligate transthiolation reaction through the active site Cys residue in RING2. In *in vitro* auto-ubiquitination assays where the RBR E3 acts as a proxy substrate, Ub transfer occurs through the active site Cys as the active site mutation C357A essentially abrogates ubiquitination activity of $HHARI_{RBR}$ (Fig 4B, LEFT panel). Remarkably, this is not the case for reactions carried out by the UBR-hybrid as the active-site-dead (C357A) version retains substantial auto-ubiquitination activity (Fig 4B, RIGHT panel). The result implies that UbcH5~Ub transfers its Ub *directly* to Lys residues when bound to the hybrid E3 construct as it does not require the active site Cys. Our UBR-hybrid construct demonstrates that the presence of an E2-binding domain that can activate E2~Ub for aminolysis creates an RBR that no longer undergoes obligate transfer to and through the active site Cys on RING2. Altogether we conclude that by favoring open E2~Ub conformations, HHARI RING1 (and likely other RING1

domains) prevents off-target ubiquitination events catalyzed by the E2~Ub and consequently enforces Ub transfer through the RING2 active site Cys.

The hydrophobic surface of Ub is required for transfer of Ub to the RBR active site

Mechanistically speaking, there is no need for RBR E3s to enhance E2~Ub ability to transfer Ub through aminolysis. Furthermore, as we demonstrated above, induction of closed E2~Ub can lead to undesirable off-target Ub transfer (Fig 4). These two rationales may be sufficient to explain why RBR E3s prefer to keep E2~Ubs in open states. However, we noted that the hydrophobic ("I44") surface of Ub that plays a critical role in protein-protein interactions is sequestered in closed E2~Ub but is exposed in open states. Furthermore, mutations of the Ub hydrophobic patch have previously been shown to decrease auto-ubiquitination activity in Parkin [40]. This raises the question whether the exposed Ub surface has a specific role in Ub transfer by RBR E3s. In *in vitro* ubiquitination assays with the RBR E3s $HHARI_{RBR}$, $Parkin_{RBR}$, and $HOIP_{RBR\text{-}LDD}$, use of Ub species that carry a mutation in a single hydrophobic patch residue led to reduced activity (Fig 5A&B, Fig EV4A). These results indicate that the Ub hydrophobic patch is required for Ub transfer by RBRs.

Current models of RBR-type mechanisms assume a two-step process for Ub transfer: first, Ub is transferred from the E2~Ub to the active site Cys on RING2 to form an E3~Ub, and second, Ub is transferred from the E3~Ub to a substrate amino group. In the case of $HOIP_{RBR\text{-}LDD}$, it has been shown that the I44-surface is not required for binding of the acceptor Ub [9]. We therefore postulated that the I44-surface might be required for the first step of the RBR Ub transfer mechanism. To test this hypothesis, we compared discharge rates for E2~Ub charged with either wt-Ub or mutant Ub prior to incubation with $Parkin_{RBR}$. In this assay, the

disappearance of E2~Ub can be observed directly by SDS-PAGE (in the absence of reducing agent). UbcH7~Ub^{WT} disappears rapidly when incubated with Parkin, whereas the UbcH7~Ub^{I44A} is stable in the presence of Parkin indicating that Ub transfer from the E2~Ub to Parkin RING2 is impaired when the Ub to be transferred is I44A-Ub (Fig 5C). Because E3~Ub intermediates for RBR E3s are often short-lived and therefore difficult to detect, it is not possible to say whether the observed disappearance of the E2~Ub is via transfer to the Parkin RING2 active site Cys or merely hydrolysis. To address this question, we took advantage of RING2 mutations in HOIP and HHARI (H887A and H359A respectively) that stabilize the E3~Ub [29, 41]. In assays with HOIP^{H887A} or HHARI^{H359A} as the E3, both the UbcH7~Ub and the E3~Ub conjugates are detected. Single mutations in the Ub hydrophobic surface show both reduced disappearance of the E2~Ub (similar to Parkin) and, importantly, decreased generation of E3~Ub (Fig 5D&E and Fig EV4B). These experiments provide strong evidence that the hydrophobic patch of Ub plays a key role in the first step of the RBR mechanism, namely for Ub transfer from the RING1-bound E2 to the Cys on RING2. Whether the Ub hydrophobic patch is also required for the second step of Ub transfer by RBR E3s remains to be addressed in future studies.

HHARI RING2 binds to the hydrophobic patch of Ub

A possible explanation for the observation that the hydrophobic patch of Ub is required for transfer of Ub from the E2 onto the E3 active site is that the Ub surface binds to the RING2 domain to recruit its active site to the E2~Ub. Consistent with this notion, some RBR RING2 domains retain weak but detectable Ub transfer activity independent of RING1, suggesting that when protein concentrations are high enough *in vitro*, RING2 can recruit an E2~Ub on its own [9, 41-44]. We reasoned that an interaction between free Ub and RING2 is likely to be of very

low affinity. Because Ub is extremely soluble, we performed NMR binding experiments using 100 μM ^{15}N-HHARI RING2 (residues 325-396) and high concentrations of Ub (1 mM; Fig 6A). A subset of resonances disappear or shift in the presence of WT-Ub but not of V70A-Ub, the Ub mutant that most affects HHARI activity (Fig 5A and Fig 6A top versus middle panels). The result has two implications: 1) the effects observed with WT-Ub are not merely due to the very high Ub concentrations used and 2) there is a direct, albeit low affinity interaction between RING2 and the hydrophobic surface of Ub. An NMR solution structure of HHARI RING2 has been solved and therefore the NMR spectrum is assigned [45], allowing perturbed residues to be identified and mapped onto the RING2 domain structure. The resulting surface forms a contiguous patch in proximity to the active site Cys357 and extends into the linker between IBR and RING2 (Fig 6B). We were surprised to see involvement of the linker which is not observed in the crystal structure [29] so we repeated the binding experiment using a RING2 construct that lacks most of the RING2-IBR linker (HHARI RING2-ΔL, residues 336-395). Remarkably, binding of Ub to ^{15}N-HHARI RING2-ΔL is substantially reduced, consistent with the linker serving as part of the binding interface (Fig 6A, bottom panel).

Mutations in HHARI residues most highly perturbed by Ub binding were tested for functional consequences in auto-ubiquitination assays. In the context of $HHARI_{RBR}$, Trp336, Glu352, and Arg363 were each mutated to Ala, and Thr341 was changed to an Asn to mimic the pathogenic mutation T415N in the analogous conserved residue in Parkin (Fig 6C). Strikingly, T341N decreases HHARI's ligase activity substantially and both W336A and E352A show a moderate reduction of ubiquitination activity while R363A has no observable effect (Fig 6D). NMR binding experiments confirm that the mutations that decrease ligase activity also decrease Ub binding to HHARI RING2 (Fig 6E). Together the results corroborate that RING2 and linker

residues are important both for Ub binding and HHARI activity, leading us to propose that the hydrophobic surface on the donor Ub binds and recruits RING2 and that this step is crucial for overall RBR activity.

Discussion

Until a few years ago, RBR E3 ligases were considered to be RING-type E3 ligases because they were thought to contain two RING domains based on primary sequence analysis. Today we know that only RING1 domains adopt a fold similar to canonical RING domains whereas RING2 domains fold into a different domain architecture that is shared by IBR domains [29-32, 41, 43, 46]. In common with canonical RING domains, RING1 binds an E2~Ub, but RING2 contains an active site Cys, similar to HECT-type E3 ligases, leading to the proposal that RBR E3 ligases act via a RING-HECT-hybrid mechanism [6] (Fig 7A). We sought here to define the mechanistic details of the RBR E3 HHARI and in so doing have discovered unique strategies that are shared among RBR E3s. Previously reported results had hinted that RBR E3s differ in essential functional ways from their eponymous RING-type E3 cousins, despite the structural similarity of RING1 domains and canonical RING domains. For example, HHARI retains the ability to transfer Ub using the UbcH5^{L104Q} mutant that abrogates Ub transfer activity with canonical RING-type E3 ligases [1]. Also, HHARI RING1 does not increase the Lys reactivity of UbcH5~Ub [6]. Together, these results suggested that HHARI RING1 does not function like a canonical RING domain. Here we demonstrate that RING1 domains not only fail to induce *closed* E2~Ub conformations – a mechanistic hallmark of canonical RING-type E3 ligases—but instead RING1s actively favor *open* E2~Ub conformations. This strategy ensures that the transfer of Ub proceeds via the active site Cys on RING2 and therefore that the type of product

generated (e.g., mono- or a specific poly-Ub chain) is determined by the RBR E3 and not by the E2 (Fig 7B).

We propose that the disfavoring of closed E2~Ub states by RING1 is a common mechanistic feature of RBR E3s for several reasons. First, we demonstrate by NMR that the RING1 domain from another RBR, RNF144 also promotes open UbcH7~Ub states (Fig 3C). Second, the RBR E3s HHARI, Parkin, TRIAD1, and HOIP all exhibit robust Ub transfer activity with UbcH5^{L104Q} *in vitro* (Fig 1A & EV1). Third, *not* promoting closed E2~Ub states is functionally important as it prevents off-target ubiquitination events catalyzed by the E2~Ub (Fig 4). In sum, RING1 domains act in an opposite manner to canonical RINGs in that they actively inhibit E2~Ub closed states and consequently, suppress E2~Ub aminolysis reactivity and therefore E2 specificity. Such a strategy can be rationalized in the context of the overall RBR mechanism in which an E2~Ub must transfer Ub specifically onto a Cys (the active site of RING2) and not to a Lys residue. RBR E3 ligases are rendered catalytically inactive when their active site Cys is mutated to an Ala proving that the Ub transfer occurs through an obligate covalent E3~Ub conjugate [6, 8-11, 22, 23]. Therefore, Ub transfer from the E2~Ub to Lys residues on either the E3 itself or another protein in its vicinity would be off-target and likely detrimental to the cellular processes that RBR E3s regulate. This unique feature of RBR RING1 domains allows RBR E3s to accept Ub from a variety of E2~Ubs including E2s that are able to transfer Ub onto either Lys or Cys, while ensuring that Ub transfer occurs through the active site Cys on RING2. Such discrimination is crucial, as in all cases known to date, it is the enzyme that carries out the *final* aminolysis reaction that determines the type of Ub modification on a given substrate. In the case of RING-type E3s it is the E2 that determines whether poly-Ub chains are built as well as the chain topology (for example K48- vs. K63-linked Ub chains). But in the case

of E3 ligases that utilize an E3~Ub intermediate, the E3 controls the final Ub product formation. For example, the E2 E2-25K possesses intrinsic ability to build K48-linked Ub chains in the absence of an E3, but this preference is suppressed when paired with the linear chain building complex that contains HOIL-1L/HOIP known to build linear Ub chains [15]. In such reactions the E2~Ub acts as a supplier of Ub for the E3, but must not modify substrates directly. Altogether, these properties enable use of the same E2s by both RING-type and RBR E3s to follow the adage "The last guy holding the activated Ub/Ubl gets to determine the product" [47].

Consistent with this general principle, the only available structure of a HECT/E2~Ub complex shows the E2~Ub in an extended conformation with non-covalent interactions between Ub and the HECT domain C-lobe, suggesting that HECT-type E3s may also promote open E2~Ub states [7]. However, the open E2~Ub state appears to be stabilized by interactions between Ub and the HECT active-site-containing C-lobe, while our NMR results show that the E2-binding domain (RING1) of RBR E3s actively disfavors E2~Ub closed states on its own. Likely, this feature is particularly important for RBR E3s like HHARI that can bind E2~Ub in their auto-inhibited states where RING1 and RING2 are very far removed as it serves to inhibit premature Ub transfer from the bound E2~Ub before an activation event allows recruitment of RING2 to occur.

Given the structural similarities between canonical RINGs and RBR RING1s, their opposite effects upon binding E2~Ub is surprising. As pointed out above, RING1 domains lack the basic linchpin residue responsible for stabilizing closed E2~Ub states, but this does not adequately explain why RING1 binding actively promotes open E2~Ubs. One possibility is that RING1 binds Ub in the context of E2~Ub as has been suggested for Parkin[33], but our NMR data for HHARI and RNF144 RING1 binding to E2~Ub presented here do not indicate Ub

binding by RING1. Instead, NMR binding experiments with either UbcH5 or UbcH7 identified an E2 surface that includes residues of the cross-over-helix that are not perturbed by canonical RING binding, suggesting that RING1 binds to a shifted or expanded surface on the E2. Notably, this "new" E2 binding surface overlaps with that contacted by Ub in closed E2~Ub states, suggesting that RING1 binding may effectively compete with Ub binding, thereby disfavoring closed conformations. The details of HHARI RING1:E2~Ub must await further structural characterization.

Our finding that mutation of Ub hydrophobic patch residues affects the first Ub transfer step for HHARI, Parkin, and HOIP led to our subsequent discovery of a Ub-binding surface on RING2. Although there are differences in severity among different Ub hydrophobic patch mutations for different RBR E3 ligases, all three E3s tested exhibit reduced activity with V70A-Ub and Q49E-Ub. Consistent with the modest degree of sequence conservation in RBR RING2s, we speculate that the Ub binding surface on RING2 is composed of some different residues in each RBR E3 (Fig 5A and Fig EV4B). That the composition of the Ub binding regions on RING2s varies is not particularly surprising. Various Ub binding domains that use the same Ub hydrophobic patch differ in primary and tertiary structure indicating that there are many possible binding modes between the Ub hydrophobic patch and a binding motif. We therefore propose that RING2 binding to the hydrophobic patch of Ub serves to recruit RING2 to the RING1-bound E2~Ub and that this feature is shared among RBR E3 ligases.

While this study was under review, a crystal structure of $HOIP_{RBR\text{-}LDD}$ bound to UbcH5~Ub was published that is consistent with the main tenets of the model presented here [48]. The structure reveals a myriad of interactions among the E3, E2, and Ub that involve multiple copies of HOIP, UbcH5, and Ub in the asymmetric unit. Nevertheless, a number of

features and interactions observed in the crystal are analogous to what we report here from solution measurements. First, the E2~Ub bound to RING1 of the $HOIP_{RBR\text{-}LDD}$ is in an open conformation. In the crystal this Ub moiety forms an extensive interface with the E3 including residues from the RING1-IBR linker and the IBR. Our work demonstrates that HHARI and RNF144 RING1 constructs (which include the RING1-IBR linker) are sufficient to induce open E2~Ub conformations, so the importance of additional contacts with the IBR during the first step of ubiquitin transfer remain to be addressed. Second, the hydrophobic patch of this Ub makes contacts to the IBR-RING2 linker and RING2 of another HOIP molecule in the crystal and this interaction is centered around Ub residues I44 and V70, in agreement with our assays showing that I44A-Ub and V70A-Ub significantly impair Ub transfer with $HOIP_{RBR\text{-}LDD.}$ (Fig EV4B). As the HOIP/E2~Ub structure is of UbcH5~Ub which is already in open states when unbound to an E3, our study provides an important additional insight that cannot be inferred from the crystal structure: RING1 binding actively opposes closed states, rather than just failing to promote them. Structural and biochemical investigations have provided rationales for the effects of many patient mutations in Parkin, but the T415N mutation has remained enigmatic [49]. Substitution of Thr415 with Asn decreases ligase activity substantially though it alters neither the structure nor solubility of Parkin [43, 50, 51]. Thr415 is proposed to be involved in a hydrogen-bonding network around the active site that is required for catalysis [43]. In our study, we found that the analogous mutation in HHARI, T341N, also decreases ligase activity and, importantly, decreases Ub binding to HHARI RING2 (Fig 6D&E, Fig EV5B). Thus, our discovery of a Ub-binding site composed of residues from RING2 and its proximal linker provides another possible mechanistic explanation for the loss of function associated with this Parkin mutation. Our results support an earlier report that peptides spanning the Parkin IBR-RING2 linker bind Ub in a peptide array

assay [40]. Thr415 is conserved in orthologs of Parkin as well as orthologs in HHARI. Altogether, the observations lead us to propose that the pathogenic Parkin T415N mutation disrupts Ub binding and consequently disables the recruitment of RING2 to the bound E2~Ub conjugate to enable the transfer of Ub onto the Parkin active site. It remains possible that the detrimental effect of T415N on Parkin activity is due to a combination of the loss of Ub binding to RING2 and the loss of a critical hydrogen-bonding network around the active site [43].

A common feature of RBR E3 ligases is that they exist in auto-inhibited states characterized by low activity [8, 10, 29-34, 40, 52]. Structures of HHARI and Parkin reveal two common features that define the auto-inhibited states [29-34]. First, the active site Cys on RING2 is at least partially buried by another domain. Second, the E2-binding RING1 domain and the RING2 domain are separated by large distances (Fig 7A). Both features imply that RBR E3 ligases must undergo major rearrangements to become active enzymes. Details of release of auto-inhibition are specific for each RBR E3 and are not yet fully defined. [8, 10, 29-34, 40, 52]. However, they share one common feature: the E2-binding RING1 domain and the active-site-containing RING2 domain must come together for transfer of Ub from the E2~Ub onto the E3 active site. In auto-inhibited conformations of HHARI and Parkin, the domains of the RBR are connected by long flexible linkers that presumably allow the domains to adopt positions that are quite remote from one another. Other than a short helix referred to as the REP (repressor) element in Parkin, linkers between IBR and RING2 domains are either not observed or are unstructured in existing crystal structures of HHARI and Parkin [29-34, 52]. However, the linker proximal to HHARI RING2 is observed in solution by NMR and in crystal structures of $HOIP_{RING2\text{-}LDD}$ and $HOIP_{RBR\text{-}LDD}$ bound to E2~Ub where in all cases it forms a short helix (Fig EV5C and [41, 45, 48]). Importantly, several of the HHARI residues that we observed to be

perturbed upon Ub binding are in the part of the IBR-RING2 linker that is seen to form a helix. We propose that the linker is extended and/or disordered in auto-inhibited states, resulting in an incomplete RING2 Ub-binding surface that will have little or no ability to bind Ub. Upon release of the inhibitory domain(s), the linker could undergo a coil-to-helix transition to complete the Ub-binding site on RING2, enabling it to be recruited to the conjugated Ub moiety bound at RING1. We propose that open E2~Ub conformations induced by RING1 binding expose the hydrophobic patch on the conjugated Ub to allow Ub within the RING1-bound E2~Ub to contact RING2 and ensure proper transfer of Ub onto the RING2 active. Although the structural details by which this mechanism is carried out may vary among RBRs, we believe that the main features defined here will be shared among them.

In closing, we note that our original proposal that RBR E3s are RING-HECT hybrids remains true in a structural sense. But findings reported here show clearly that the RBRs have evolved their own distinctive mechanistic strategies to achieve their function. Most remarkably, the centerpiece of the canonical RING allosteric mechanism for Ub transfer has been turned on its head by the RBRs.

Experimental Procedures

Cloning and constructs

The following constructs were used in this study. If not stated otherwise the following constructs are human and full-length: HHARI-RBR (aa 177-395), HHARI-RING2 (aa 325-396), HHARI-RING2-ΔL (aa 336-395), HHARI-RING1 (aa 177-270), GST-Parkin- RBR (aa 217-465, rat), TRIAD1-ΔARI (aa 1-348), RNF144 RING1 (aa 2-108), HOIP-RBR-LDD (aa 697-1072), HOIP-RING2 (aa 853-1072), E4BU (aa 1142-1173, mouse), BRCA1/BARD1 (aa 1-100/26-

140), UbcH7^{WT} or UbcH7^{C86S}, UbcH5c^{WT} or UbcH5c^{C85S} , His$_6$-Ubc13^{C87S}, E4BU-HHARI-hybrid (mouseE4BU aa1142-1173, HHARI aa 271-396) with either WT HHARI RING2 active site C357 or C357A. HHARI RING1 and E4BU-HHARI-hybrid were cloned into pGEX-4T in-frame with thrombin-cleavable, N-terminal GST-tag. RNF144 RING1 was cloned into a His$_6$-Sumo vector (N-terminal tag). TRIAD1-ΔARI was cloned into pet28a in-frame with His$_6$-T7 at the N-terminus.

Expression and purification of recombinant proteins

Proteins were expressed either in LB or minimal M9 medium supplemented with [^{15}N]-ammonium chloride or ^{13}C-glucose in *Escherichia Coli* (BL21 DE3 cells) and induced with 200 μM IPTG at 16°C for 18-22 hours. Media for E3s (except E4BU) was supplemented with 0.2mM Zn^{2+}. UbcH5c, UbcH7, His$_6$-Ubc13, BRCA1/BARD1, E4BU, GST-HHARI-RBR, GST-Parkin-RBR, HOIP-RBR-LDD, HOIP-RING2 were purified as previously described [6, 8, 35, 36, 41, 53]. GST-E4BU-HHARI-hybrid was purified as GST-HHARI-RBR.HHARI RING1 and RING2 constructs were purified using GST columns (GE Healthcare and Life Sciences) in 50mM TRIS, 200mM NaCl, pH8.0 and eluted with 10mM Glutathione. GST-tags cleaved with thrombin (Sigma Aldrich) and removed by size-exclusion chromatography (25mM $NaPO_4$, 150mM NaCl, pH7.0). His$_6$-T7-TRIAD1-ΔARI and His$_6$-Sumo-RNF144-RING1 were purified using Ni^{2+}-affinity chromatography. His$_6$-Sumo-tag was removed from RNF144-RING1 using sumo protease in 50mM TRIS, 200mM NaCl, 1mM DTT, pH8.0. Finally, size-exclusion chromatography in 25mM $NaPO_4$, 150mM NaCl, pH7.0 was performed on His$_6$-T7-TRIAD1-ΔARI and cleaved RNF144-RING1.

E2~Ub discharge assays

2 μM wheat E1, 20 μM UbcH7 or UbcH5, 10 μM of Ub or HA-Ub (WT or mutant), 5mM ATP were mixed at 37°C in 25 mM $NaPO_4$, 150 mM NaCl, pH 7.0 for 20min. Charging reactions were quenched with the addition of 0.1 units of apyrase (Sigma Aldrich)/10 μl reaction for 5min. A zero minute time point was taken using non-reducing SDS-PAGE load dye prior to incubation with either free nucleophile and/or E3. *Cys reactivity assays*: Charging reactions were diluted twofold and incubated at 37°C with a final concentration of either 5 mM Cys in the absence or presence of 75 μM E3 (HHARI RING1). Reactions were quenched at given time points by addition of non-reducing SDS-PAGE load dye. Products were visualized with Coomassie blue stain. *Parkin discharge assays:* Charging reactions were diluted twofold and incubated at 37°C with a final concentration of 4 μM GST-Parkin-$_{RBR}$. Reactions were quenched at given time points by addition of non-reducing SDS-PAGE load dye. UbcH7~Ub discharge and E3-Ub product formation was visualized by western blotting for HA-Ub (HA antibody from Life Tein, LT0422). *HOIP~Ub/HHARI~Ub capture assay:* 50 μl charging reactions were quenched with addition of 5 μl apyrase for 5min at room temperature (RT). Time point zero was taken immediately prior to addition of H887A-$HOIP_{RBR\text{-}LDD}$ or H359A-$HHARI_{RBR}$ to a final concentration of 5 μM E3. Reactions were performed at RT and quenched at given time points by addition of non-reducing SDS-PAGE load dye. Product formation was visualized by western blotting for HA-Ub and GST (HHARI).

Ubiquitination assays

For E3 auto-ubiquitination assays 0.5 μM wheat E1, 2 μM E2, 2 μM E3 (GST-$HHARI_{RBR}$, T7-$TRIAD1_{\Delta ARI}$, GST-Parkin$_{\text{-}RBR}$, Flag-BRCA1/BARD1) and 20 μM Ub were incubated at incubated at 37°C in 25 mM $NaPO_4$, 150 mM NaCl, pH 7.0. Reactions were

initiated with 10 mM ATP and quenched with SDS-PAGE reducing buffer. Samples were run on SDS-PAGE gel and visualized on Western blots (blotting for tags on E3). Antibodies used: GST antibody - Life Tein, LT0423 (Fig 1, 4, 6); Flag antibody -Sigma Aldrich, F3165 (Fig 1); T7 antibody- EMD Millipore, 69522 (Fig 1). Free linear chain building assays using $HOIP_{RBR\text{-}LDD}$ were done as described previously [41].

Generation of stable E2-O-Ub

10 μM human E1, 250 μM E2 ($UbcH7^{C86S}$, $UbcH5c^{C85S}$ or His_6-$Ubc13^{C87S}$), 750 μM Ub, 12.5 mM ATP where incubated at 37°C for 8 hours in 25 mM $NaPO_4$, 150 mM NaCl, pH 7.0. Charged species were separated from uncharged species using size exclusion chromatography.

NMR experiments

The same buffer (25 mM $NaPO_4$, 150 mM NaCl, pH7.0, 10% D_2O) and temperature (298K) were used for all experiments. All (^1H,^{15}N)-HSQC-TROSY experiments were acquired at field strengths of 500 Mhz except for data collected for Fig 6A where 600 Mhz was used instead. The following concentrations where used for each Figure. Fig 1: 220 uM ^{15}N-UbcH5-O-^{15}N-Ub Fig 2: 250 μM of ^{15}N-$UbcH7^{C86S}$ and ^{15}N-UbcH7-O-Ub^{I44A}, 200 μM of ^{15}N-UbcH7-O-Ub; Fig EV2: 250 μM free ^{15}N-$UbcH7^{C86S}$ and 250 μM ^{15}N-$UbcH7^{C86S}$ + 125 μM HHARI RING1; Fig3A, left panel: 50 μM ^{15}N-Ub, 200 μM free UbcH7-O-^{15}N-Ub, 160 μM UbcH7-O-^{15}N-Ub + 200 μM HHARI RING1; Fig 3C: 200 μM free UbcH7-O-^{15}N-Ub, 160 μM UbcH7-O-^{15}N-Ub + 200 μM HHARI RING1; 70 μM UbcH7-O-^{15}N-Ub + 200 μM RNF144 RING1; 220 μM UbcH7-O-^{15}N-Ub + 220 μM BRCA1/BARD1; Appendix Fig S4: 160 μM UbcH7-O-^{15}N-Ub + 510 μM E4BU; Fig EV3: 50 μM ^{15}N-Ub, 100 μM UbcH13-O-^{15}N-Ub, 100uM Ubc13-O-^{15}N-Ub + 300

μM HHARI RING1.Fig 6A: 100 μM free ^{15}N-HHARI RING2(-ΔL), 100 μM ^{15}N-HHARI RING2(-ΔL)+ 1 mM Ub (either WT or V70A); Fig 6E: 50 μM free ^{15}N-Ub, 50 μM ^{15}N-Ub + 500 μM HHARI RING2 (WT or mutants).

(^{1}H,^{13}C)-HSQC-TROSY experiments for Fig 3B & Appendix Fig S3 were acquired at 500 Mhz (200 μM free ^{13}C-UbcH7^{C86S}, 200 μM ^{13}C-UbcH7-O-Ub, 125 μM ^{13}C-UbcH7-O-Ub + 150 μM HHARI RING1) or 600Mhz (300 μM ^{13}C-UbcH7^{C86S} + 360 μM HHARI RING1).

NMRPipe/NMRDraw [54] was used to process NMR data. NMRViewJ (One Moon Scientific) was used for data visualization [55]. The equation $\Delta\delta = [(\Delta\delta^{15}N/5)^2 + (\Delta\delta\ ^{1}H)^2]^{1/2}$ was used to calculated chemical shift perturbations of 2D Trosy-HSQC NMR experiments.

ACKNOWLEDGEMENTS

We thank M. Stewart and P. DaRosa for insightful discussions and critical reading of the manuscript; P. Brzovic, S. Delbecq, and L. Martino for useful discussion; M. Cook and K. Reiter for proof reading the manuscript. This work was supported by National Institute of General Medical Sciences grant R01 GM088055 (REK), the Francis Crick Institute (grant number FCI01) which receives its core funding from Cancer Research UK, the UK Medical Research Council, and the Wellcome Trust (KR), UW Hurd Fellowship Fund, and PHS NRSA 5T32 GM007270 (KKD).

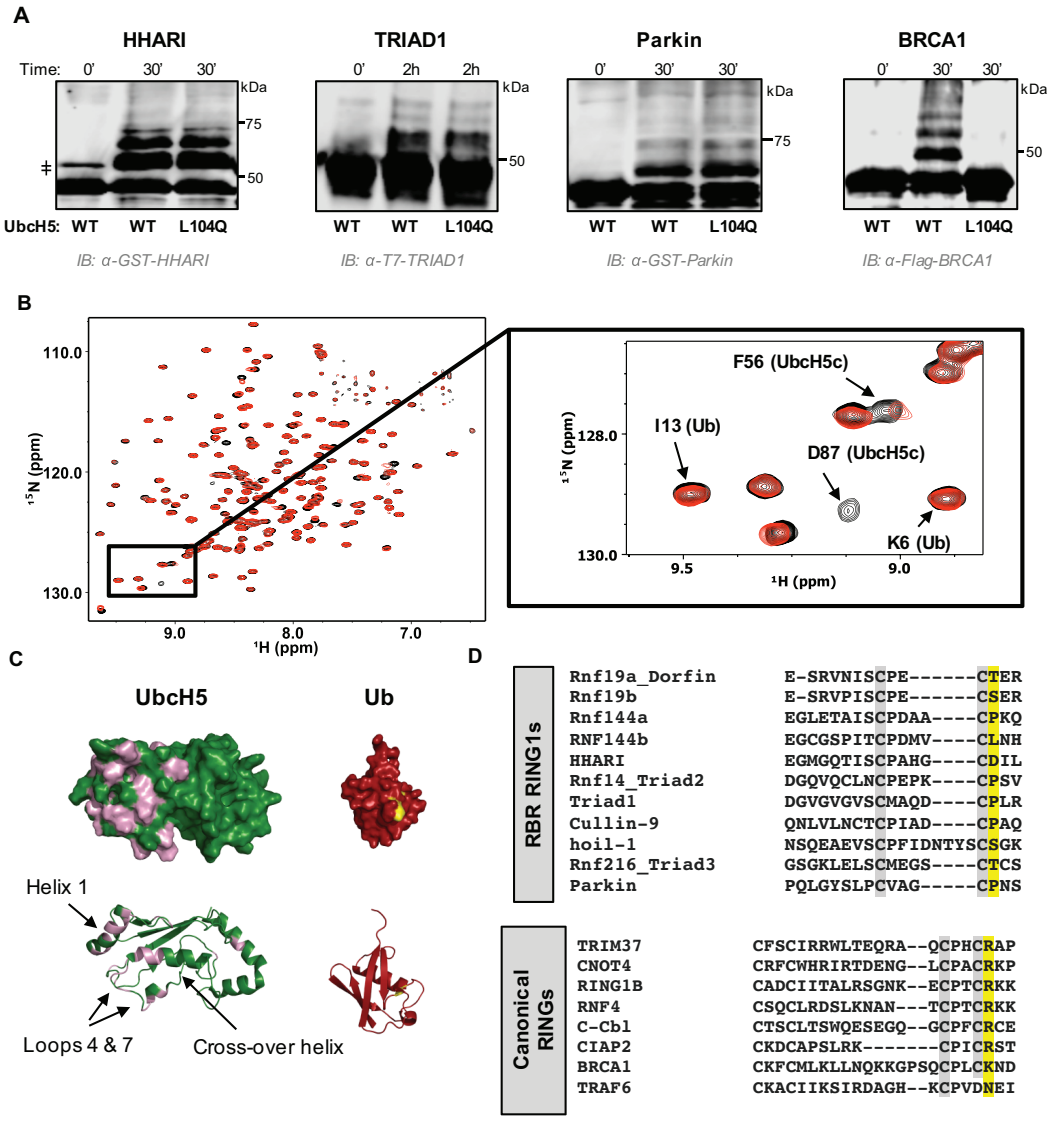

Figure 1. RBR E3 ligases do not require closed states of E2~Ub for ubiquitin transfer. a) Auto-ubiquitination assays in which the E3 acts as both an E3 and as proxy substrate were performed with GST-HHARI$_{RBR}$, T7-Triad1$_{\Delta Ari}$, GST-Parkin$_{RBR}$, and Flag-BRCA1/BARD1 and either UbcH5^{WT} or UbcH5^{L104Q} as the E2. Products were visualized by western blotting against indicated tags on E3s. Times given are post-ATP addition. b) Overlay of (^{1}H,^{15}N)-HSQC-TROSY spectra of ^{15}N-UbcH5-O-^{15}N-Ub in the absence (black) and presence (red) of 0.5mol equiv. HHARI RING1. A subset of UbcH5 peaks, but not Ub peaks, shift and broaden upon HHARI RING1 binding. c) CSPs from (b) are mapped onto the structures of UbcH5c (PDB 2fuh) and Ub (PDB 1ubq). Residues that exhibit loss of intensity > 1 stdv upon RING1 binding (intensity < 0. 47) are colored on each structure: UbcH5 residues 5, 6, 7, 16, 20, 22, 56, 62, 74, 87, 90, 91, 96, 97, 99-103, 137, 138 (pink) and Ub residues 48, 50 (yellow). The lack of CSPs on the UbcH5 cross-over helix and on the surface of Ub signifies that HHARI RING1 does not

induce closed UbcH5~Ub. d) CLUSTAL OMEGA alignments of the C-terminal sequences of RBR RING1 domains (top) and canonical RING domains (bottom). Each alignment includes the 7^{th} and 8^{th} Zn^{2+} coordinating positions (gray). The allosteric linchpin position critical for E2~Ub activation by RING-type E3s is highlighted in yellow. RBR RING1 domains lack the allosteric linchpin.

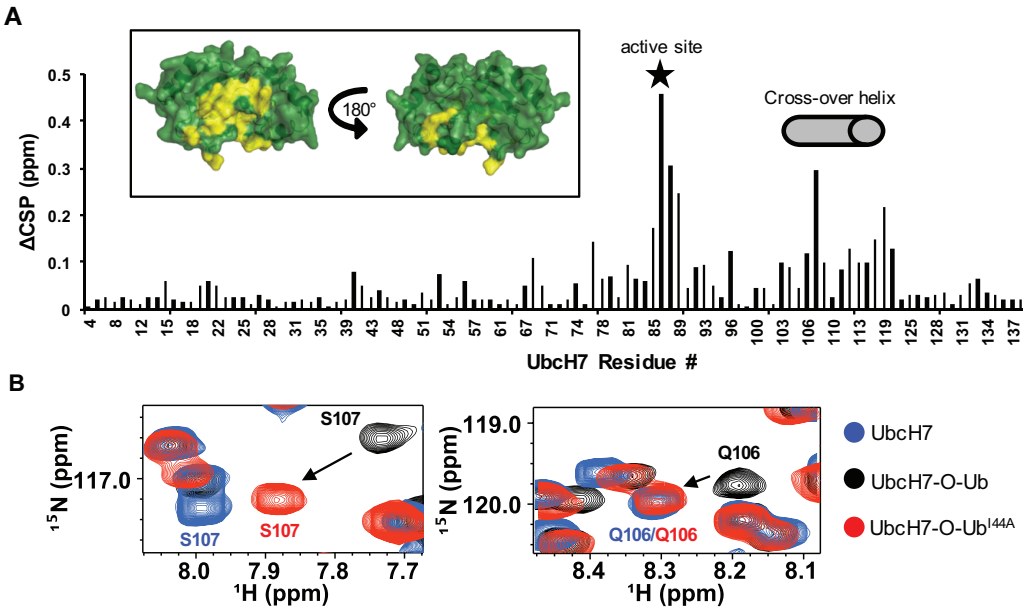

Figure 2. UbcH7~Ub populates E3-independent closed conformations. a) Histogram of CSPs between free ^{15}N-UbcH7 and ^{15}N-UbcH7-O-Ub identifies UbcH7 residues affected by conjugation to Ub. Active site (Ser86) is indicated with a star and cross-over helix residues (101-113) are marked with a gray cylinder. *INSET*. CSPs greater than 1 stdv (> 0.115 ppm) are highlighted in yellow on a surface representation of UbcH7 (PDB 1fbv). The view on the left shows the surface that contains the UbcH7 cross-over helix. b) Region of ^{1}H-^{15}N-HSQC TROSY spectra containing resonances of the cross-over helix residues S107 and Q106 are overlaid: unconjugated ^{15}N-UbcH7 (blue), ^{15}N-UbcH7-O-Ub (black), and ^{15}N-UbcH7-O-Ub^{I44A} (red). Peaks representing S107 and Q106 in the context of UbcH7~Ub-I44A (red) are closer to peaks observed in free UbcH7(blue) than UbcH7~Ub-WT (black) indicating that I44A of Ub disrupts interactions with the cross-over helix of UbcH7.

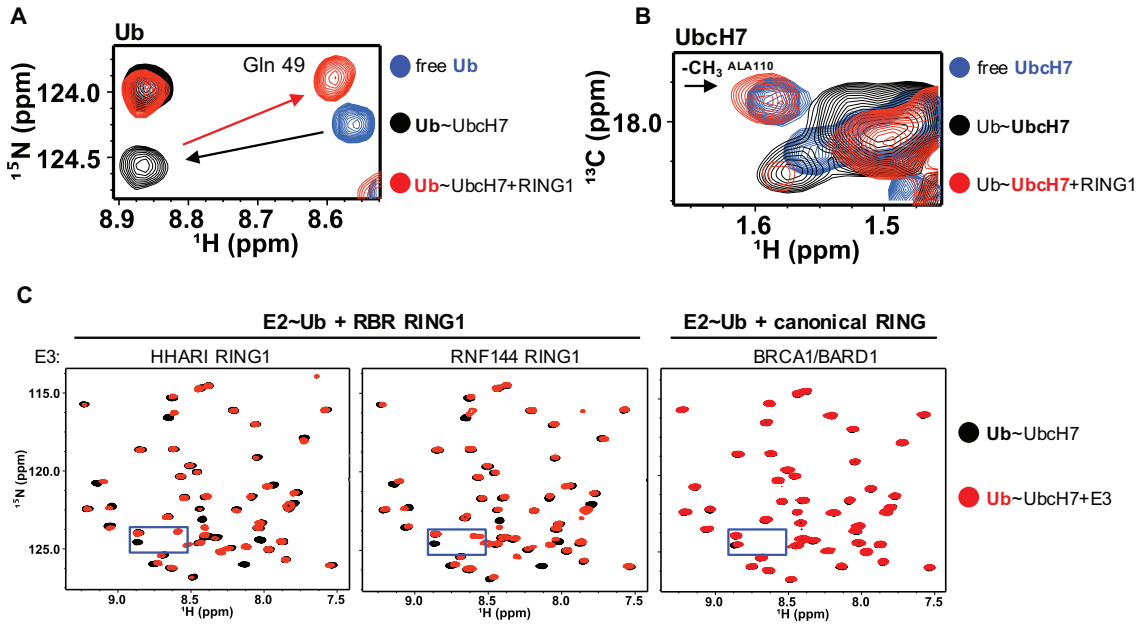

Figure 3. HHARI RING1 disfavors closed E2~Ub conformations. a) Region of ^{1}H-^{15}N-HSQC TROSY spectra that contains Gln49 Ub resonance are overlaid: free ^{15}N-Ub (blue), UbcH7-O-^{15}N-Ub (black), and HHARI RING1-bound UbcH7-O-^{15}N-Ub (red). Black arrow highlights perturbation upon conjugation to UbcH7 (black arrow) and red arrow highlights perturbation of conjugated Ub upon HHARI RING1 binding to UbcH7. b) Region of ^{1}H-^{13}C-HSQC spectra of ^{13}C-UbcH7 (blue), ^{13}C-UbcH7-O-Ub (black), and HHARI RING1-bound ^{13}C-UbcH7-O-Ub (red) that includes the methyl ($^{13}CH_3$) resonance of the surface-exposed UbcH7 cross-over helix residue, Ala 110 (black arrow) is shown. The $^{13}CH_3$ peak of Ala110 either broadens dramatically or shifts to an unknown position in the spectrum of ^{13}C-UbcH7-O-Ub (black) and reappears at its position in *free* UbcH7 in the presence of HHARI RING1, consistent with disruption of closed UbcH7~Ub conformations. Pairwise overlays and larger spectra are provided in Appendix Fig S3. c) Regions of ^{1}H-^{15}N-HSQC-TROSY spectra of UbcH7-O-^{15}N-Ub in the absence (black) and presence (red) of a RING1 domain from the RBR E3s HHARI (left) or RNF144 (middle) or a canonical RING domain of BRCA1/BARD1 (right). The perturbations on Ub due to binding of HHARI RING1 and RNF144 RING1 are remarkably similar, while binding of the canonical RING domain of BRCA1/BARD1 has no observable effect on the Ub spectrum. Gray boxes mark area expanded in a)

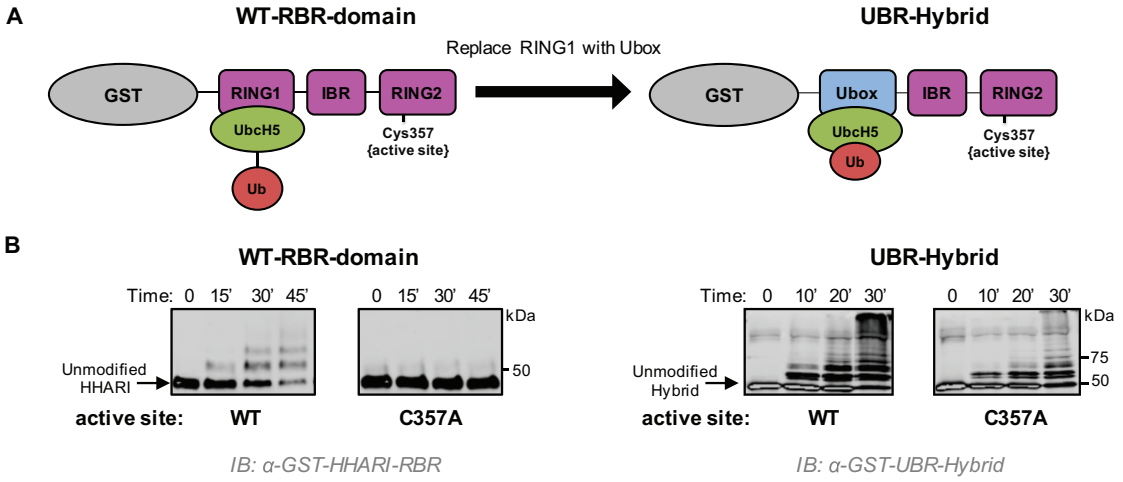

Figure 4. RING1 opening of E2~Ub enforces transfer via the RING2 active site. a) Schematic representation of the two constructs used. *LEFT*. GST-tagged $HHARI_{RBR}$ with its native RING1 domain that does not induce closed conformations of UbcH5~Ub. *RIGHT*. GST-tagged HHARI construct in which the RING1 domain was replaced with the Ubox domain of E4BU to generate the UBR-hybrid that promotes closed conformations of UbcH5~Ub. b) *LEFT*. Auto-ubiquitination assays were performed with wild-type $HHARI_{RBR}$ or an active site-dead mutant (C357A- $HHARI_{RBR}$). Products were visualized by western blotting against GST. The zero time point was taken immediately prior to ATP addition, all other times are post-ATP addition. *RIGHT*. Identical assays as shown on left were performed with the UBR-hybrid. The active site-dead mutant (C357A) retains substantial auto-ubiquitination activity signifying that UbcH5~Ub is able to transfer Ub *directly* onto the GST-UBR-hybrid construct, bypassing the RING2 active site Cys.

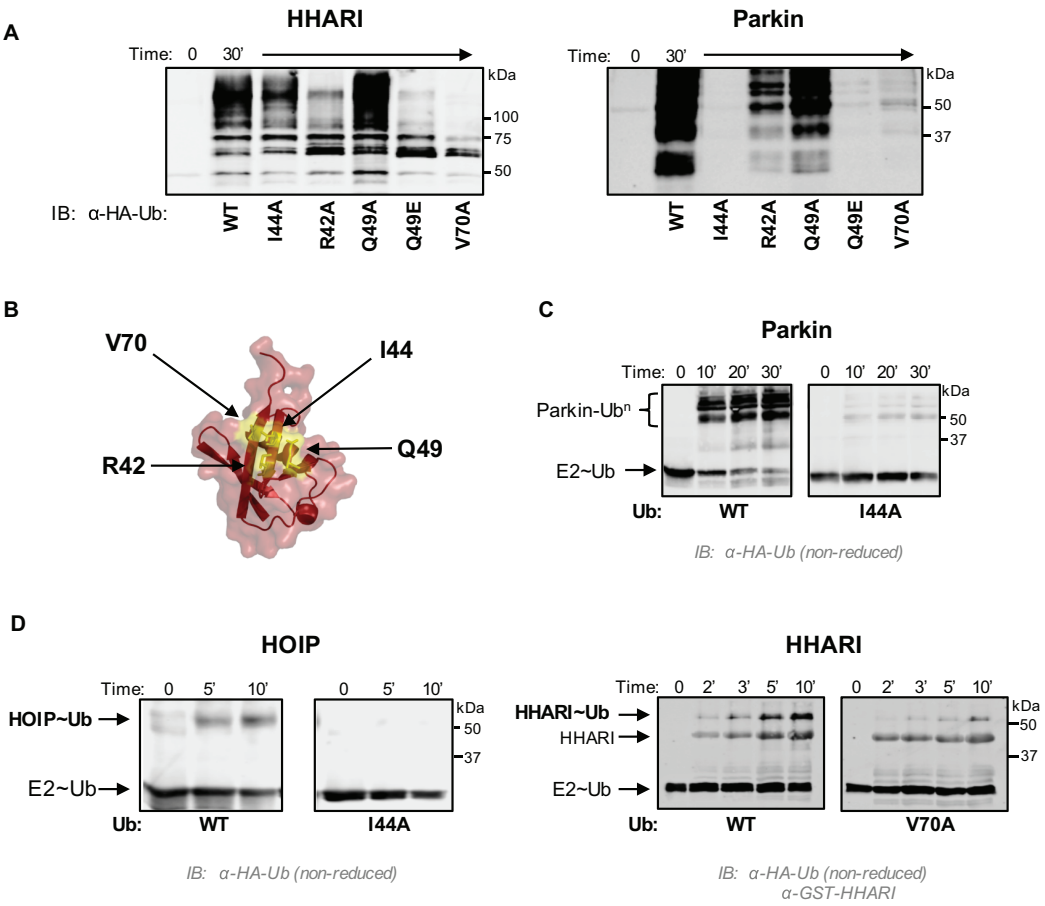

Figure 5. The Ub hydrophobic patch plays a role in Ub transfer from E2~Ub onto RING2 of RBR E3 ligases. a) *LEFT*. E3 auto-ubiquitination assays were performed using various Ub mutants (I44A, R42A, Q49A, Q49E, and V70A) and the RBR E3s $HHARI_{RBR}$ (left) and $Parkin_{RBR}$ (right). Products were visualized by western blotting against HA-Ub. Samples were analyzed 30 minutes after ATP addition. b) The hydrophobic patch of Ub (PDB 1ubq) is colored yellow on a surface representation and positions of each mutation are noted. c) UbcH7~Ub conjugates were preformed with either with WT-Ub or I44A-Ub. After the addition of apyrase to quench the charging reaction, UbcH7~Ub^{WT} (left) or UbcH7~Ub^{I44A} (right) was incubated with $Parkin_{RBR}$. The disappearance of each UbcH7~Ub species and appearance of auto-ubiquitinated E3 was visualized under non-reducing conditions by western blotting for HA-Ub. Time was recorded post addition of $Parkin_{RBR}$. E2~Ub conjugated with I44A-Ub does not disappear over the timecourse of the reaction. d) UbcH7 conjugated with WT-Ub, I44A-Ub, or V70A Ub as indicated was incubated with either H887A-$HOIP_{RBR\text{-}LDD}$ (left) or H359A-$HHARI_{RBR}$ (right) mutants that allow trapping of the E3~Ub thioester with WT-Ub (Stieglitz et al, 2013;[29]). While a HOIP~Ub thioester species is observed when UbcH7 was charged with WT-Ub, no detectable transfer occurs with the I44A-Ub conjugate (left). Similarly, V70A-Ub shows reduced formation of the HHARI~Ub thioester (right). In addition to blotting for HA-Ub, the blot on the right was also blotted for GST-HHARI.

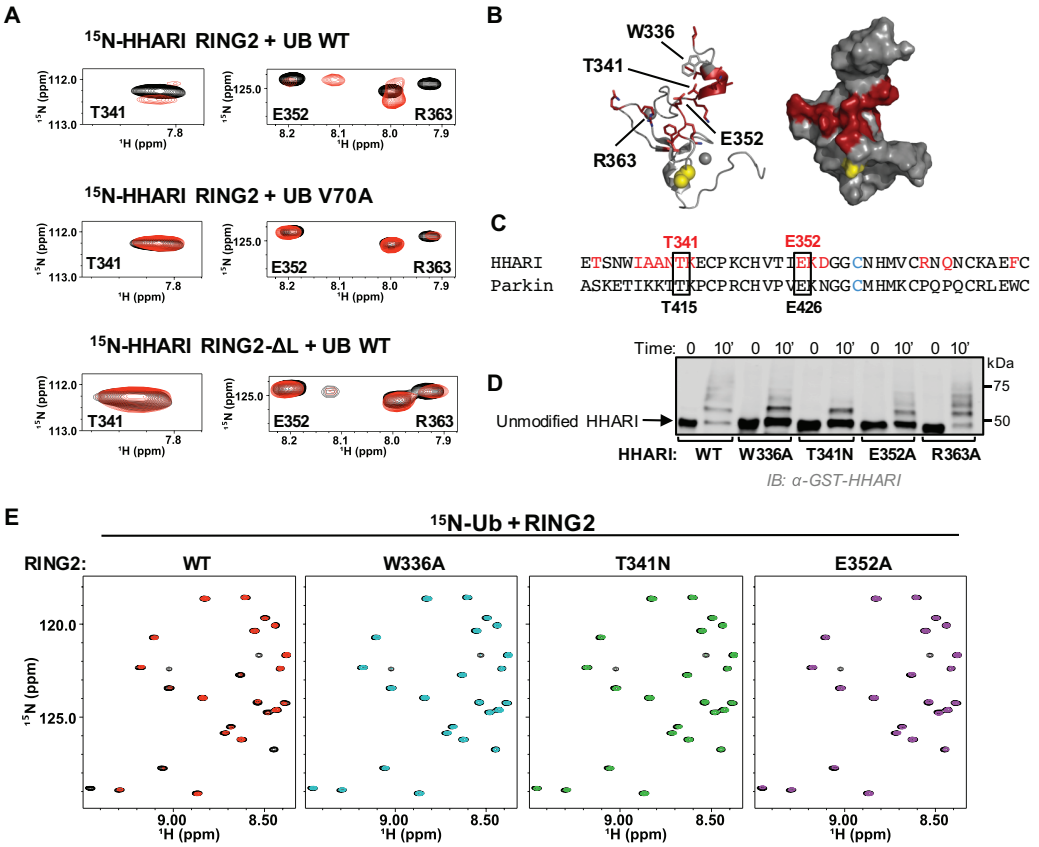

Figure 6. HHARI RING2 binds to Ub. a) *Top panel*. Regions of ^{1}H-^{15}N-HSQC TROSY spectra of ^{15}N-HHARI RING2 in the absence (black) and presence of excess Ub (red). *Middle panel*. Identical spectral region, but in the presence of Ub-V70A (red). *Bottom panel*. Identical spectral region, but spectra are from a truncated HHARI RING2 construct that lacks N-terminal residues 325-335 (HHARI RING2-ΔL). b) Residues with CSPs greater than 1 stdv (HHARI residues 333, 337-342, 352-354, 363, 365, 371) are colored red in a cartoon (left) and surface (right) representation of HHARI RING2 (PDB 2m9y). The active site C357 is in shown in yellow. c) Sequence alignment of HHARI and Parkin RING2 domains. HHARI residues perturbed by Ub binding (panel a) are in red. Residues that decrease auto-ubiquitination activity when mutated in HHARI$_{RBR}$ are indicated with black boxes. d) Mutations in the Ub binding surface of RING2 decrease activity in E3 auto-ubiquitination assays. Time points (10min) are visualized by western blotting for the GST-tag on HHARI. Relative activity of HHARI WT and mutant forms is clearest when the intensity of the unmodified HHARI band is compared. e) ^{1}H-^{15}N-HSQC TROSY spectra of ^{15}N-Ub demonstrate binding by WT HHARI RING2, but not by mutant HHARI RING2 constructs that exhibit decreased auto-ubiquitination activity. Overlay of ^{15}N-Ub spectra in the absence (black) and presence of WT-HHARI RING2 (red), W336A-HHARI RING2 (blue), T341N-HHARI RING2 (green), or E352A-HHARI RING2 (purple). HHARI mutations that exhibited reduced binding to Ub also show decreased ubiquitination activity in panel d).

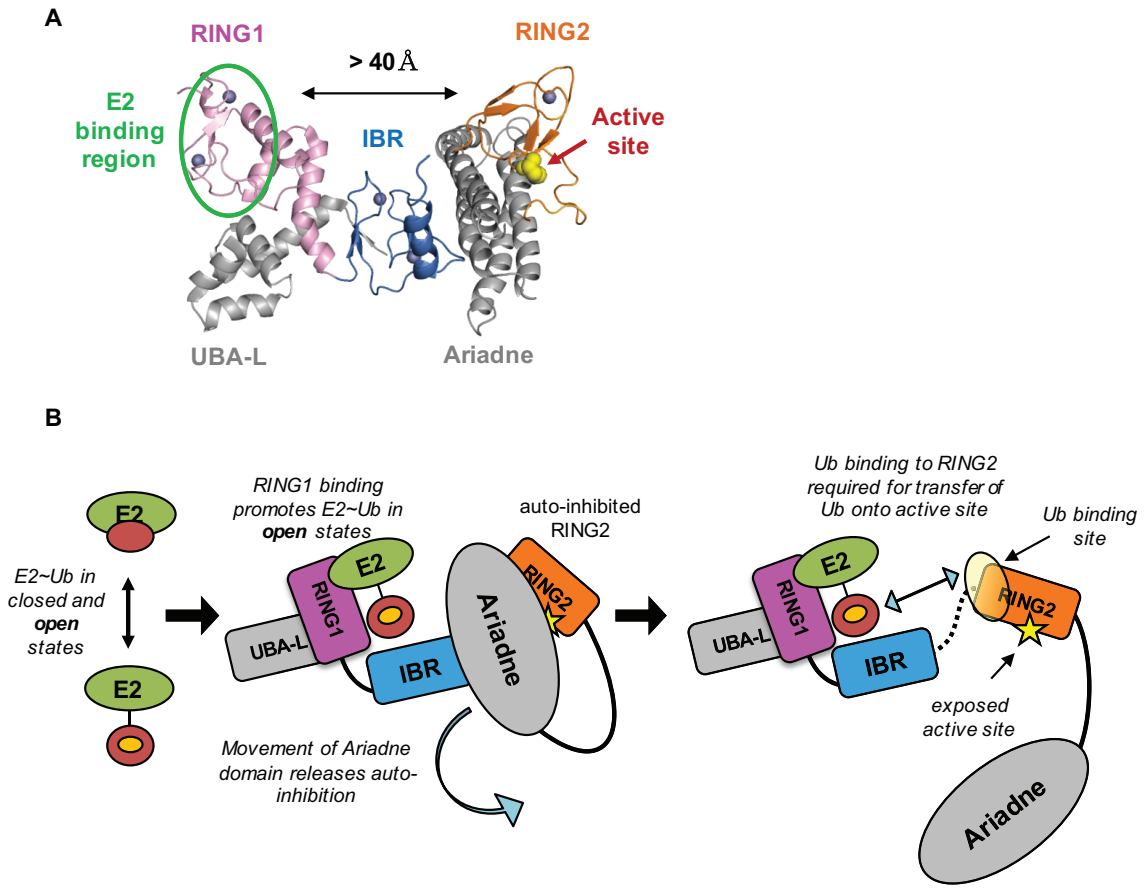

Figure 7. Model of RBR E3 Ub transfer mechanisms. a) Auto-inhibited HHARI structure is shown in cartoon representation (PDB 4KC9). The E2-binding site (green oval) on RING1 (pink) is separated from the active site Cys (yellow spheres) on RING2 (orange) by more than 40 Å. The IBR domain (dark blue) connects RING1 and RING2 and the Ariadne domain (grey) occludes the active site Cys. b) A model depicts the events required for Ub transfer by HHARI (with no intended order). E2~Ub binding to RING1 favors open E2~Ub conformations (middle panel) that expose the Ub hydrophobic patch (orange circle). Movement of the Ariadne domain (middle panel) exposes the active site Cys (right panel, yellow star) and may allow a disorder-to-helix transition of the IBR-RING2 linker (dotted black line in right panel, not seen in structure in A) which completes the Ub binding site on RING2 (yellow sphere, right panel). Open E2~Ub conformations make the hydrophobic patch of Ub (orange circle) available for recruitment by RING2 to ensure transfer of Ub to the active cite Cys.

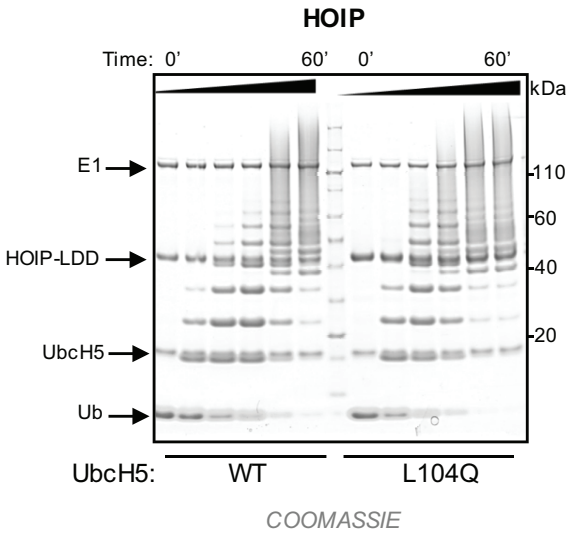

Figure EV1. HOIP does not require closed states of E2~Ub for linear chain formation.
Linear Ub chain building reactions were performed using $HOIP_{RBR\text{-}LDD}$ and either $UbcH5^{WT}$ or $UbcH5^{L104Q}$. Product formation (free linear Ub chains) was visualized by Coomassie-blue staining.

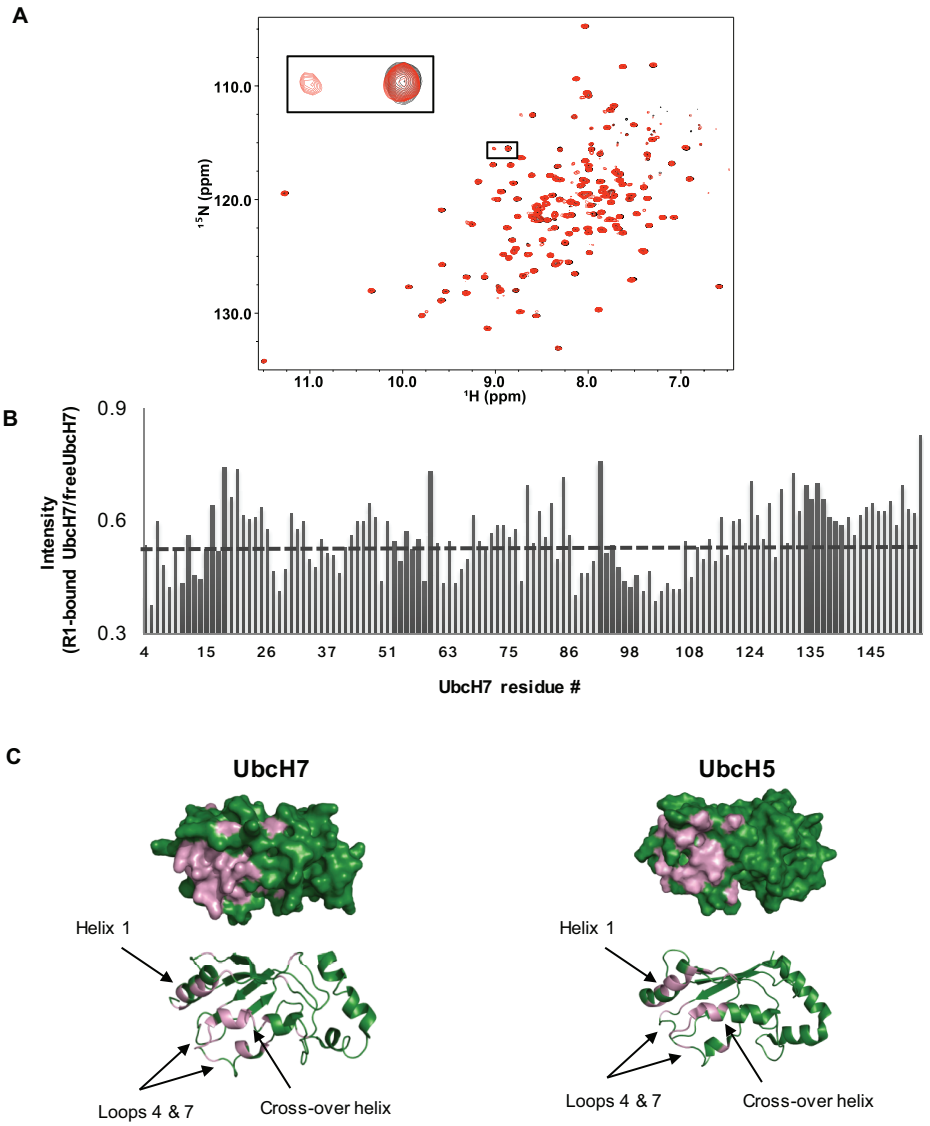

Figure EV2. NMR mapping of HHARI RING1 binding to UbcH7. a) Spectral overlay of ^{15}N-UbcH7 in the absence (black) and presence (red) of 0.5 mol equiv. HHARI RING1. Affected resonances show peak doubling, characteristic of a high-affinity complex, where a new set of resonances that correspond to resonances from the complex appear simultaneously with resonances of the unbound species. b) Histogram displays the ratio of peak intensity of UbcH7 residues (bound/free) measured from the spectra shown above. The average intensity ratio is indicated with a grey dashed line. c) *LEFT.* Surface (top) and cartoon (bottom) representation of UbcH7 (pdb 1fbv). Residues that exhibit loss of intensity > 1 stdv from the average upon RING1 binding (intensity < 0.448) are colored in pink (residues 6, 11, 13, 14, 28, 40, 57, 61, 64, 78, 87, 89, 90, 96, 98-100, 102-106, 108). *RIGHT.* For comparison, UbcH5 residues that are perturbed (either CSP or intensity loss) upon RING1 binding are indicated in pink (CSPs: > 0.028ppm and intensity <0. 44)

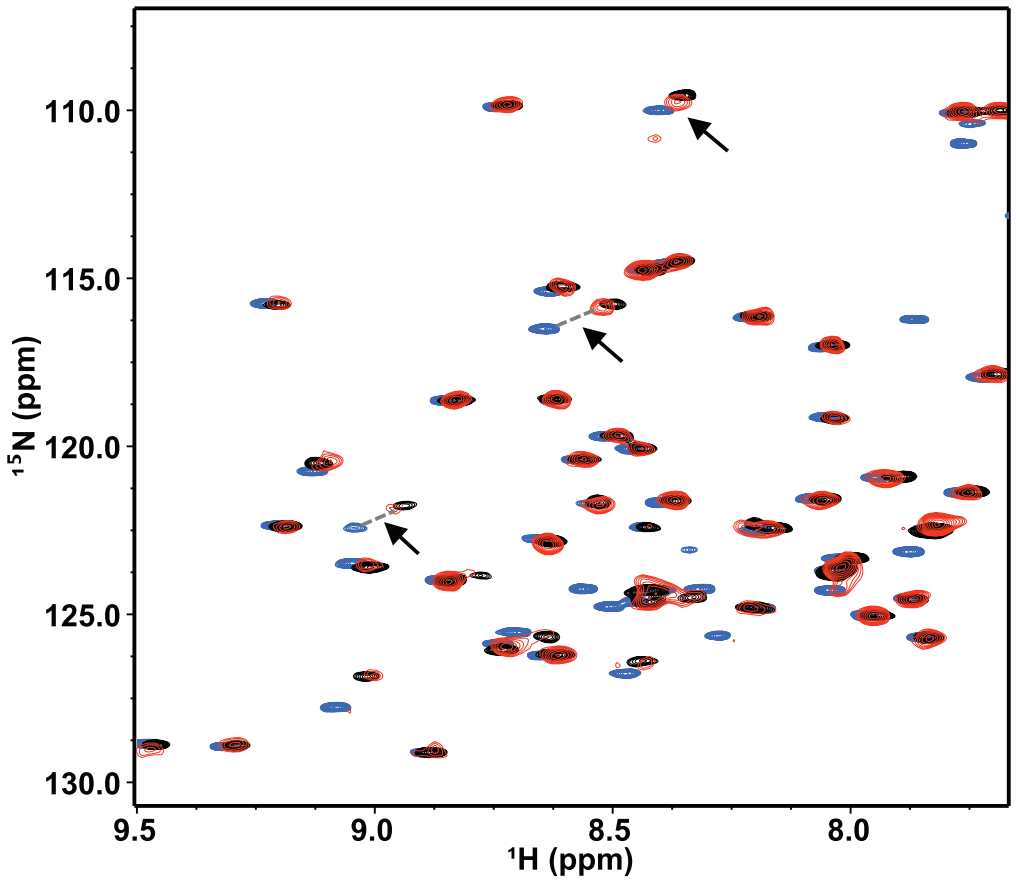

Figure EV3. HHARI RING1 disruption of (E3-independent) closed E2~Ub conformations. a) Similar to UbcH7, Ubc13~Ub populates closed states in the absence of an E3 [35]. Shown here are three ^{1}H-^{15}N-HSQC TROSY spectra of Ub overlaid: free ^{15}N-Ub (blue), Ubc13-O-^{15}N-Ub (black), and Ubc13-O-^{15}N-Ub in the presence of 3 mol equiv. HHARI RING1 (red). Due to the weak affinity binding of Ubc13 to HHARI RING1, the complex is far from saturation and the spectrum exhibits fast-to-intermediate exchange behavior. Therefore, the observed CSPs for the effects of RING1 binding to Ubc13-O-^{15}N-Ub are quite small (black versus red). Black arrows highlight several Ub resonances that shift along the same trajectory (but opposite direction) upon binding HHARI RING1 as experienced when Ub is conjugated to Ubc13, consistent with Ubc13~Ub populating more open-like states when in complex with HHARI RING1.

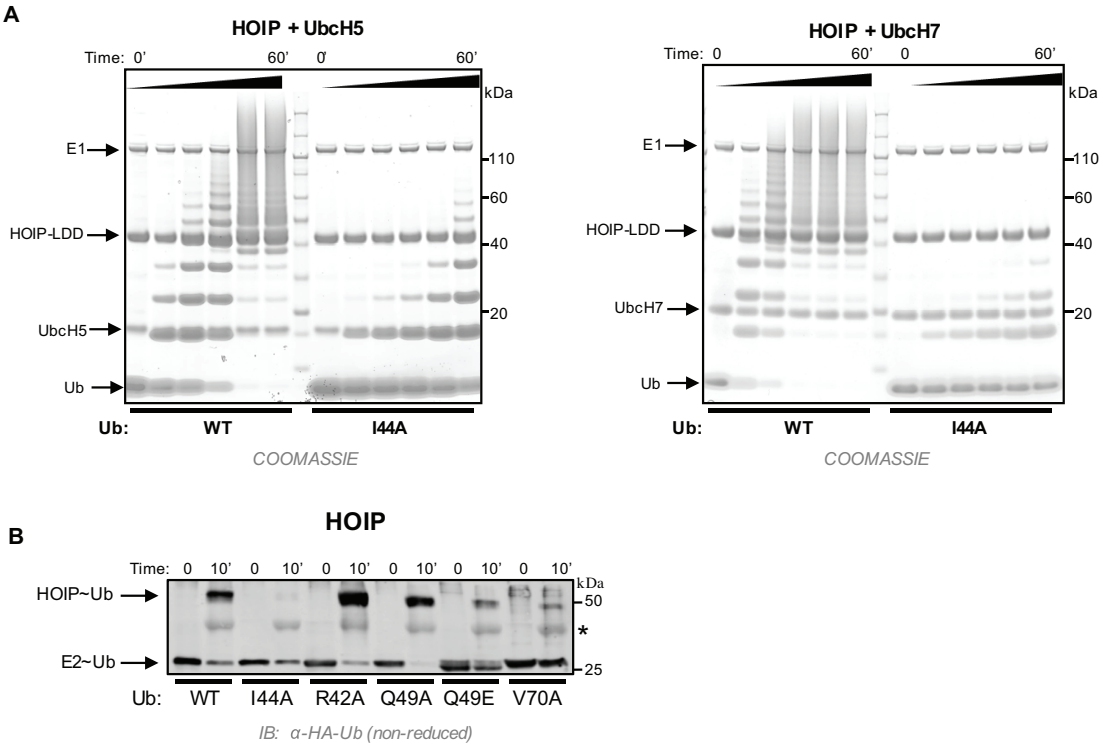

Figure EV4. Ub hydrophobic patch involvement in linear chain building by the RBR E3 HOIP. a) Time courses of linear-chain-building assays using $HOIP_{RBR\text{-}LDD}$ and either UbcH5 (left) or UbcH7 (right) conjugated with WT-Ub or I44A-Ub as followed by Coomassie-stained gels. The I44A mutation in the donor Ub does not impair the formation of di-Ub (Smit et al, 2012), yet I44A-Ub significantly reduces linear chain building ability by $HOIP_{RBR\text{-}LDD}$. b) UbcH7 was pre-conjugated with either WT- or mutant-Ub (as indicated) and the reaction was quenched with apyrase. Each UbcH7~Ub species was incubated with H887A-$HOIP_{RBR\text{-}LDD}$ to enable detection of the E3~Ub intermediate (Stieglitz et al, 2013). Samples were analyzed on SDS-page under non-reducing conditions and subsequently visualized by western blotting for the HA-tag on Ub. Time was recorded post addition of H887A-$HOIP_{RBR\text{-}LDD}$. Note: The HA-antibody cross-reacts with free HOIP (see *).

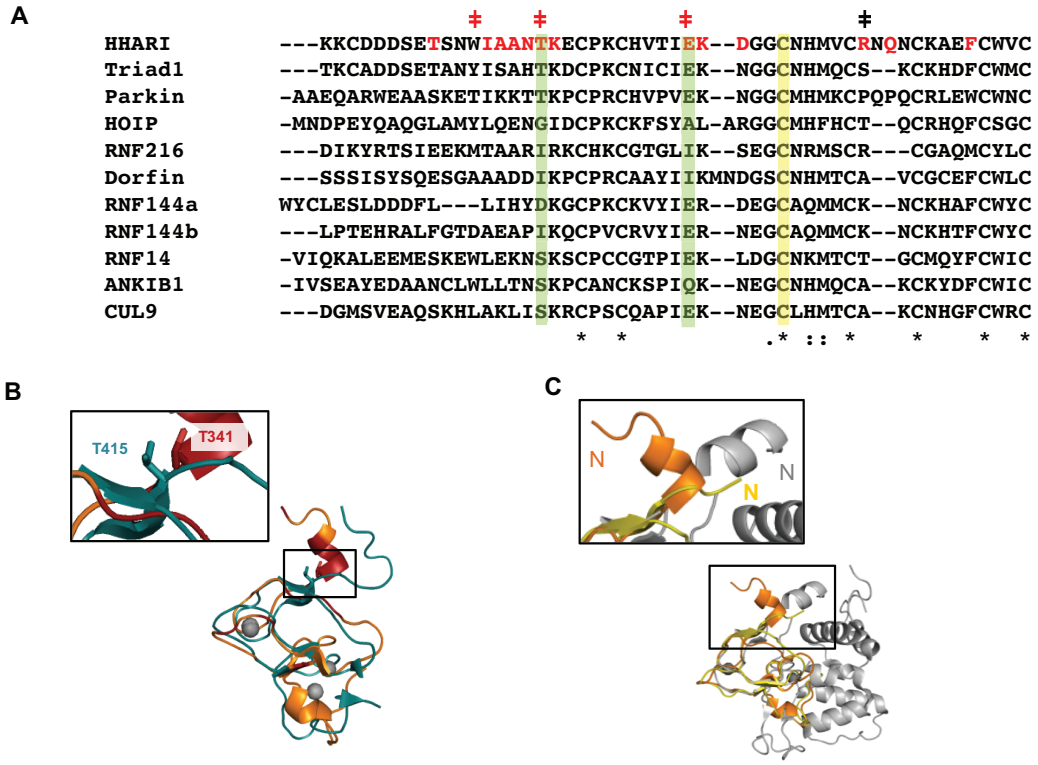

Figure EV5. Comparison of RBR RING2 domains. a) RING2 sequence alignments were generated using CLUSTAL OMEGA. Residues observed to be perturbed upon Ub binding to HHARI RING2 in NMR titration experiments are highlighted in red. HHARI residues that were mutated and tested for change in activity are marked with a (ǂ) with red indicating decreased and black indicating no observable change in activity (see Fig 6C). Green bars highlight residues that are important for Ub binding of HHARI RING2 that are well conserved among RBR RING2s. The active site Cys is marked with a yellow bar. 7th and 8th Zn^{2+}coordinating residues are not shown. b) Structural overlay of NMR solution structures of Parkin (teal, PDB 2lwr) and HHARI (orange, PDB 2m9y) RING2 domains. RING2 residues perturbed upon Ub binding (Fig 6A) are colored dark red on HHARI RING2. The HHARI RING2 mutations T341N abrogates Ub binding and decreases ligase activity (Fig 6D&E). *INSET*. The analogous mutation in Parkin, T415N, has been linked to early-onset Parkinson's disease (Abbas et al, 1999). c) Structural overlay of three RING2 domains: a HHARI NMR solution structure (orange, PDB 2m9y), a HHARI crystal structure (yellow, PDB 4kc9) and a HOIP crystal structure (grey, PDB 4ljq). An enlargement of the N-terminal region that is part of the IBR-RING2 linker shows a helical disposition of the linker in the HOIP and HHARI NMR, but not in the HHARI crystal structure.

	Name used in manuscript	Residues	species	tags	Figure where construct was used
Canonical RINGs Constructs	BRCA1/BARD1	1-304/25-327	human	N-terminal Flag-tag on BRCA1	Fig 1A
	BRCA1/BARD1	1-100/26-140	human	none	Fig 3C
	E4BU	1142-1173	mouse	none	Appendix Fig S4
HHARI Constructs	$HHARI_{RBR}$	177-395	human	N-terminal GST-tag	Fig 1A, Fig 4B, Fig 5A&E, Fig 6C
	HHARI RING1	177-270	human	none	Fig 1B, Fig 3, Fig EV2A, Appendix Fig S3&5, Fig EV3
	HHARI RING2	325-396	human	none	Fig 6A&E
	HHARI RING2-ΔL	336-396	human	none	Fig 6A
Other RBR Constructs	$HOIP_{RBR\text{-}LDD}$	697-1072	human	none	Fig 5D, Fig EV4
	RNF144 RING1	2-108	human	none	Fig 3C
	$Parkin_{RBR}$	217-465	rat	N-terminal GST-tag	Fig 1A, Fig 4B, Fig 5A&C
	$Triad1_{\Delta ARI}$	1-348	human	N-terminal His-T7-tag	Fig 1A
Hybrid construct	UBR-hybrid	1142-1173 (E4BU)	mouse	N-terminal GST-tag	Fig 4
		271-396 (HHARI)	human		

Appendix Table S1. Constructs of all RBR E3 ligases used in this study.

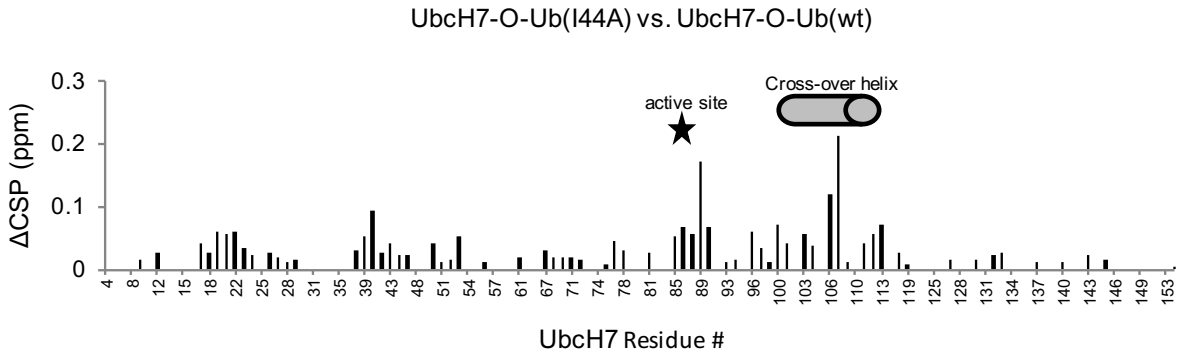

Appendix Figure S1. I44A-Ub disrupts UbcH7~Ub closed conformations. Histogram of CSPs between ^{15}N-UbcH7-O-Ub-I44A and ^{15}N-UbcH7-O-Ub-WT. Residues that are initially perturbed upon Ub conjugation to UbcH7 (Fig 2A) are *less* perturbed by conjugation of I44A-Ub to UbcH7 (Fig 2B). As a consequence, the histogram (above) displaying CSPs for ^{5}N-UbcH7-O-Ub-I44A vs. ^{15}N-UbcH7-O-Ub-WT highlights UbcH7 residues that are involved in the formation of closed conformations. The active site serine residue is indicated with a star and cross-over helix residues (101-113) are marked with a gray cylinder.

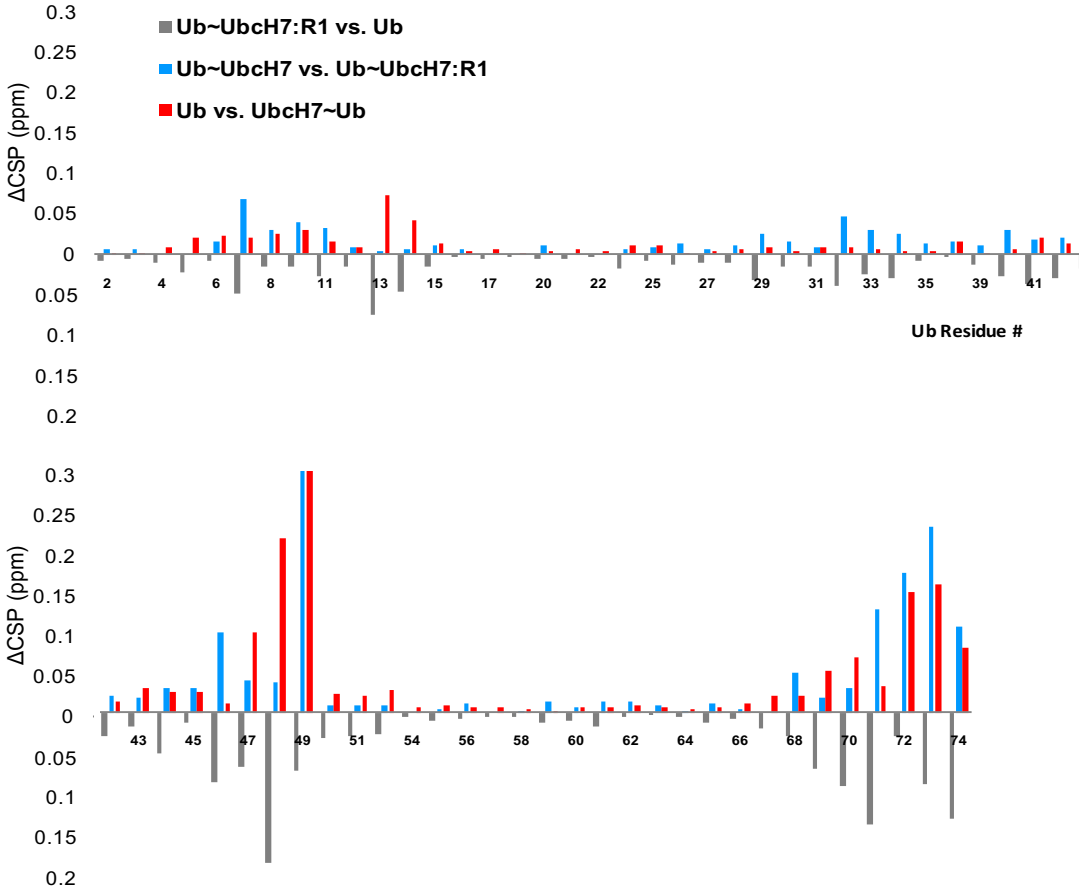

Appendix Figure S2. HHARI RING1 disrupts closed UbcH7~Ub conformations. The histogram shown summarizes comparisons of the three NMR spectra shown in Fig3: free ^{15}N-Ub, UbcH7-O-^{15}N-Ub, and HHARI RING1-bound UbcH7-O-^{15}N-Ub. CSPs that Ub residues undergo upon conjugation to UbcH7 are shown as red bars. These CSPs are characteristic of formation of closed UbcH7-O-Ub formations. CSPs that Ub residues undergo when HHARI RING1 binds to UbcH7-O-Ub are shown as blue bars. Most, though not all, Ub residues that shift upon conjugation (red bars) also shift upon RING1 binding (blue bars), consistent with disruption of closed UbcH7-O-Ub by RING1 binding. The grey bars (inverted for readability) compare resonance positions in free Ub to Ub in the context of HHARI RING1-bound UbcH7-O-Ub.

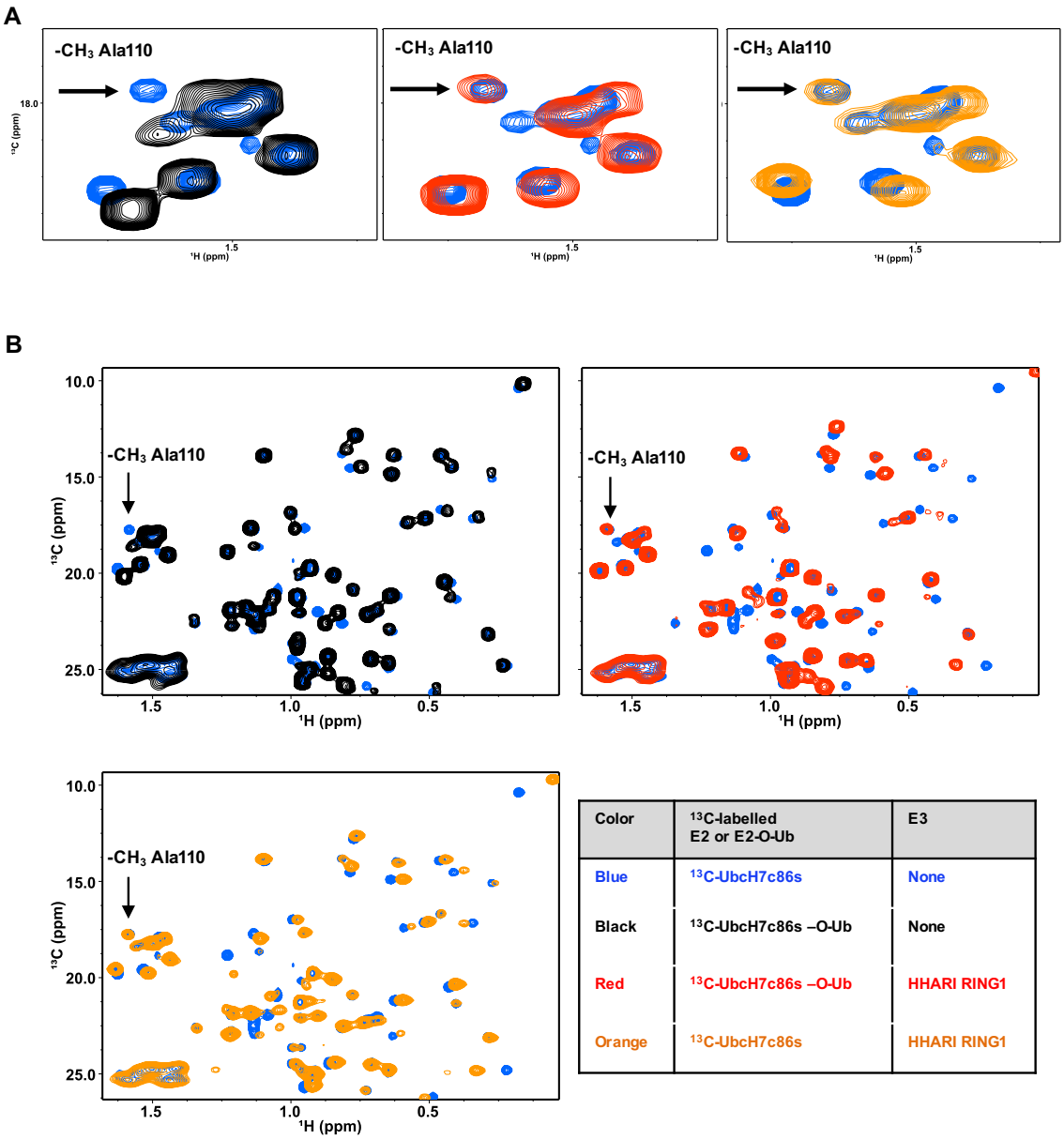

Appendix Figure S3. HHARI RING1 disrupts closed UbcH7~Ub conformations. a) Regions of ^{1}H-^{13}C-HSQC spectral overlays that contain sidechain methyl resonance of Ala110 are shown: free ^{13}C-UbcH7 (black), ^{13}C-UbcH7-O-Ub (red), HHARI RING1-bound ^{13}C-UbcH7-O-Ub (orange), and HHARI RING1-bound ^{13}C-UbcH7 (blue) are shown. The methyl resonance of cross-over residue Ala 110 (red arrow) shifts to an unknown position when Ub is conjugated to UbcH7 (red spectrum), indicating Ub interacts with the sidechain of Ala110. The peak reappears in its original position when HHARI RING1 binds to UbcH7-O-Ub (orange spectrum), consistent with disruption of closed UbcH7~Ub conformations in the complex. The Ala110 resonance is not perturbed when unconjugated UbcH7 binds to HHARI RING1 (blue spectrum), showing that that effect observed is due specifically to the presence of conjugated Ub and not to RING1 directly. b) Full methyl resonance-containing region of spectra shown in a) are provided.

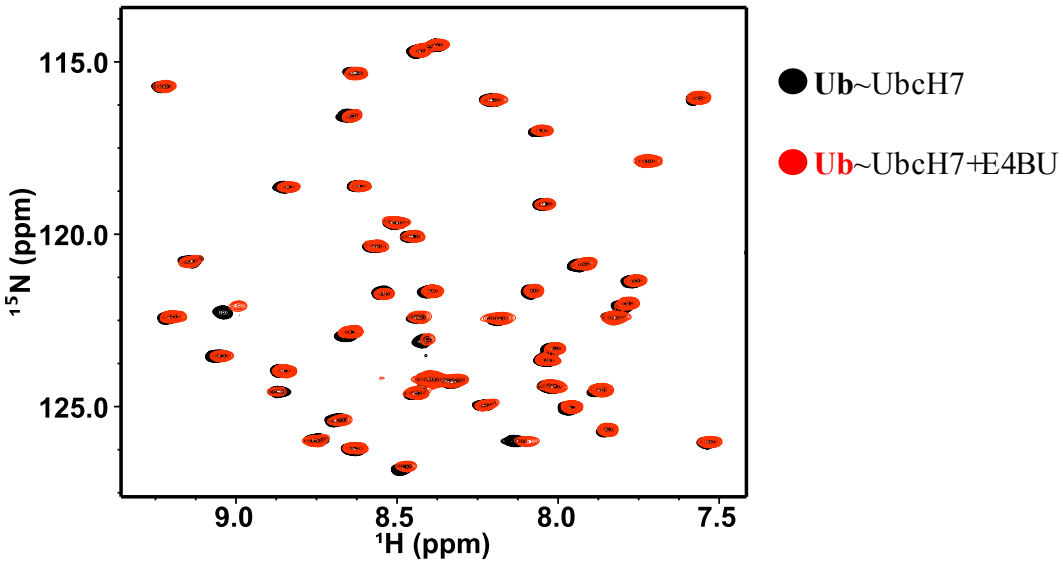

Appendix Figure S4. E4BU Ubox binding does not disrupt closed UbcH7~Ub conformations. ^{1}H-^{15}N-HSQC-TROSY spectra of UbcH7-O-^{15}N-Ub in the absence (black) and presence (red) of 3 mol equiv. Ubox domain of E4BU. Similar to BRCA1/BARD1 binding, E4BU has little effect on the Ub spectrum while HHARI RING1 and RNF144 RING1 significantly perturb Ub resonances upon binding to UbcH7-O-^{15}N-Ub (Fig 3c). Together these data demonstrate that RBR RING1s, but not canonical RING-type E3s disrupt closed UbcH7~Ub conformations.

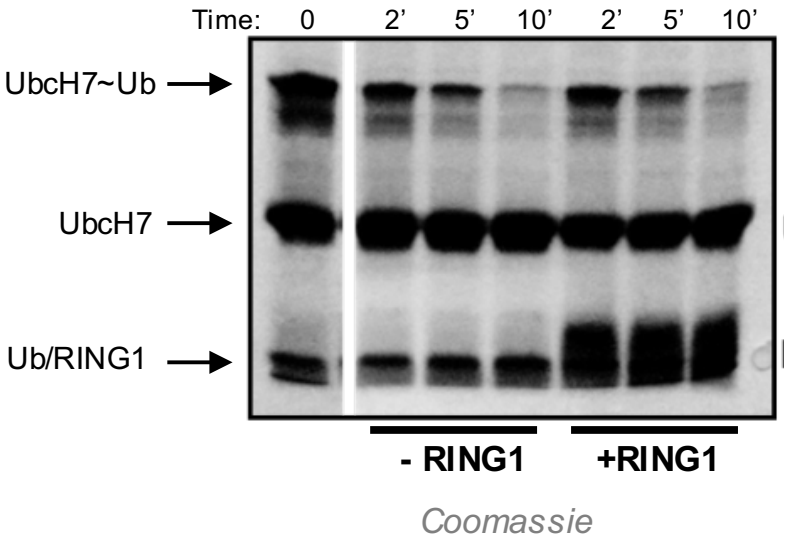

Appendix Figure S5. HHARI RING1 does not increase Cys reactivity of UbcH7~Ub. Cys reactivity assays of UbcH7~Ub were performed in the absence (left) or presence of excess HHARI RING1 (right). Reactions were quenched upon the addition of non-reducing SDS-page load dye. The zero min time point was taken immediately before addition of free Cys. The reaction timecourse shows the disappearance of the conjugate following addition of Cys, monitored by Coomassie-stained SDS-PAGE.

References

1. Pruneda JN, Littlefield PJ, Soss SE, Nordquist KA, Chazin WJ, Brzovic PS, Klevit RE (2012) Structure of an E3:E2~Ub complex reveals an allosteric mechanism shared among RING/U-box ligases. Molecular cell 47: 933-42

2. Dou H, Buetow L, Sibbet GJ, Cameron K, Huang DT (2012) BIRC7-E2 ubiquitin conjugate structure reveals the mechanism of ubiquitin transfer by a RING dimer. Nature structural & molecular biology 19: 876-83

3. Plechanovova A, Jaffray EG, Tatham MH, Naismith JH, Hay RT (2012) Structure of a RING E3 ligase and ubiquitin-loaded E2 primed for catalysis. Nature 489: 115-20

4. Branigan E, Plechanovova A, Jaffray EG, Naismith JH, Hay RT (2015) Structural basis for the RING-catalyzed synthesis of K63-linked ubiquitin chains. Nature structural & molecular biology 22: 597-602

5. Saha A, Lewis S, Kleiger G, Kuhlman B, Deshaies RJ (2011) Essential role for ubiquitin-ubiquitin-conjugating enzyme interaction in ubiquitin discharge from Cdc34 to substrate. Molecular cell 42: 75-83

6. Wenzel DM, Lissounov A, Brzovic PS, Klevit RE (2011) UBCH7 reactivity profile reveals parkin and HHARI to be RING/HECT hybrids. Nature 474: 105-8

7. Kamadurai HB, Souphron J, Scott DC, Duda DM, Miller DJ, Stringer D, Piper RC, Schulman BA (2009) Insights into ubiquitin transfer cascades from a structure of a UbcH5B approximately ubiquitin-HECT(NEDD4L) complex. Molecular cell 36: 1095-102

8. Stieglitz B, Morris-Davies AC, Koliopoulos MG, Christodoulou E, Rittinger K (2012) LUBAC synthesizes linear ubiquitin chains via a thioester intermediate. EMBO reports 13: 840-6

9. Smit JJ, Monteferrario D, Noordermeer SM, van Dijk WJ, van der Reijden BA, Sixma TK (2012) The E3 ligase HOIP specifies linear ubiquitin chain assembly through its RING-IBR-RING domain and the unique LDD extension. The EMBO journal 31: 3833-44

10. Kelsall IR, Duda DM, Olszewski JL, Hofmann K, Knebel A, Langevin F, Wood N, Wightman M, Schulman BA, Alpi AF (2013) TRIAD1 and HHARI bind to and are activated by distinct neddylated Cullin-RING ligase complexes. The EMBO journal 32: 2848-60

11. Ho SR, Mahanic CS, Lee YJ, Lin WC (2014) RNF144A, an E3 ubiquitin ligase for DNA-PKcs, promotes apoptosis during DNA damage. Proceedings of the National Academy of Sciences of the United States of America 111: E2646-55

12. Kitada T, Asakawa S, Hattori N, Matsumine H, Yamamura Y, Minoshima S, Yokochi M, Mizuno Y, Shimizu N (1998) Mutations in the parkin gene cause autosomal recessive juvenile parkinsonism. Nature 392: 605-8

13. Matsumine H, Saito M, Shimoda-Matsubayashi S, Tanaka H, Ishikawa A, Nakagawa-Hattori Y, Yokochi M, Kobayashi T, Igarashi S, Takano H, et al. (1997) Localization of a gene for an autosomal recessive form of juvenile Parkinsonism to chromosome 6q25.2-27. American journal of human genetics 60: 588-96

14. Ikeda F, Deribe YL, Skanland SS, Stieglitz B, Grabbe C, Franz-Wachtel M, van Wijk SJ, Goswami P, Nagy V, Terzic J, et al. (2011) SHARPIN forms a linear ubiquitin ligase complex regulating NF-kappaB activity and apoptosis. Nature 471: 637-41

15. Kirisako T, Kamei K, Murata S, Kato M, Fukumoto H, Kanie M, Sano S, Tokunaga F, Tanaka K, Iwai K (2006) A ubiquitin ligase complex assembles linear polyubiquitin chains. The EMBO journal 25: 4877-87

16. Gerlach B, Cordier SM, Schmukle AC, Emmerich CH, Rieser E, Haas TL, Webb AI, Rickard JA, Anderton H, Wong WW, et al. (2011) Linear ubiquitination prevents inflammation and regulates immune signalling. Nature 471: 591-6

17. Tokunaga F, Nakagawa T, Nakahara M, Saeki Y, Taniguchi M, Sakata S, Tanaka K, Nakano H, Iwai K (2011) SHARPIN is a component of the NF-kappaB-activating linear ubiquitin chain assembly complex. Nature 471: 633-6

18. Aguilera M, Oliveros M, Martinez-Padron M, Barbas JA, Ferrus A (2000) Ariadne-1: a vital Drosophila gene is required in development and defines a new conserved family of ring-finger proteins. Genetics 155: 1231-44

19. Tan NG, Ardley HC, Scott GB, Rose SA, Markham AF, Robinson PA (2003) Human homologue of ariadne promotes the ubiquitylation of translation initiation factor 4E homologous protein, 4EHP. FEBS letters 554: 501-4

20. Qiu X, Fay DS (2006) ARI-1, an RBR family ubiquitin-ligase, functions with UBC-18 to regulate pharyngeal development in C. elegans. Developmental biology 291: 239-52

21. Elmehdawi F, Wheway G, Szymanska K, Adams M, High AS, Johnson CA, Robinson PA (2013) Human Homolog of Drosophila Ariadne (HHARI) is a marker of cellular proliferation associated with nuclear bodies. Experimental cell research 319: 161-72

22. Lazarou M, Narendra DP, Jin SM, Tekle E, Banerjee S, Youle RJ (2013) PINK1 drives Parkin self-association and HECT-like E3 activity upstream of mitochondrial binding. The Journal of cell biology 200: 163-72

23. Zheng X, Hunter T (2013) Parkin mitochondrial translocation is achieved through a novel catalytic activity coupled mechanism. Cell research 23: 886-97

24. Mani K, Fay DS (2009) A mechanistic basis for the coordinated regulation of pharyngeal morphogenesis in Caenorhabditis elegans by LIN-35/Rb and UBC-18-ARI-1. PLoS genetics 5: e1000510

25. Fiesel FC, Moussaud-Lamodiere EL, Ando M, Springer W (2014) A specific subset of E2 ubiquitin-conjugating enzymes regulate Parkin activation and mitophagy differently. Journal of cell science 127: 3488-504

26. Lim GG, Chew KC, Ng XH, Henry-Basil A, Sim RW, Tan JM, Chai C, Lim KL (2013) Proteasome inhibition promotes Parkin-Ubc13 interaction and lysine 63-linked ubiquitination. PloS one 8: e73235

27. Zhang Y, Gao J, Chung KK, Huang H, Dawson VL, Dawson TM (2000) Parkin functions as an E2-dependent ubiquitin- protein ligase and promotes the degradation of the synaptic vesicle-associated protein, CDCrel-1. Proceedings of the National Academy of Sciences of the United States of America 97: 13354-9

28. Haddad DM, Vilain S, Vos M, Esposito G, Matta S, Kalscheuer VM, Craessaerts K, Leyssen M, Nascimento RM, Vianna-Morgante AM, et al. (2013) Mutations in the intellectual disability gene Ube2a cause neuronal dysfunction and impair parkin-dependent mitophagy. Molecular cell 50: 831-43

29. Duda DM, Olszewski JL, Schuermann JP, Kurinov I, Miller DJ, Nourse A, Alpi AF, Schulman BA (2013) Structure of HHARI, a RING-IBR-RING ubiquitin ligase: autoinhibition of an Ariadne-family E3 and insights into ligation mechanism. Structure 21: 1030-41

30. Riley BE, Lougheed JC, Callaway K, Velasquez M, Brecht E, Nguyen L, Shaler T, Walker D, Yang Y, Regnstrom K, et al. (2013) Structure and function of Parkin E3 ubiquitin ligase reveals aspects of RING and HECT ligases. Nature communications 4: 1982

31. Trempe JF, Sauve V, Grenier K, Seirafi M, Tang MY, Menade M, Al-Abdul-Wahid S, Krett J, Wong K, Kozlov G, et al. (2013) Structure of parkin reveals mechanisms for ubiquitin ligase activation. Science 340: 1451-5

32. Wauer T, Komander D (2013) Structure of the human Parkin ligase domain in an autoinhibited state. The EMBO journal 32: 2099-112

33. Kumar A, Aguirre JD, Condos TE, Martinez-Torres RJ, Chaugule VK, Toth R, Sundaramoorthy R, Mercier P, Knebel A, Spratt DE, et al. (2015) Disruption of the autoinhibited state primes the E3 ligase parkin for activation and catalysis. The EMBO journal 34: 2506-21

34. Sauve V, Lilov A, Seirafi M, Vranas M, Rasool S, Kozlov G, Sprules T, Wang J, Trempe JF, Gehring K (2015) A Ubl/ubiquitin switch in the activation of Parkin. The EMBO journal 34: 2492-505

35. Pruneda JN, Stoll KE, Bolton LJ, Brzovic PS, Klevit RE (2011) Ubiquitin in motion: structural studies of the ubiquitin-conjugating enzyme approximately ubiquitin conjugate. Biochemistry 50: 1624-33

36. Brzovic PS, Keeffe JR, Nishikawa H, Miyamoto K, Fox D, 3rd, Fukuda M, Ohta T, Klevit R (2003) Binding and recognition in the assembly of an active BRCA1/BARD1 ubiquitin-ligase complex. Proceedings of the National Academy of Sciences of the United States of America 100: 5646-51

37. DaRosa PA, Wang Z, Jiang X, Pruneda JN, Cong F, Klevit RE, Xu W (2015) Allosteric activation of the RNF146 ubiquitin ligase by a poly(ADP-ribosyl)ation signal. Nature 517: 223-6

38. Xu Z, Kohli E, Devlin KI, Bold M, Nix JC, Misra S (2008) Interactions between the quality control ubiquitin ligase CHIP and ubiquitin conjugating enzymes. BMC structural biology 8: 26

39. Serniwka SA, Shaw GS (2008) 1H, 13C and 15N resonance assignments for the human E2 conjugating enzyme, UbcH7. Biomolecular NMR assignments 2: 21-3

40. Chaugule VK, Burchell L, Barber KR, Sidhu A, Leslie SJ, Shaw GS, Walden H (2011) Autoregulation of Parkin activity through its ubiquitin-like domain. The EMBO journal 30: 2853-67

41. Stieglitz B, Rana RR, Koliopoulos MG, Morris-Davies AC, Schaeffer V, Christodoulou E, Howell S, Brown NR, Dikic I, Rittinger K (2013) Structural basis for ligase-specific conjugation of linear ubiquitin chains by HOIP. Nature 503: 422-6

42. Capili AD, Edghill EL, Wu K, Borden KL (2004) Structure of the C-terminal RING finger from a RING-IBR-RING/TRIAD motif reveals a novel zinc-binding domain distinct from a RING. Journal of molecular biology 340: 1117-29

43. Spratt DE, Martinez-Torres RJ, Noh YJ, Mercier P, Manczyk N, Barber KR, Aguirre JD, Burchell L, Purkiss A, Walden H, et al. (2013) A molecular explanation for the recessive nature of parkin-linked Parkinson's disease. Nature communications 4: 1983

44. Rankin CA, Galeva NA, Bae K, Ahmad MN, Witte TM, Richter ML (2014) Isolated RING2 domain of parkin is sufficient for E2-dependent E3 ligase activity. Biochemistry 53: 225-34

45. Spratt DE, Mercier P, Shaw GS (2013) Structure of the HHARI catalytic domain shows glimpses of a HECT E3 ligase. PloS one 8: e74047

46. Beasley SA, Hristova VA, Shaw GS (2007) Structure of the Parkin in-between-ring domain provides insights for E3-ligase dysfunction in autosomal recessive Parkinson's disease. Proceedings of the National Academy of Sciences of the United States of America 104: 3095-100

47. Stewart MD, Ritterhoff T, Klevit RE, Brzovic PS (2016) E2 enzymes: more than just middle men. Cell research 26: 423-40

48. Lechtenberg BC, Rajput A, Sanishvili R, Dobaczewska MK, Ware CF, Mace PD, Riedl SJ (2016) Structure of a HOIP/E2~ubiquitin complex reveals RBR E3 ligase mechanism and regulation. Nature 529: 546-50

49. Abbas N, Lucking CB, Ricard S, Durr A, Bonifati V, De Michele G, Bouley S, Vaughan JR, Gasser T, Marconi R, et al. (1999) A wide variety of mutations in the parkin gene are responsible for autosomal recessive parkinsonism in Europe. French Parkinson's Disease Genetics Study Group and the European Consortium on Genetic Susceptibility in Parkinson's Disease. Human molecular genetics 8: 567-74

50. Matsuda N, Kitami T, Suzuki T, Mizuno Y, Hattori N, Tanaka K (2006) Diverse effects of pathogenic mutations of Parkin that catalyze multiple monoubiquitylation in vitro. The Journal of biological chemistry 281: 3204-9

51. Sriram SR, Li X, Ko HS, Chung KK, Wong E, Lim KL, Dawson VL, Dawson TM (2005) Familial-associated mutations differentially disrupt the solubility, localization, binding and ubiquitination properties of parkin. Human molecular genetics 14: 2571-86

52. Wauer T, Simicek M, Schubert A, Komander D (2015) Mechanism of phospho-ubiquitin-induced PARKIN activation. Nature 524: 370-4

53. Nordquist KA, Dimitrova YN, Brzovic PS, Ridenour WB, Munro KA, Soss SE, Caprioli RM, Klevit RE, Chazin WJ (2010) Structural and functional characterization of the monomeric U-box domain from E4B. Biochemistry 49: 347-55

54. Delaglio F, Grzesiek S, Vuister GW, Zhu G, Pfeifer J, Bax A (1995) NMRPipe: a multidimensional spectral processing system based on UNIX pipes. Journal of biomolecular NMR 6: 277-93

55. Johnson BA, Blevins RA (1994) NMR View: A computer program for the visualization and analysis of NMR data. Journal of biomolecular NMR 4: 603-14

Chapter III: Structural studies of the HHARI/UbcH7~Ub reveal unique RBR RING1 elements

The following manuscript is currently under review by the journal ***Structure***.

Katja K. Dove[1], Jennifer L. Olszewski[2], Luigi Martino[4], David M. Duda[2,3,] Xiaoli S. Wu[1], Darcie J. Miller[2], Katrin Rittinger[4], Brenda A. Schulman[*2,3], Rachel E. Klevit[*1]

[1]Department of Biochemistry, University of Washington, Seattle, Washington, USA.

[2] Department of Structural Biology, St. Jude Children's Research Hospital, Memphis, TN, USA

[3]Howard Hughes Medical Institute, St. Jude Children's Research Hospital, Memphis, TN, USA

[4]The Francis Crick Institute, 1 Midland Road, London NW1 1AT, UK.

* Corresponding authors; email: klevit@uw.edu and Brenda.Schulman@stjude.org

Author contributions

K.K.D., K.R., M.L., D.M.D., J.L.O., B.A.S and R.E.K. conceived the experiments and/or wrote the manuscript. K.K.D. performed the NMR. K.K.D and X.S.W. ran auto-ubiquitination assays. M. L. collected all ITC measurements. D.M.D., J.L.O., and D.J.M. generated the isopeptide-linked UbcH7~Ub-HHARI complex and performed the crystallography experiments.

Introduction

Post-translational modification of substrate with ubiquitin (Ub) requires the coordination of two types of enzymes: Ub-conjugating enzymes (E2s) and Ub ligases (E3s). While E3s are generally thought to bind substrates, substrate ubiquitination can be performed by either an E2 or an E3, depending on the type of E3 ligase. The large family of RING (Really Interesting New Gene)-type E3s (including U-box E3s) bind a substrate and an E2~Ub simultaneously, but Ub transfer occurs from the E2 *directly* onto the substrate. As a result, the E2 determines the type of Ub modification for a given substrate (Christensen et al., 2007; Kim et al., 2007; Rodrigo-Brenni and Morgan, 2007). In contrast, substrate ubiquitination by HECT (Homologous to E6AP C-Terminus)-type E3s and by RING-in-between-RING (RBR) E3s is performed in two steps. First, the E3 binds a cognate E2~Ub as a prelude to forming an obligatory E3~Ub thioester intermediate. Second, Ub is transferred to from the E3 to the substrate. Therefore, for HECTs and RBRs it is the E3 that dictates the type of Ub modification independent of the E2 (Kim and Huibregtse, 2009; Kim et al., 2007; Wang et al., 2006; Wang and Pickart, 2005).

RBR E3s share structural features with RING-type E3s in that they contain an E2-binding RING domain (called "RING1" in RBRs) (Wenzel et al., 2011). Structures of RBR RING1 domains from Parkin, HHARI, HOIP, and RNF144 confirm that they are highly similar in structure to canonical RINGs (Fig. 1A) (Duda et al., 2013; Lechtenberg et al., 2016; Miyamoto, 2004; Riley et al., 2013; Trempe et al., 2013; Wauer and Komander, 2013). However, there is growing evidence that canonical RINGs and RBR RING1s are mechanistically distinct. Specifically, canonical RINGs promote *closed* conformations of E2~Ubs that are required for direct transfer of Ub from the E2 to substrate, while RBR RING1s promote *open* E2~Ub that

may be a feature of functioning with a thioester-forming E3 (Dou et al., 2012; Dove et al., 2016; Plechanovova et al., 2012; Pruneda et al., 2012).

Consistent with a two-step mechanism, RBR E3s display mechanistic parallels to HECT type-E3s, with a distinct active-site-containing domain, although the catalytic "RING2" domain in RBRs lacks structural homology with the catalytic C-lobe domain in HECT E3s. In the structure of a HECT domain/E2~Ub complex, the conjugate is in an open conformation with the E2 contacting the HECT N-lobe and Ub contacting the HECT C-lobe (Kamadurai et al., 2009). Interestingly, a structure representing an active E2~Ub-RBR species of the RBR E3 HOIP likewise showed extensive contacts between the donor Ub and the catalytic RING2 domain.

Despite progress in understanding how RING, HECT, and RBR E3s form catalytic complexes with E2~Ub intermediates, existing structures have not explained how isolated RING1 domains from RBRs are sufficient to disrupt closed states of E2~Ubs without any detectable contact with Ub, as evidenced by NMR studies on HHARI and RNF144 (Dove et al., 2016). This implies that features of RING1 domains somehow promote *open* E2~Ub states while highly similar canonical RING domains promote *closed* E2~Ub states. Here we address this conundrum for the RBR E3 HHARI and UbcH7~Ub conjugate. Mutagenesis and NMR results reveal that the second Zn^{2+}-loop (Zn^{2+}-loop II) in RING1 is largely responsible for the disruption of closed UbcH7~Ub states. A new crystal structure of HHARI in complex with UbcH7~Ub confirms that the E2~Ub conjugate is in an open state and shows that Zn^{2+}-loop II contacts UbcH7 on a surface that would conflict with Ub in a closed E2~Ub conformation. The structure verifies that E2~Ub binding does not release HHARI from its auto-inhibited conformation

implying that additional events must occur to release the E3 into its active form. Relevant to the reported activation of HHARI by binding to neddylated Cullins, we extend previous results (Kelsall et al., 2013) to demonstrate that HHARI can bind free NEDD8 and free Ub through its UBA-Like domain.

Results

Zn^{2+}-loop II of HHARI RING1 differs from canonical RINGs and promotes open UbcH7~Ub conformations.

To understand how RING1s promote opening of E2~Ubs, we compared primary sequence alignments of RING1s and canonical RING domains. Only a few conserved residues define RING and RING1 domains, most of which are required for coordination of two Zn^{2+} ions. In addition, most canonical RINGs contain structural elements that stimulate E2~Ub activity including a conserved "linchpin" residue that RBR RING1s appear not to contain (Fig. 1B, (Das et al., 2009; Dou et al., 2012, 2013; Koliopoulos et al., 2016; Plechanovova et al., 2012; Pruneda et al., 2012; Scott et al., 2014)). Lack of a linchpin could explain why RING1s do not promote closed E2~Ubs but it does not explain how they *actively* disfavor closed E2~Ubs (Dove et al., 2016). A unique feature of RING1s is the extension of Zn^{2+}-loop II, a loop involved in E2 binding (Metzger et al., 2014; Spratt et al., 2014). Specifically, while the last two Zn^{2+}-coordinating Cys residues are consistently separated by exactly two residues in canonical RINGs (C_{7th}-X-X-C_{8th}) there are up to four residues in RING1s (Fig. 1B, (Spratt et al., 2014)). Furthermore, the Zn^{2+}-loop II of canonical RINGs typically contacts E2s via loop 7, which is in close proximity to the E2 cross-over helix, a surface needed to contact Ub in closed E2~Ubs (Fig. S1) (Dou et

al., 2012, 2013; Plechanovova et al., 2012; Pruneda et al., 2012). However, the HHARI RING1 binding surface mapped on the E2 UbcH7 by NMR included the cross-over helix suggesting a potential overlap with the Ub contact site of closed E2~Ubs (Dove et al., 2016). Putting those two observations together, we hypothesized that the longer Zn^{2+}-loop II of HHARI RING1 (C_{7th}-P-A-H-G-C_{8th}) might sterically impede closed states of E2~Ubs.

To test our hypothesis, we designed two HHARI RING1 mutants and assessed their ability to disrupt closed UbcH7~Ubs. In one mutant, two "extra" loop residues were deleted to create a more canonical two-residue loop (ΔH234G235) and in the other, the side chain of His234 was trimmed to Gly (H234G) to remove a bulky side chain. Binding affinities measured by ITC reveal that HHARI RING1 binds UbcH7~Ub with high affinity (K_D 116nM; Fig. 1C & Table 1) and that each mutant has an only modest decrease in affinity (K_D of 625nM and 1.7μM for H234G and ΔH234G235 RING1, respectively; Fig. 1C & Table 1). We therefore characterized each mutants' ability to disrupt close UbcH7~Ubs conformations.

To assess whether the above RING1 mutants affect the open/closed status of UbcH7~Ub, we focused on key NMR resonances in the Ub spectrum that report on these states, using a stable oxyester mimic (active site Cys-to-Ser mutant) of UbcH7~Ub as done before (Dove et al., 2016). As shown previously, the NMR spectrum of ^{15}N-Ub within UbcH7~Ub exhibits chemical shifts that are hallmarks of the closed state (Dove et al., 2016). In particular, the Q49-Ub NH resonance undergoes a large chemical shift relative to its position in free ^{15}N-Ub upon conjugation to UbcH7 and shifts back close to its position in free ^{15}N-Ub upon HHARI RING1 binding to UbcH7~Ub (Fig. 1D from black to green to blue, respectively). The observations indicate that

UbcH7~Ub is predominantly in a closed state on its own but it is predominantly in open conformations when bound to RING1 (Dove et al., 2016). The Q49-Ub resonance falls along a trajectory defined by the resonances of unbound UbcH7~Ub (green) and bound to wild-type (WT) HHARI RING1 (blue) when bound to the mutant HHARI RING1s (ΔH234G235 and H234G; Fig. 1D, red and orange). The most parsimonious explanation is that the RING1 mutants affect the fractional populations of closed and open UbcH7~Ub states. Specifically, the Q49-Ub resonance position remains closer to the "closed-state" position (Fig. 1D, red) when bound to the loop deletion mutant, ΔH234G235, while it shifts almost to the WT RING1-bound position when bound to H234G RING1. Therefore, RING1 lacking the His234 side chain can still disrupt closed E2~Ubs while RING1 with a shortened two-residue loop has diminished ability to perform this function (Fig. 1D, orange). This observation cannot be explained by a decreased binding affinity of the mutants as NMR experiments were performed under saturating conditions. Altogether, the results indicate that the length of Zn^{2+}-loop II rather than the nature of its side chains is responsible for HHARI RING1's ability to promote open UbcH7~Ubs. Consistent with this conclusion, RNF144 RING1 also disrupts closed UbcH7~Ubs yet it contains an Ala at the position analogous to HHARI His234 (Fig. 1B) (Dove et al., 2016). The loop deletion mutant of HHARI does still elicit a small shift away from the closed state position, indicating that there may be another contributory factor. Nevertheless, the data reveal that the extension of Zn^{2+}-loop II is largely responsible for HHARI and RNF144 RING1's promotion of open E2~Ubs that ensures that transfer of Ub from the bound E2~Ub proceeds via the RBR active site Cys.

Structure of HHARI bound to UbcH7~Ub

To obtain a more detailed view of the interactions between HHARI and UbcH7~Ub, we determined a crystal structure of HHARI bound to UbcH7~Ub, using a truncated HHARI construct (residues 90-557, for simplicity referred to as HHARI) and the active site Cys-to-Lys mutant of UbcH7 to increase conjugate stability (referred to as UbcH7~Ub). The asymmetric unit contains two copies of HHARI each bound to UbcH7~Ub, with only weak density observed for the two Ub moieties (only one was placed in the final model). The interface between the two copies of the complex is composed of two RING1 and two UbcH7 molecules. However, based on NMR relaxation parameters of HHARI RING1 bound to UbcH7 in solution we can conclude that this dimer interface is due to crystal packing (Dove et al., 2016).

Two features are immediately apparent in the structure of the complex (Fig. 2). First, although there is an E2~Ub bound to RING1, the E3 is in an auto-inhibited conformation similar to previous structures of HHARI (pdb 4kc9 & 4kbl; (Duda et al., 2013)). Second, UbcH7~Ub is in an open conformation consistent with earlier conclusions that HHARI RING1 promotes open states of UbcH7~Ub (Dove et al., 2016). Though weak, the electron density observed for the Ub moiety does not contact its cognate HHARI partner. This contrasts with two structures of UbcH5~Ub bound to thioester-forming E3s: the HECT domain from NEDD4L where the HECT C-lobe makes intimate contact with a hydrophobic surface of Ub (Kamadurai et al., 2009), and an “active” form of HOIP RBR-LDD that interacts with the Ub moiety of UbcH5~Ub (Lechtenberg et al., 2016). Below we further analyze and compare the new structure with existing RBR structures to gain insights into how an RBR E3 is restrained prior to activation, even when bound to its cognate E2~Ub intermediate.

HHARI is auto-inhibited even when bound to UbcH7~Ub

An emerging property of RBR E3s is that their activity is kept in check by adoption of auto-inhibited states. Full-length HHARI, as well as the construct used in this study, has very low E3 ligase activity *in vitro* (Duda et al., 2013; Scott et al., 2016). From its auto-inhibited state, HHARI can bind UbcH7 or its conjugate, but that binding does not relieve the inhibition (Duda et al., 2013; Scott et al., 2016). Consistent with that observation, HHARI is still in an auto-inhibited conformation in the structure of the HHARI/ UbcH7~Ub complex reported here, with the active site Cys far from the UbcH7 active site and occluded by the Ariadne domain (Fig.2). Comparison to a structure of the HOIP RBR-LDD module bound to an E2~Ub reveals some similarities, but also striking differences (Fig. S3) (Lechtenberg et al., 2016; Smit et al., 2012; Stieglitz et al., 2012). As in HHARI/ UbcH7~Ub, HOIP RING1 binds UbcH5~Ub in an open conformation. But in the latter case, the E3 makes substantial contacts to the ~Ub (Ub conjugated to the E2) via the C-terminal helix of RING1, the IBR, and RING2 (Fig. S3). The ~Ub/RING2 contacts observed involve a non-cognate molecule of HOIP in the crystal, but are similar to those seen in a structure of an E3~Ub mimic of the HOIP RING2-LDD module (Stieglitz et al., 2013). Together, these observations suggest that Ub/RING2 interactions play a role both prior to and after the transthiolation step from E2~Ub to E3~Ub and that the contact observed in *trans* in the HOIP/E2~Ub crystal is a proxy for a mechanistically relevant interaction (Lechtenberg et al., 2016; Stieglitz et al., 2013). Two recent studies have concluded that similar Ub/RING2 contacts are important in the formation of the HHARI~Ub intermediate (Dove et al., 2016; Scott et al., 2016). However, structural details regarding the large conformational change required to bring E2~Ub and RING2 in close proximity remains to be defined.

Unique Interactions between HHARI RING1 and UbcH7

UbcH7 can bind to canonical RINGs, but can only transfer Ub to Cys residues and therefore its only known RING-dependent activity is with RBR E3s (Brzovic et al., 2003; Christensen et al., 2007; Wenzel et al., 2011; Zheng et al., 2000). Comparison of functional E2/RING pairs, mostly containing the E2 UbcH5, with the C-cbl/UbcH7 structure confirms a similar binding mode. Here we discuss unique features of the functional HHARI RING1/UbcH7 interaction.

The overall architecture of the RING1/UbcH7 interface is similar to interfaces seen in other RING/E2 pairs (Brown et al., 2014; Brzovic et al., 2003; DaRosa et al., 2015; Dou et al., 2012; Koliopoulos et al., 2016; Lechtenberg et al., 2016; Li et al., 2015; Plechanovova et al., 2012; Pruneda et al., 2012; Scott et al., 2014; Xu et al., 2008; Zheng et al., 2000). UbcH7 residues from loops 4 and 7 and the N-terminus of helix 1 and HHARI RING1 residues from both Zn^{2+}-loops and the central helix make canonical E2/RING interactions (Fig. 3A & S1). Residues that are shared between UbcH7 and UbcH5 in the RING-binding regions makes similar contacts. For example, UbcH7 loop 4 residue Phe63 contacts HHARI RING1 residues Ile188 in Zn^{2+}-loop I and Tyr215 in the central helix (Fig. S4A). UbcH7 Phe63 is analogous to Phe62 in UbcH5 which makes contacts to canonical RINGs; Ile188 is analogous to a highly conserved Ile residue (for example, Ile26 in BRCA1) that plays a pivotal role in canonical RING/E2 interactions; and hydrophobic residues emanating from the central helix of RINGs are also involved in E2 interactions. Substitution at any of these three positions with alanine results in a substantial decrease in HHARI auto-ubiquitination activity (Fig. S4B, (Duda et al., 2013; Scott et

al., 2016)) and the HHARI double mutant I188A/Y215A-RING1 exhibits a complete loss of detectable ligase activity under the same conditions (Fig. S4C).

HHARI functions with both UbcH7 and UbcH5 but has markedly higher affinity for UbcH7 than for UbcH5 (Table 1, Fig. S2 & S5A, (Wenzel et al., 2011)). We examined the RING1/UbcH7 contacts in the structure to identify features that might explain why HHARI binds tighter to UbcH7, focusing on positions that differ between the two E2s. While loop 4 is well conserved between UbcH7 and UbcH5, residues in loop 7 vary in the two E2s (Fig. S5B). There are extensive, intimate contacts between RING1 Zn^{2+}-loop II and UbcH7 loop 7, with virtually every residue of HHARI's loop extending from residue 230-237 in contact with UbcH7's loop 7 and the beginning of the cross-over helix (Fig. 3A). Of particular note, the previously discussed HHARI His234 in Zn^{2+} loop II reaches out and appears to make a hydrogen bond with UbcH7 residue Gln103 (Fig. 3A). The analogous position to Gln103 is a Lys in UbcH5 (Lys101 in UbcH5, Fig. S5B). Substitution of His234 with a Gly decreases the affinity of HHARI-RING1 for UbcH7 from ~300nM to 1000nM (Table 1). This decrease corresponds to a $\Delta\Delta G$ of 0.4 kcal/mol, consistent with the loss of an H-bond (Sheu et al., 2003).

Another UbcH7-specific interaction involves Lys96 in loop 7 of UbcH7. Lys96 is in the position normally held by a Ser residue in the highly conserved "WSPAL" motif in loop 7 of numerous E2s including UbcH5 (Fig. S5B). The structure reveals an extensive hydrogen-bond network emanating from Lys96 to three RING1 Zn^{2+}-loop II residues (Ser230, Cys23, and Asp237; Fig. 3B). HHARI residue Asp237 is in what would be the linchpin position of RING1 (based on primary sequence). A charge-swap mutant of Lys96, K96E-UbcH7, shows greatly

diminished activity in auto-ubiquitination of HHARI (Fig. 3C). Similarly, a charge-swap mutant of HHARI residue Asp237, D237R-HHARI, has decreased activity relative to the WT E3 (Fig. 3C). As predicted from the structure, mutation of the Lys that interacts with three groups shows a greater reduction in activity than mutation of RING1 D237 that disrupts a single contact. Notably, when the charge-swapped E2 and E3 mutants are combined in the same assay, increased activity is observed relative to the activity of either mutant paired with the WT partner (Fig. 3C). The results confirm that an ionic interaction between Lys96 in UbcH7 and Asp237 in HHARI inferred from the crystal structure contributes to the formation of a functional UbcH7/HHARI-RING1 complex.

Our NMR results indicate that Zn^{2+} loop II of HHARI is largely responsible for disfavoring the closed state of UbcH7~Ub (Fig. 1D). Furthermore, previous NMR mapping revealed that the HHARI RING1 binding surface extends onto the cross-over helix of UbcH7 and includes residue 103 (Dove et al., 2016). Consistent with those observations, the tip of Zn^{2+}-loop II reaches past UbcH7's loop 7 to contact the E2's cross-over helix, most notably, with Q103 (Fig. 3A). The analogous side chain in UbcH5, Lys101, contacts Ub in the closed state of UbcH5~Ub when bound to a canonical RING domain (Dou et al., 2012; Koliopoulos et al., 2016; Plechanovova et al., 2012). Altogether, the observations suggest that RING1 Zn^{2+} loop II may conflict with the position of Ub in closed E2~Ub. To assess this possibility, we built a model of RING1/UbcH7~Ub with Ub in the closed state by superimposing the structure of closed UbcH5~Ub from the complex with BIRC7 (pdb 4auq, Fig. S5C). In the model, the tip of Zn^{2+}-loop II of HHARI RING1 clashes with Ub in the closed state of E2~Ub, providing a structural explanation for results presented in Figure 1D.

The HHARI UBA-L domain binds to Ubiquitin and NEDD8

Analysis of the HHARI/UbcH7~Ub crystal structure revealed that a Ub from a UbcH7~Ub moiety bound to HHARI contacts the UBA-L domain of a HHARI molecule in a neighboring symmetry unit (denoted with a (‘), Fig. 4A). This Ub/UBA-L interface is comprised of the hydrophobic surface of Ub (including residues Leu8, Ile44 and Val70) and residues Val123, Met146, and Phe150 of the UBA-L. To see whether the UBA-L binds Ub in solution, we took advantage of the ability of NMR to detect weak binding by collecting ^{1}H-^{15}N-HSQC-type NMR spectra of ^{15}N-Ub in the absence (black) and presence (red) of full-length HHARI (Fig. 4B). Chemical shift perturbations (CSPs) in the form of peak shifting and broadening are clearly visible, indicating a specific interaction between Ub and HHARI (Fig.4B & S6A). CSP mapping onto the Ub structure reveals a binding surface centered around the Ile44 hydrophobic patch (Fig. S6B). Mutation of residues on that surface abrogate the observed binding, as shown in the NMR overlay obtained with ^{15}N-Ub-L8A/I44A in the absence and presence of HHARI (Fig. 4B). Furthermore, the HHARI UBA-L double mutant V123D/F150D shows substantially reduced binding to ^{15}N-Ub (Fig. 4B), corroborating that the Ub/UBA-L’ contact site observed in the crystal is similar to the interaction in solution.

Although a functional significance for a HHARI UBA-L/Ub remains undefined, the domain is implicated in binding to the Ub-like protein, NEDD8, via the interaction between HHARI and neddylated Cullins (Kelsall et al., 2013; Scott et al., 2016). NMR binding experiments carried out on ^{15}N-NEDD8 in the absence (black) or presence WT HHARI confirm that HHARI also binds weakly to NEDD8 in solution (Fig. S6C). That both Ub and NEDD8 bind similarly to the UBA-L is not surprising based on the high similarity between the two proteins on their

hydrophobic surface (>90% of residues at UBA-L/Ub' interface are conserved between Ub and NEDD8, Fig. S6D). But while binding to neddylated Cullins has been shown to activate HHARI E3 activity, neither NEDD8 nor Ub alone are thought to cause conformational changes in HHARI that lead to its activation(Kelsall et al., 2013; Scott et al., 2016).

Discussion

In this study, we set out to define how RBR RING1 domains recognize E2~Ubs using HHARI and UbcH7~Ub as an example. We discovered how subtle differences between the strikingly similar E2-binding domains of canonical RING and RBR E3s dictate essentially opposite mechanisms for activating E2~Ub intermediates. We demonstrate that a two-residue extension of Zn^{2+}-loop II of HHARI RING1 is largely responsible for disrupting closed UbcH7~Ubs. Deletion of the two "extra" residues in HHARI Zn^{2+}-loop II to create a two-residue loop as found in canonical RING domains generates a RING1 with diminished ability to disrupt closed UbcH7~Ub (Fig. 1D). In the crystal structure presented here, the tip of the elongated Zn^{2+}-loop II contacts the cross-over helix of UbcH7, thereby utilizing a surface that has been shown to stabilize closed E2~Ub conjugates (Dou et al., 2012, 2013; Koliopoulos et al., 2016; Plechanovova et al., 2012; Pruneda et al., 2012; Scott et al., 2014). Modeling a HHARI RING1/UbcH7~Ub complex with an E2~Ub in the closed conformation confirms that segments of Zn^{2+}- loop II would sterically clash with ~Ub of closed UbcH7~Ubs (Fig. S5C). We therefore propose that the elongated loop serves as a wedge to prevent closed E2~Ub states when bound to RING1.

RBR E3s are highly active E3s that keep their activity in check through adoption of auto-inhibited states. Auto-inhibited HHARI can bind E2~Ub so it is crucial to prevent the formation of highly active closed E2~Ub to inhibit non-productive discharge of Ub until the E3 is ready to accept the Ub onto its RING2 active site. In contrast, auto-inhibited Parkin cannot bind E2~Ub because its E2-binding site is partly occluded (Kumar et al., 2015; Riley et al., 2013; Sauve et al., 2015; Trempe et al., 2013; Wauer and Komander, 2013; Wauer et al., 2015). It may therefore be less important for Parkin to disfavor closed E2~Ub states. Our results show that deletion of two residues in HHARI's Zn^{2+}-loop II decreases its ability to open UbcH7~Ub substantially, but some of this ability is retained (Fig. 1D). Therefore, it is possible that Parkin's three-residue loop helps to promote open E2~Ubs states once its E2-binding site is accessible.

Some RBR E3s possess a more canonical two-residue Zn^{2+}-loop II and may different mechanisms to direct conformational opening of their bound E2~Ub. Indeed, HOIP binds UbcH5~Ub in an open state despite its two-residue loop, and as predicted by our results, its short Zn^{2+}-loop II does not contact UbcH5 cross-over helix residues (Lechtenberg et al., 2016), implying a different mechanism is in play. Notably, while the ~Ub in our structure appears to make no contacts to its cognate HHARI, the analogous ~Ub in the crystal structure of UbcH5~Ub/HOIP-RBR-LDD makes contacts with RING1 and the IBR, reminiscent of a HECT/E2~Ub complex (Kamadurai et al., 2009; Lechtenberg et al., 2016). The HOIP-RBR-LDD/UbcH5~Ub structure appears to represent a partially activated state as the E2~Ub is well positioned for Ub transfer, but the acceptor RING2 domain belongs to a different polypeptide due to a dimer swap. Therefore, details of the fully activated E2~Ub/HOIP complex with its RING2 correctly positioned must await further studies.

We propose a model for RING and RING1 function with E2~Ubs based on known and emerging properties (Fig. 5). E2~Ub conjugates exist as ensembles of closed and open states and the distribution among those states varies depending on the E2 in question (Dove et al.; Pruneda et al., 2011). Canonical RINGs actively stabilize closed E2~Ubs via a combination of contacts to ~Ub, often including a linchpin interaction to activate transfer to amino groups (Dou et al., 2012; Plechanovova et al., 2012; Pruneda et al., 2012) (Brown et al., 2014; Dou et al., 2013; Koliopoulos et al., 2016; Scott et al., 2014). In contrast, RBR- and HECT-type E3s promote open E2~Ubs (Dove et al., 2016; Kamadurai et al., 2009). Our results indicate that a distinguishing feature of some but not all RING1 domains, an extended Zn^{2+}-loop II, serves as a wedge to prevent ~Ub from adopting a closed conformation on the E2. One consequence of keeping E2~Ub in minimally reactive, open states is to prevent off-target ubiquitination (Dove et al., 2016). Furthermore, we have shown previously that open UbcH7~Ub exposes the hydrophobic surface of Ub that plays a role in recruiting HHARI RING2 (Dove et al., 2016). As the transfer of Ub from the E2 to E3 active sites is a shared step in RBR-catalyzed Ub transfer, presentation of an open E2~Ub, either through the wedge mechanism defined here (RBRs with extended loops) or potentially through additional interactions with the ~Ub (HOIP and possibly other two-residue loop-containing RBRs) is a unifying theme.

It appears that many E3 ligases contain parallel domains that mediate parallel interactions, but despite this relationship, the detailed mechanisms can differ substantially with important functional implications. Our study provides a structural explanation for the fundamentally different action of RING1s as compared to their eponymous cousins, the

canonical RING domains. RING E3s couple E2~Ub binding and activation in a single event that enable the E2~Ub to "fire" directly onto substrate. By promoting an open E2~Ub, RBR E3s inhibit E2~Ub firing to allow formation of the E3~Ub intermediate once the E3 is activated and its RING2 active site is exposed. The activation step and subsequent transfer of Ub to a substrate must involve large scale domain rearrangements in the RBR E3s. Details of how HHARI and other RBR E3s achieve these important final steps are undoubtedly the next structural mystery to solve.

Acknowledgements

We thank I. Kurinov for help with crystallography data collection, and D.W. Miller for support for experiments in the Schulman lab. This work was supported by National Institute of General Medical Sciences grant R01 GM088055 (REK), the Francis Crick Institute, which receives its core funding from Cancer Research UK (FC001142), the UK Medical Research Council (FC001142), and the Wellcome Trust (FC001142) (KR), UW Hurd Fellowship Fund, PHS NRSA 5T32 GM007270 (KKD), ALSAC, NIH R37GM069530, NIH P30CA021765, and Howard Hughes Medical Institute (BAS). NE-CAT was supported by NIH P41GM103403, NIH-ORIP HEI grant (S10 RR029205) and APS by DOE DE-AC02-06CH11357.

Conflict of Interest

The authors declare that they have no conflict of interest.

Experimental Procedures

Protein expression and purification

All proteins described are human and full-length unless stated otherwise. Wheat and mouse E1, Ub, UbcH5, UbcH7, HHARI RING1 (aa 177-270), HHARI-RBR (aa 177-395), HHARI full-length were produced as described (Dove et al., 2016; Duda et al., 2013). All point mutations were introduced using the Quikchange mutagenesis kit. The construct expressing His-Uba1 was a gift from C. Wolberger.

Isotopically labeled proteins used for NMR were expressed as described previously (Dove et al., 2016). GST-NEDD8 lysate was applied to GST resin (GE Healthcare) in 50mM Tris-HCL, 200mM NaCl, pH8.0. GST was cleaved with thrombin (Sigma Aldrich) on column at 37°C followed by size-exclusion chromatography (25mM $NaPO_4$, 150mM NaCl, pH7.0).

HHARI (aa 90-557, $HHARI^{90-557}$) used for crystallography was cloned as described (Scott et al., 2016) and purified by glutathione affinity chromatography, followed by TEV proteolysis to liberate GST, size exclusion chromatography, glutathione affinity chromatography to remove remaining GST/uncleaved fusion protein, and size exclusion chromatography in 25mM Tris-HCl pH7.6, 150mM NaCl, 1mM DTT. $UbcH7^{C86K}$ was expressed similarly, but with dialysis during proteolysis with TEV and a final size exclusion chromatography step. His-Ub was purified by Ni pulldown, followed by dialysis, size exclusion chromatography in 25mM Tris-HCl pH7.6, 150mM NaCl, 1mM DTT. Purified $HHARI^{90-557}$ and $UbcH7^{C86K}$-His-Ub used in crystallography were mixed 1:1 and concentrated to form a complex. The complex was purified by size exclusion chromatography in 25mM Tris-HCl pH7.6, 150mM NaCl, 1mM DTT.

Crystallization, Data collection and Structure determination

Crystals of HHARI$^{90-557}$/UbcH7^{C86K}-His-Ub were grown with the hanging drop vapor diffusion method at room temperature. 2 ul drops contained 1 ul protein mixture (10-12 mg/ml protein in 25mM Tris, pH7.0, 150mM NaCl, 1mM DTT) and 1ul well solution (7-10% PEG 5000 monomethyl ether (MME), 0.1M HEPES pH7.0, and 5% Tacsimate pH 7.0) over a 1ml reservoir volume. Crystals were flash frozen in 30% PEG 5000 MME, 0.1M HEPES 7.0, and 5% Tacsimate pH7.0. Due to the limited diffraction quality of these crystals, a relatively poor molecular replacement solution was obtained with limited usefulness for initial model building. Therefore, de novo structure determination was pursued. To this end, there are 6 naturally occurring Zn clusters per HHARI protomer. Zn SAD data (peak, 1.2862 Å) was collected at the Advanced Photon Source NE-CAT Sector 24-IDC beamline and processed to 3.6 Å using the RAPD pipeline (https://github.com/RAPD). The structure was solved using ShelxC/D/E (Sheldrick, 2010) as implemented in the automated CRANK CCP4 pipeline (Ness et al., 2004). Autotracing efforts yielded limited results. Therefore, a difference anomalous map was generated for location of the zinc atoms and placement of the 2 HHARI moieties in the asymmetric unit (ASU) using our previously published HHARI structure (pdb 4KBL (Duda et al., 2013)). After manual placement of HHARI using COOT (Emsley et al., 2010), UbcH7 moieties were identified in the experimental map. UbcH7 pdb 5HPT (Zhang et al., 2016) was used for initial model building. The full ASU was built without addition of the relatively weak Ub moieties. Furthermore, significant sub-domain movements for HHARI and UbcH7 relative to the reference structures were apparent. Therefore, models were broken down into sub-domains for rigid body refinement with Refmac (Murshudov et al., 1997). Following rigid body refinement, the Ub portion of the complex was modeled using available structures in the pdb. Due to insufficient

electron density, only one of the two Ubs could be confidently placed in the AU corresponding to chain E of complex A/C/E. Although the second copy of the Ub was not included in refinement, superimposition of the two complexes based on HHARI and UbcH7 reveal a similar location for the Ubs in their respective larger complex. Next, the low resolution DEN refinement protocol was implemented using CNS (Brunger et al., 1998; Schroder et al., 2010). Best results (model with lowest R_{free}, reduced R_{work}/R_{free} spread, and good Ramachandran statistics and best overall map quality) were obtained using the rigid body refined model as the reference model, a maximum likelihood target function, and DEN parameters γ 0.4 and κ 300. Phenix (Adams et al., 2010) was then used for successive rounds of positional and B-factor refinement. After many rounds of crystal optimization and screening of hundreds of crystals, data from a single crystal diffracting to 3.24 Å was obtained using the NE-CAT Sector 24-IDC beamline. The isomorphous data was integrated and scaled with XDS (Kabsch, 2010). Following rigid body refinement, the improved electron density maps allowed for further additions to the model, including loop regions and termini. Further refinement was carried out using Phenix and Refmac. The A/C/E complex is described throughout the manuscript unless otherwise noted. The final model includes HHARI chain A residues 98-162, 181-329, 339-392, 410-448, and 451-554; HHARI chain B 98-152, 184-328, 340-391, 409-441, and 457-552; UbcH7 chain C 1-151; UbcH7 chain D 1-153; Ub chain E 1-73. According to Molprobity (Chen et al., 2010), 96% and 0% of residues are within the favored and outlier regions of the Ramachandran plot, respectively. See Table 2 for pertinent data collection and refinement statistics. Structural cartoon figures were generated using PyMOL (Schrödinger, 2002).

Auto-ubiquitination assays

The following proteins were combined in 25mM $NaPO_4$, 150mM NaCl, pH7.0: 0.5μM wheat E1, 2μM E2, 2μM GST-HHARI^{RBR} (aa 177-395), and 20μM Ub and incubated at 37°C. 10mM ATP was added to start reactions and SDS-PAGE reducing buffer was used to quench reaction. Samples were run on SDS-PAGE gel, followed by western blots, which were visualized using GST antibody (Life Tein, LT0423) against GST-HHARI^{RBR}.

Generation of stable E2~Ubs for NMR and crystallography

Formation of isopeptide linked UbcH7(C86K)~Ub:

150uM UbcH7^{C86K}, 15μM E1, 450μM His-Ub in 30mM Tris pH8.8, 50mM NaCl, 5mM ATP, 10mM $MgCl_2$ was incubated for ~18 hours at 30°C. The resulting UbcH7~Ub was purified by size exclusion chromatography in 25mM Tris-HCl pH7.6, 150mM NaCl, 1mM DTT. The UbcH7-C86S-Ub oxyester for all NMR studies was generated as described (Dove et al., 2016).

Isothermal titration calorimetry

ITC experiments were performed at 293K using a Microcal iTC200 calorimeter (Malvern). Samples were prepared in a degassed buffer (25mM Hepes pH7.5, 150mM NaCl, 0.5mM TCEP). Cell solutions contained 25-30μM E2 or E2~Ub and syringe solutions contained of 250-300μM RING1 constructs. For each titration 20 injections of 2μL were performed. Where possible, the integrated data, corrected for heats of dilution, were fitted using a nonlinear least-squares algorithm to a 1:1 binding curve, using the MicroCal Origin 7.0 software package. The fitting parameters are $\Delta H°$ (reaction enthalpy change in kcal·mol^{-1}), K_b (equilibrium binding constant in M^{-1}), and n

(number of binding sites). Each experiment was repeated at least twice and average values are reported.

NMR experiments

All NMR experiments were performed at 298K in 25mM $NaPO_4$, 150mM NaCl, pH7.0, 10% D_2O. UbcH7-O-Ub was used for increased stability. The following protein concentrations and field strengths were used for (^1H,^{15}N)-HSQC-TROSY experiments: Fig.1D (500 Mhz): 50μM ^{15}N-Ub, 200μM free UbcH7-O-^{15}N-Ub, 160μM UbcH7-O-^{15}N-Ub + 200μM HHARI RING1, 150μM UbcH7-O-^{15}N-Ub + 250μM HHARI RING1 mutants (H234G or ΔH234G235) ; Fig. 4B (800Mhz): 50μM ^{15}N-Ub, 50μM ^{15}N-Ub + 20μM of either WT or V123DF150D-HHARI FL; 500 (Mhz): 50μM ^{15}N-L8A/ I44A-Ub, 50μM ^{15}N-L8A/ I44A-Ub + 20μM HHARI FL; Fig.S6C (800 Mhz): 50μM ^{15}N-NEDD8, 50μM ^{15}N-NEDD8 + 20μM HHARI FL. NMRPipe/NMRDraw (Delaglio et al., 1995) was used to process NMR data. NMRViewJ (One Moon Scientific) was used for data visualization (Johnson and Blevins, 1994). The equation $\Delta\delta = [(\Delta\delta\ ^{15}N/5)^2 + (\Delta\delta\ ^{1}H)^2]^{1/2}$ was used to calculated chemical shift perturbations of 2D HSQC-TROSY NMR experiments.

Interactions	n	Kd (nM)	ΔH Kcal/mol	-TΔS Kcal/mol	ΔG Kcal/mol
RING1/UbcH7	1.0±0.1	294±25	4.3±0.1	-12.7±0.8	-8.4±0.7
RING1/UbcH7~Ub	1.0±0.1	116±34	3.7±0.1	-12.7±2.7	-8.9±2.6
RING1/UbcH5a	No binding detected				
RING1/UbcH5a~Ub	No binding detected				
RING1-HGXX/UbcH7	0.8±0.2	2380±300	4.2±0.9	-11.7±1.8	-7.5±0.9
RING1-HGXX/UbcH7~Ub	0.9±0.1	1695±152	6.9±0.9	-14.6±1.6	-7.7±0.7
RING1-H234G/UbcH7	0.8±0.2	1000±102	7.2±0.8	-15.2±1.6	-8.0±0.8
RING1-H234G/UbcH7~Ub	1.0±0.1	625±79	4.5±0.5	-12.8±1.5	-8.3±1.0

Table 1. ITC data for the interaction between HHARI RING1 and its mutants with UbcH7, UbcH7~Ub, UbcH5a and Ubc5a~Ub

	HHARI/UbcH7~Ub (Zn-SAD)	HHARI/UbcH7~Ub (Native)
Data Collection		
Space group	*C*2	*C*2
Unit cell *a, b, c* (Å), α, β, γ (°)	183.71, 75.82, 147.61, 90, 107.15, 90	184.57, 76.79, 147.72, 90, 107.33, 90
Resolution (Å)	141.04–3.56 (3.85-3.56)[a]	48.45–3.24 (3.45-3.24)
Completeness (%)	96.4 (97.9)	98.9 (96.0)
No. reflections (unique)	65,236 (22,642)	183,340 (31,387)
Redundancy	2.9 (2.9)	5.8 (5.9)
R_{sym} (%)	7.5 (56.1)	9.3 (88.3)
R_{meas} (%)	9.1 (68.3)	10.2 (96.6)
$CC_{1/2}$	1.00 (0.72)	1.00 (0.76)
I/σI	13.3 (2.1)	13.1 (1.9)
Refinement		
Resolution range (Å)		48.45–3.24
R_{work}/R_{free}		22.7/27.9
No. atoms protein/Zn		9166/12
RMSD bond lengths (Å)		0.009
RMSD bond angles (°)		1.4
B factor ($Å^2$) protein/Zn		116.6/122.4

[a]Values in parentheses are for the highest-resolution shell and preceding values are for all data.

Table 2. Data Collection and Refinement Statistics

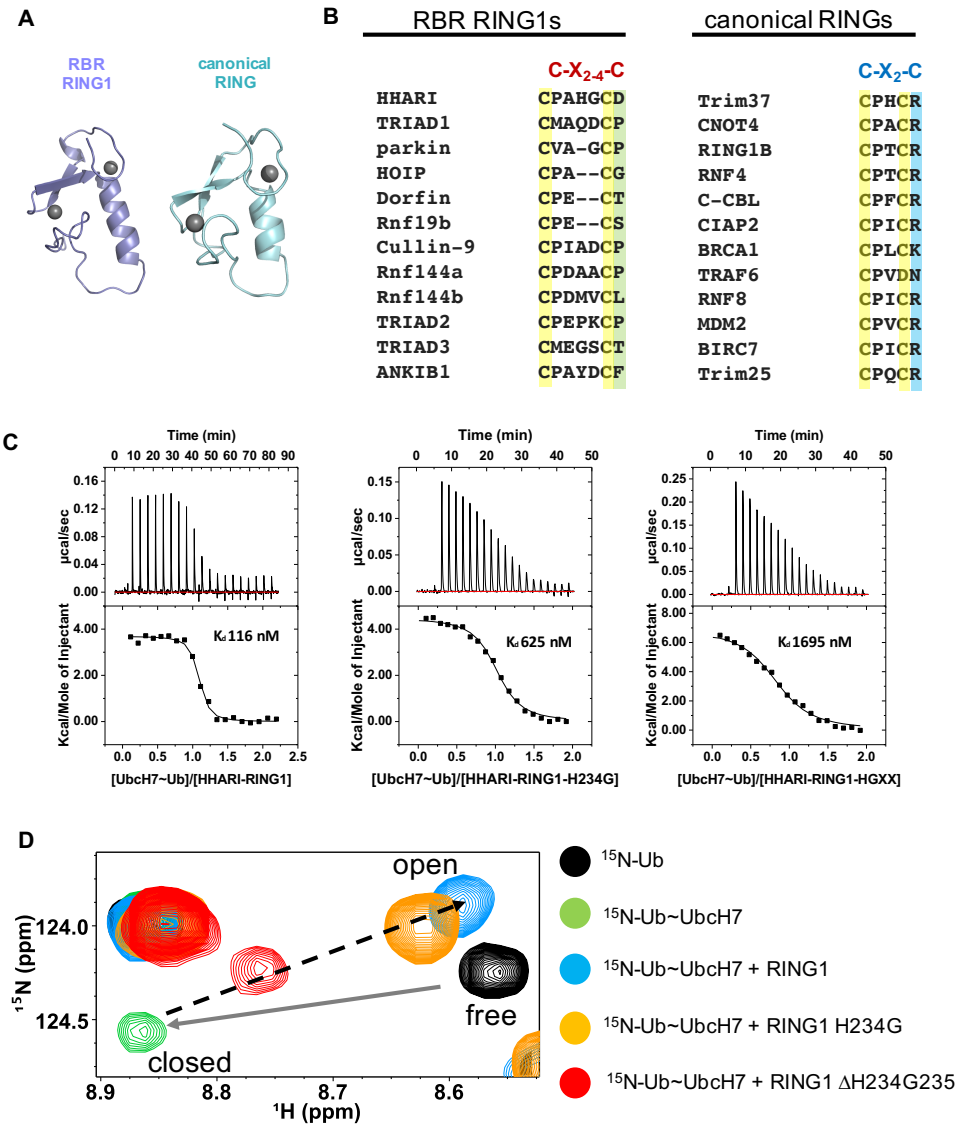

Figure 1. Comparison of RING1 and RING domains. **A.** The structures of RING1 of HHARI (slate, pdb 4KC9) and the RING domain of BRCA1 (cyan, pdb1JM7) illustrate the similar overall topologies of the two related domains. **B.** KALIGN sequence alignment of Zn^{2+}-loop II segments of RBR RING1 (left) and canonical RING domains (right). The 7th and 8th zinc-coordinating Cys residues for each domain are highlighted in yellow. The allosteric linchpin found in >50% of canonical RINGs is highlighted in blue; there are no functionally analogous residues at this position in RING1s (green). Zn^{2+}-loop II is invariably two residues long in canonical RING domains (C-X_2-C), but varies in length in RBR RING1s (C-X_{2-4}-C). **C.** Calorimetric titrations of UbcH7~Ub and HHARI RING1 wild-type (left), H234G (middle), and ΔH234G235 (right). Both the raw data and normalized binding curves are shown. Calorimetric titrations with unconjugated UbcH7 are shown in Fig. S1. **D.** The length of Zn^{2+}-loop II is largely responsible for the ability of HHARI RING1 to promote UbcH7~Ub open states. A signature of closed states populated by UbcH7~Ub in the absence of E3 is a large chemical shift perturbation of Gln49 ^{15}N-Ub (black vs. green spectra; grey arrow). Binding of HHARI RING1 to UbcH7~Ub reverses the chemical shift of

Gln49 (green-to-blue spectrum; black arrow) indicative of disruption of closed UbcH7~Ub (Dove et al., 2016). Shortening of HHARI RING1 Zn^{2+}-loop II by two residues (ΔH234G235) reduces the ability of HHARI RING1 to promote open UbcH7~Ub (red spectrum), but RING1 harboring a mutation of His to Gly still promotes open states of UbcH7~Ub (orange spectrum,).

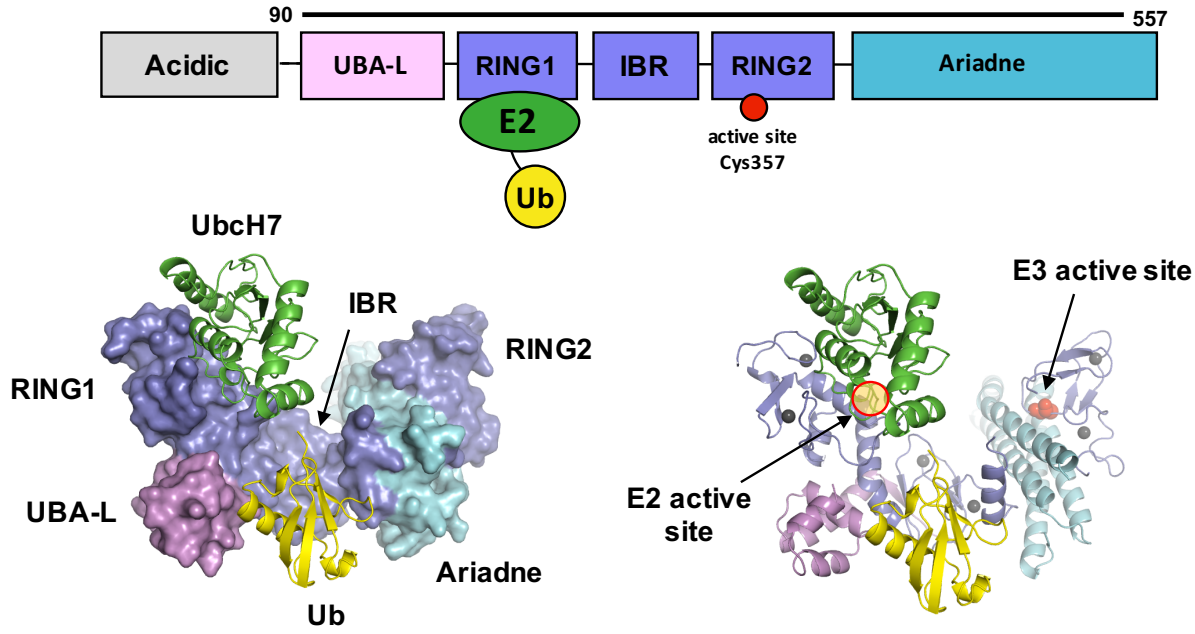

Figure 2. Structure of HHARI/UbcH7~Ub. *Top***.** The domain architecture of HHARI. The construct used for crystallography is denoted by the black bar. *Bottom***.** HHARI is shown in surface (left) and cartoon (right) representation, with same domain coloring as in top panel. UbcH7~Ub is shown in cartoon representation (UbcH7 in green, Ub in yellow). Auto-inhibited HHARI binds to UbcH7~Ub in an open conformation and no contacts are observed between Ub and its cognate HHARI. The UbcH7 active site (yellow circle, right) and HHARI active site (red spheres, right) are indicated. The HHARI active site Cys on RING2 is not visible in the surface representation (left) as it is occluded by the Ariadne domain (cyan).

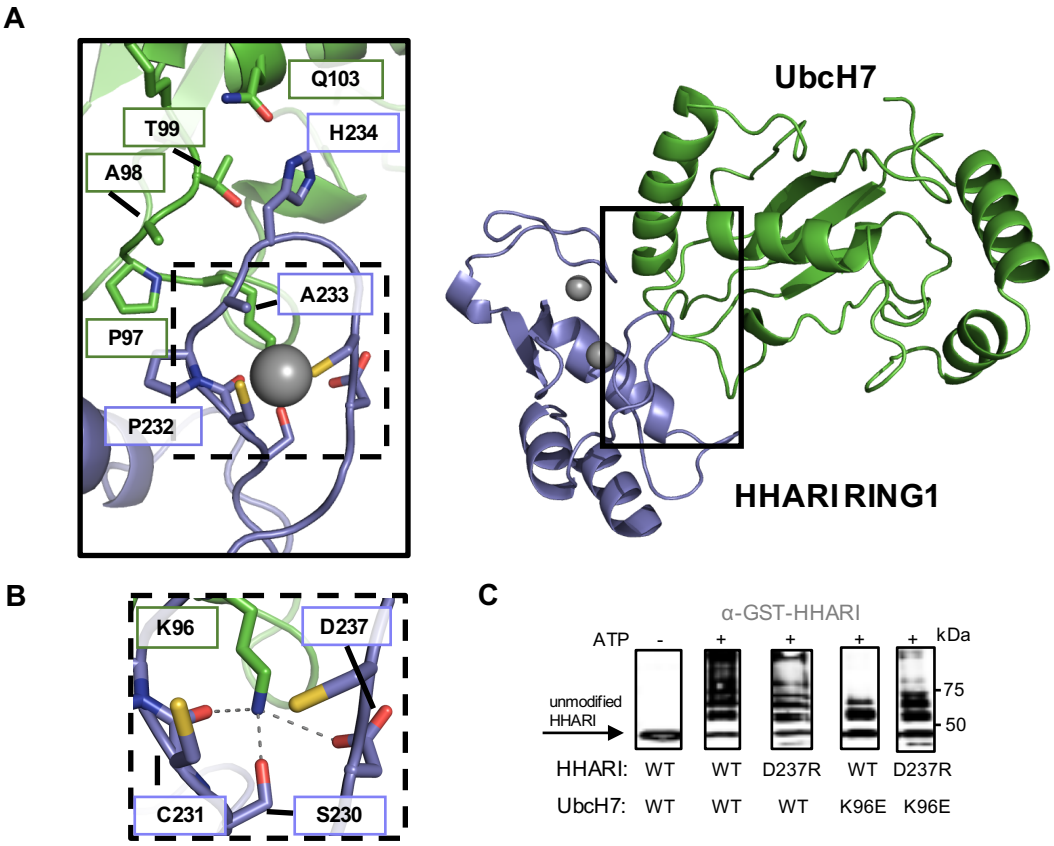

Figure 3. A. Unique features of the RING1/UbcH7 interface. UbcH7 loop 7 and the beginning of the cross-over-helix form extensive contacts with HHARI Zn^{2+}-loop II residues Ser230-Asp237. UbcH7 cross-over helix residue Gln103 is within hydrogen-bound distance of RING1 His234. **B.** UbcH7 Lys96 forms hydrogen bonds to RING1 Zn^{2+}-loop II residues Ser230, Cys231, and Asp237. Zn^{2+}not shown for clarity. **C**. Auto-ubiquitination assays with UbcH7 and GST-$HHARI^{RBR}$ which acts as both E3 and proxy substrate. This construct lacks the Ariadne domain and is therefore active (Duda et al., 2013). Single charge-swap mutation of RING1 (D237R) or UbcH7 (K96E) reduced auto-ubiquitination activity when combined with either WT UbcH7 or WT HHARI, respectively. When D237R-HHARI is combined with K96E-UbcH7, higher levels of activity are observed compared to K96E-UbcH7 and WT HHARI providing further evidence that RING1 Asp237 and UbcH7 Lys96 form a salt bridge at the RING1/UbcH7 interface. Reactions were quenched after 15min post ATP addition with SDS-page load dye and products were visualized by western blotting against GST.

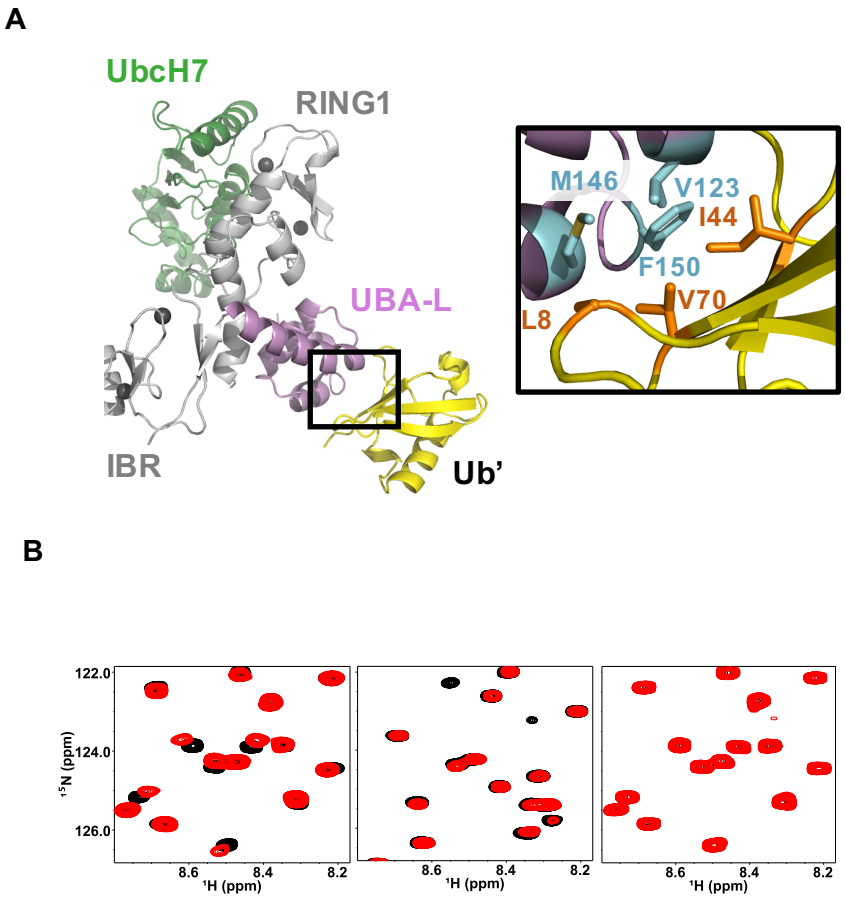

Figure 4. HHARI UBA-L domain binds Ub. **A.** HHARI UBA-L contacts Ub from a neighboring molecule (denoted as Ub') in the crystal structure. *INSET*. Central residues of the UBA-L/Ub' interface include V123, M146, & F150 (HHARI) and L8, I44, & V70 (Ub). **B**. *Left*. Overlay of ^{1}H-^{15}N-HSQC-type NMR spectra of wild-type (WT) Ub (black) and Ub in the presence of HHARI (red). Ub residues affected by HHARI binding are identified by shifting and broadening of red peaks relative to black peaks. *Middle*. The spectrum of L8A/I44A Ub in the presence of WT HHARI exhibits smaller perturbations which indicate reduced binding. *Right*. The HHARI mutant V123D/F150D shows substantially reduced binding to WT Ub, suggesting that HHARI residues V123 and F150 are critical for Ub binding.

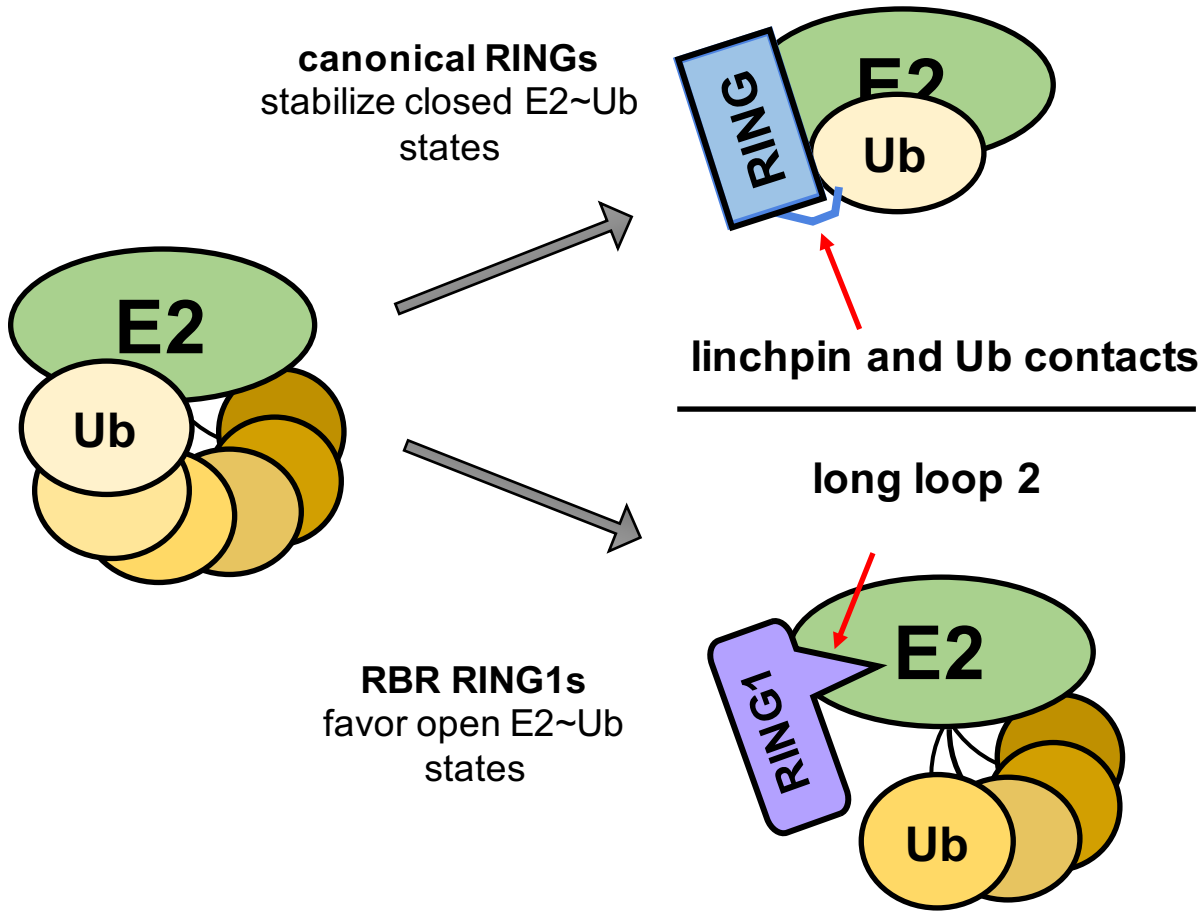

Figure 5. Model for action of canonical RING and RING1 domains with E2~Ubs. *Left*. E2~Ub conjugates exist as ensembles of closed and open states whose populations vary depending on the E2 in question (Dove et al.; Pruneda et al., 2011). *Upper Right*. Canonical RINGs stabilize closed E2~Ubs via RING/Ub contacts and a linchpin interaction to activate transfer to amino groups. *Bottom Right*. RBR RING1s bind to an E2~Ubs and protrusion of the extended Zn^{2+}-loop II inhibits adoption of closed states.

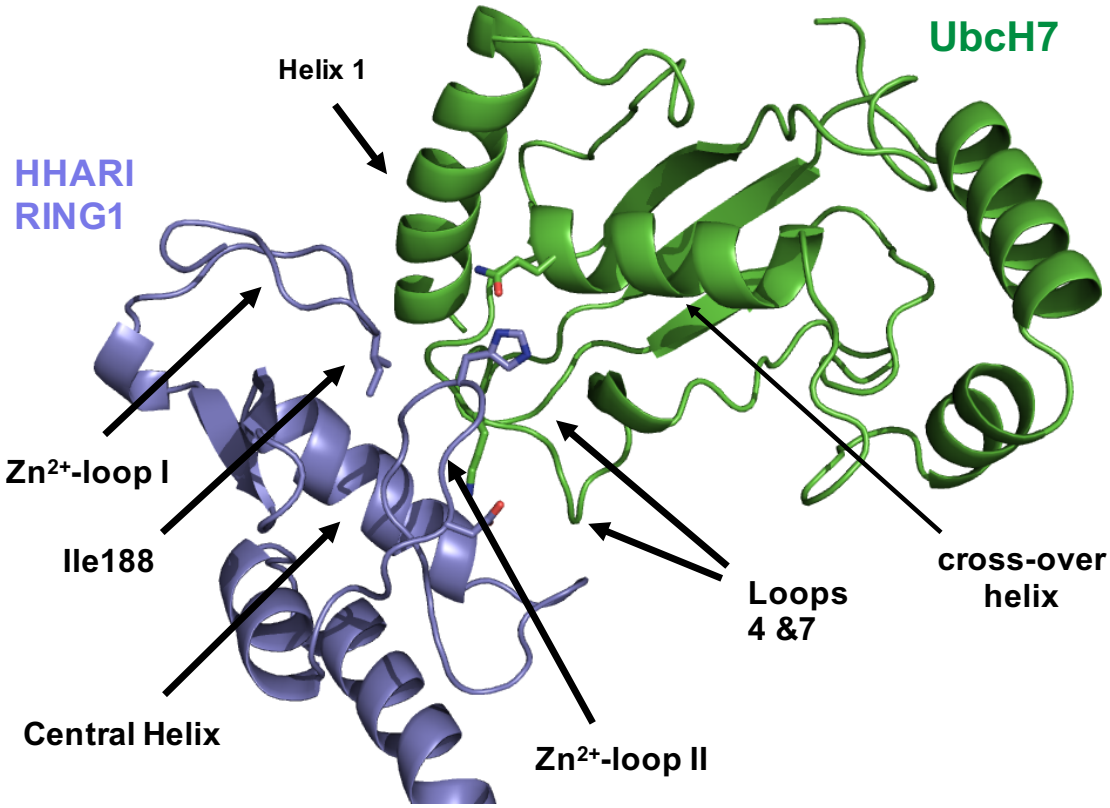

Figure S1. Related to Figure 1. Structural elements involved in the RING1:UbcH7 interface. Loops 4 and 7 and the N-terminus of helix 1 of UbcH7 and Zn^{2+}-loops I & II and the central helix of HHARI RING1 are identified.

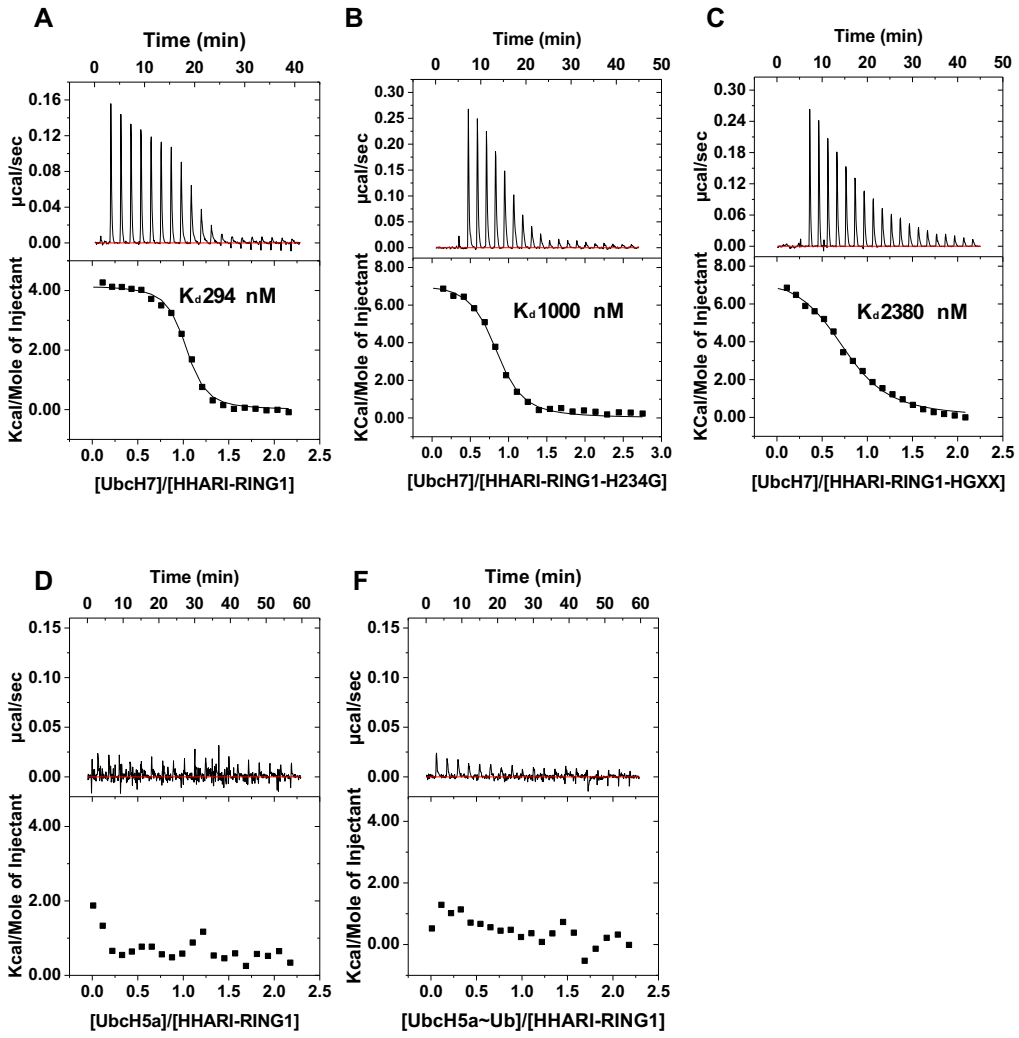

Figure S2. Related to Figure 1. Calorimetric titrations of UbcH7 and HHARI RING1 wild-type, H234G, and ΔH234G235 (A-C, respectively). D) and E) Calorimetric titrations of HHARI RING1 and UbcH5a and UbcH5a~Ub. For each titration the raw data and the normalized binding curve are reported. When measurable, dissociation constants are reported.

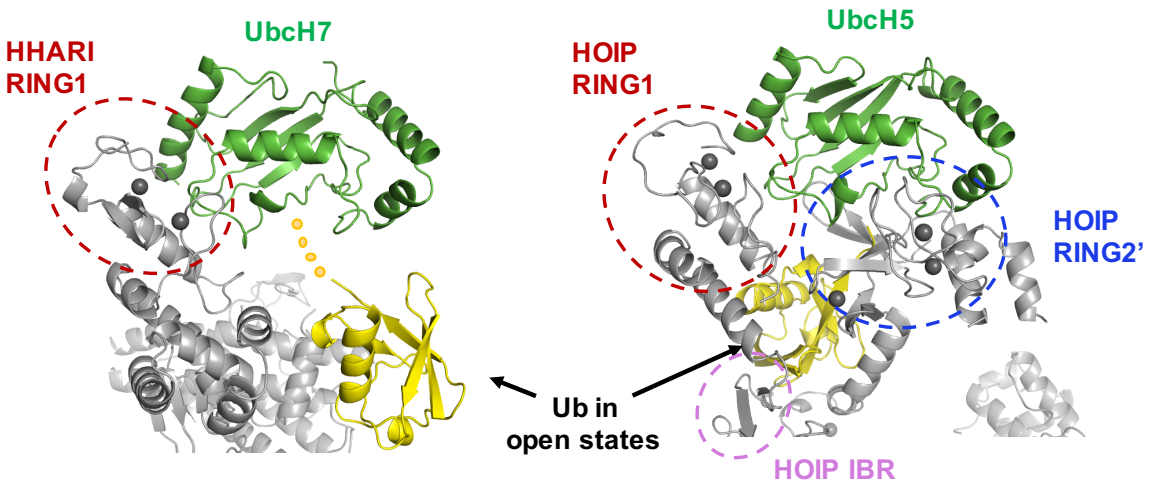

Figure S3. Related to Figure 2. Comparison of HHARI/UbcH7~Ub and HOIP-LDD/UbcH5~Ub**.** In both structures, the RING1 domain binds the E2 (green) and the E2~Ub is in an open conformation. *Left.* The Ub moiety (yellow) of UbcH7~Ub bound to HHARI does not contact any cognate HHARI domains. Yellow dots represent the C-terminus of Ub for which there is no observable density. *Right.* Ub of UbcH5~Ub bound to HOIP-LDD makes substantial contacts with the E3 via the C-terminal helix of RING1, the IBR, and RING2' of a neighboring polypeptide.

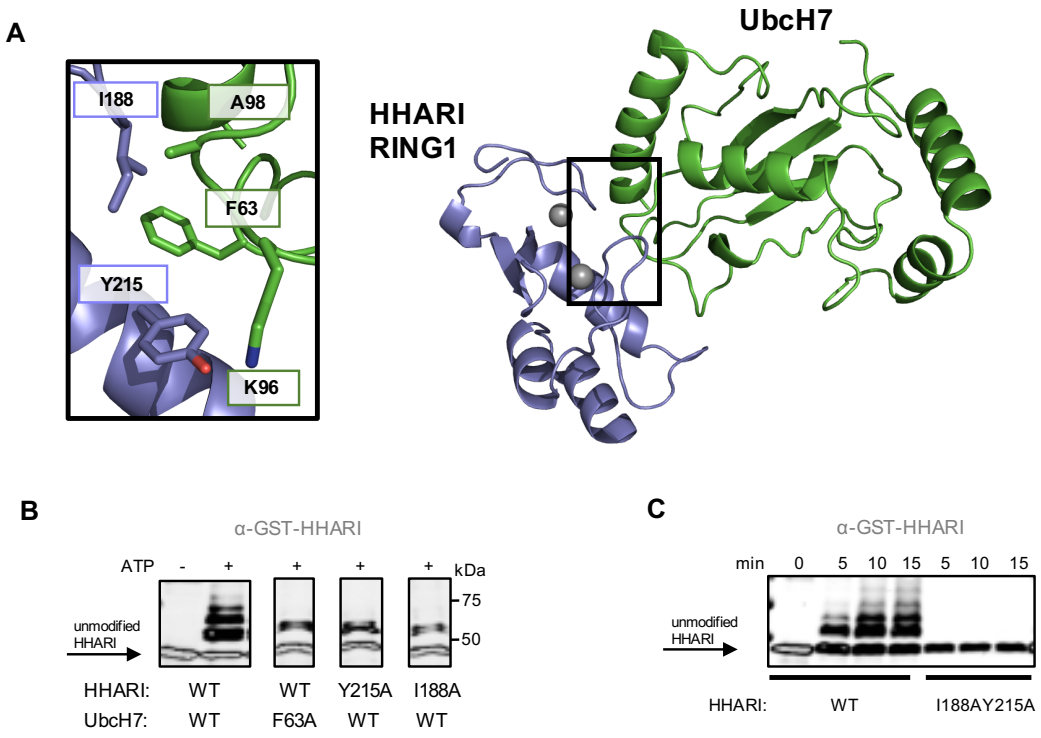

Figure S4. Related to Figure 3. **A.** Features of the RING1/UbcH7 interface that are reminiscent of canonical RING/E2 complexes. UbcH7 loop 4 residue Phe63 contacts HHARI RING1 residues Ile188 in Zn^{2+}-loop I and Tyr215 in the central helix. UbcH7 Phe63 is analogous to Phe62 in UbcH5 and RING1 Ile188 is analogous to a highly conserved Ile residue in canonical RINGs (for example, Ile26 in BRCA1) both of which play a pivotal role in canonical RING/E2 interactions; and hydrophobic residues emanating from the central helix of RINGs are also known to be involved in E2 interactions. **B.** Auto-ubiquitination assays with UbcH7 and GST-$HHARI^{RBR}$ which acts as both E3 and proxy substrate. This construct lacks the Ariadne domain and is therefore active (Duda et al., 2013). Mutation of UbcH7 residue (F63A) or HHARI RING1 residues Y215A and I188A at the RING1/UbcH7 interface reduce auto-ubiquitination activity (Duda et al., 2013; Scott et al., 2016). Reactions were quenched after 5min post ATP addition with SDS-page load dye and products were visualized by western blotting against GST. **C.** Auto-ubiquitination assays with UbcH7 and GST-$HHARI^{RBR}$. The double mutant I188A/Y215A of HHARI RING1 residues found at the RING1:UbcH7 interface drastically reduces auto-ubiquitination activity. Each indicated time post-ATP addition was quenched with SDS-page load dye and products were visualized by western blotting against GST.

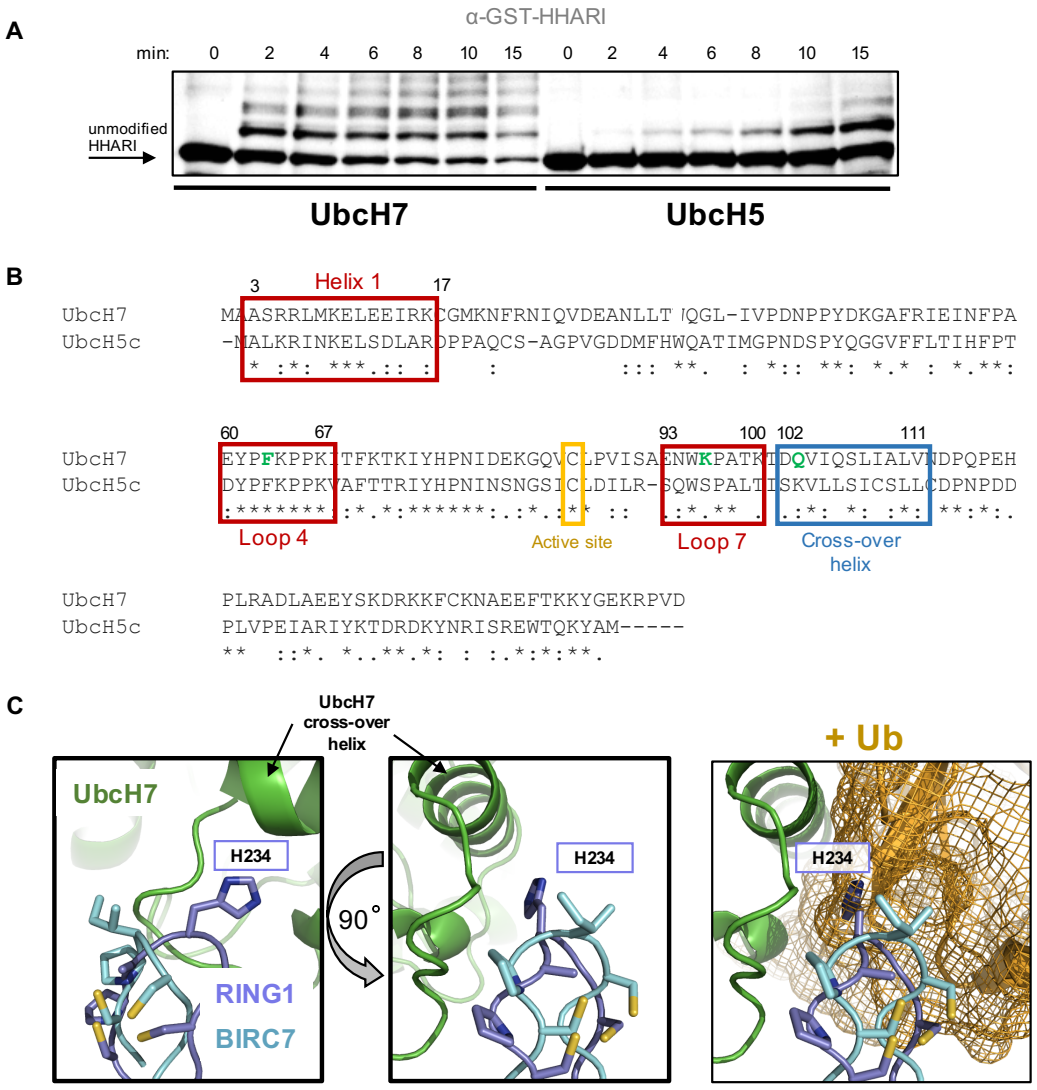

Figure S5. Related to Figure 3. Comparison of UbcH7 and UbcH5. **A.** Auto-ubiquitination assays comparing activity of UbcH7 and UbcH5 with GST-HHARI^{RBR} that acts as both an E3 and as proxy substrate. This construct lacks the Ariadne domain and is therefore active (Duda et al., 2013). Times given are post-ATP addition and products were visualized by western blotting against GST. **B.** Clustal Omega sequence alignment of UbcH7 and UbcH5c. Structural elements (Helix 1, Loops 4 & 7) typically involved in RING binding are marked with red boxes. Loop 4 is highly conserved between UbcH5c and UbcH7, while Helix 1 and Loop 7 are variable. Residues in the cross-over helix are indicated with a blue box. Active site Cys residues are highlighted by a yellow box. UbcH7 residues Phe63, Lys96, and Gln103 (highlighted in Fig. 3) are colored green. **C.** Structural overlays centered on the E2s of HHARI RING1:UbcH7~Ub and the canonical RING BIRC7:UbcH5~Ub. *Left & Middle*. Overlay of HHARI RING1 and BIRC7 shows that Zn^{2+}-loop II of HHARI RING1 (with His234 at its tip), but not BIRC7 reaches toward the cross-over helix of the E2 UbcH7 (UbcH5~Ub bound to BIRC7 not shown). *Right*. Same view as in the middle panel with the Ub moiety from the closed state of UbcH5~Ub bound to BIRC7 displayed in yellow mesh. The structural overlay reveals that the tip of HHARI Zn^{2+}-loop II, C^{231}-P-A-H-G-C^{236}, would clash sterically with Ub in the closed state.

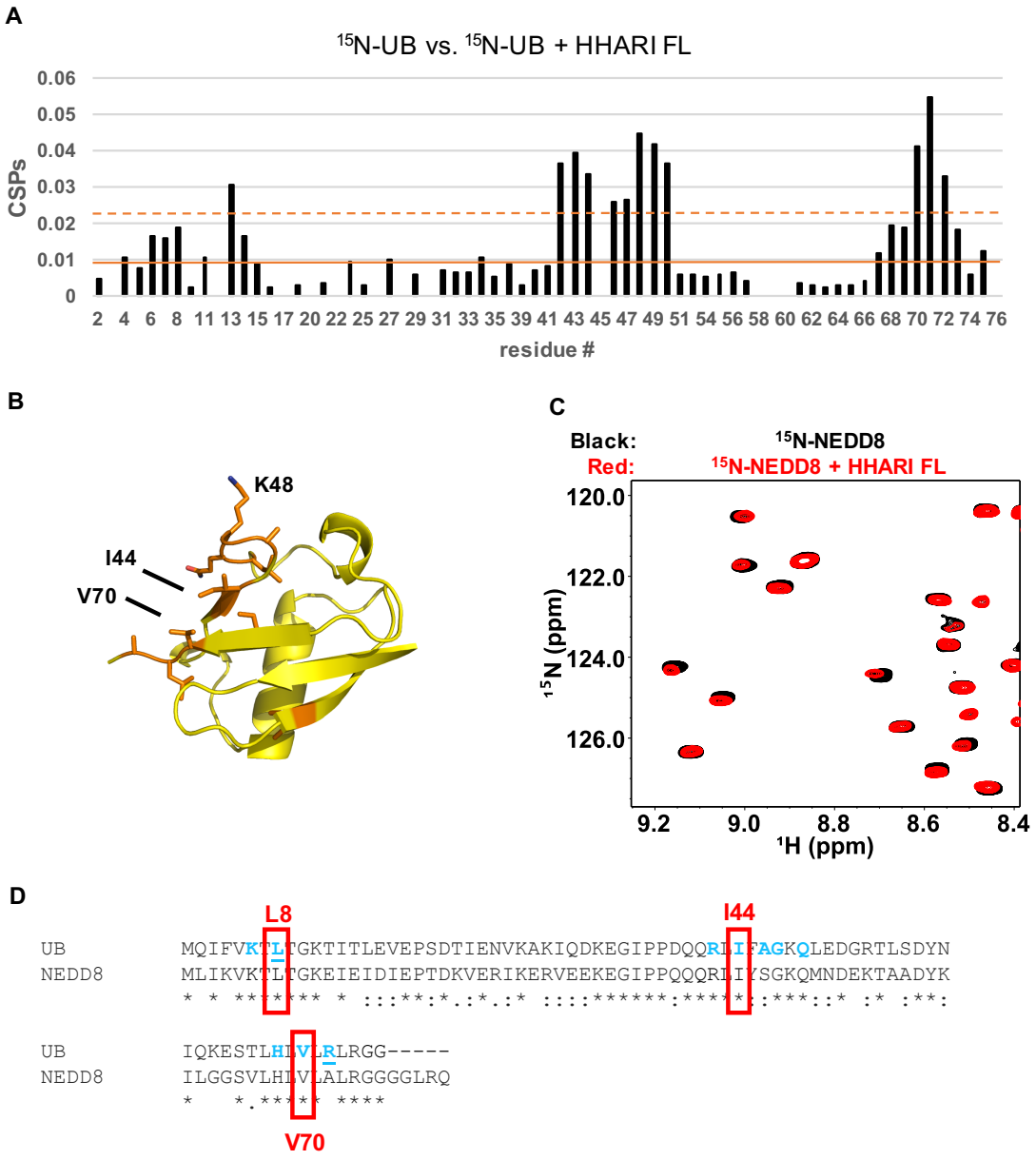

Figure S6. Related to Figure 4. HHARI binds Ub and NEDD8. **A.** Histogram of Chemical Shift Perturbations (CSPs) between ^{15}N-Ub in the absence and presence of 0.4 mole equiv. HHARI full-length (FL). The average (0.012) and AVG+1STDV (0.025) are indicated with a solid and dashed orange line, respectively. **B.** CSPs for wild-type Ub bound to HHARI-FL (Fig. 4B) are mapped onto a Ub structure (PDB 1UBQ). Ub residues with CSPs larger than 1STDV are colored orange. **C.** Overlay of ^{1}H-^{15}N-HSQC NMR spectra of free NEDD8 in the absence (black) and presence (red) of 0.4 mol equiv. of HHARI FL. Peaks shift and broaden in the presence of HHARI indicative of HHARI binding to NEDD8. **D.** Clustal Omega sequence alignment of Ub and NEDD8 reveals that UB residues (Leu8, Ile44 & Val70) central to HHARI UBA-L binding (Fig. 4 A&B) are conserved in NEDD8 (red boxes). Ub residues that contact a UBA-L of a neighboring HHARI subunit are highlighted in blue; of those, Leu8 and Val70 lack observable side chain density (underlined).

References

Adams, P.D., Afonine, P.V., Bunkoczi, G., Chen, V.B., Davis, I.W., Echols, N., Headd, J.J., Hung, L.W., Kapral, G.J., Grosse-Kunstleve, R.W.*, et al.* (2010). PHENIX: a comprehensive Python-based system for macromolecular structure solution. Acta Crystallogr D Biol Crystallogr *66*, 213-221.

Brown, N.G., Watson, E.R., Weissmann, F., Jarvis, M.A., VanderLinden, R., Grace, C.R., Frye, J.J., Qiao, R., Dube, P., Petzold, G.*, et al.* (2014). Mechanism of polyubiquitination by human anaphase-promoting complex: RING repurposing for ubiquitin chain assembly. Mol Cell *56*, 246-260.

Brunger, A.T., Adams, P.D., Clore, G.M., DeLano, W.L., Gros, P., Grosse-Kunstleve, R.W., Jiang, J.S., Kuszewski, J., Nilges, M., Pannu, N.S.*, et al.* (1998). Crystallography & NMR system: A new software suite for macromolecular structure determination. Acta Crystallogr D Biol Crystallogr *54*, 905-921.

Brzovic, P.S., Keeffe, J.R., Nishikawa, H., Miyamoto, K., Fox, D., 3rd, Fukuda, M., Ohta, T., and Klevit, R. (2003). Binding and recognition in the assembly of an active BRCA1/BARD1 ubiquitin-ligase complex. Proc Natl Acad Sci U S A *100*, 5646-5651.

Chen, V.B., Arendall, W.B., 3rd, Headd, J.J., Keedy, D.A., Immormino, R.M., Kapral, G.J., Murray, L.W., Richardson, J.S., and Richardson, D.C. (2010). MolProbity: all-atom structure validation for macromolecular crystallography. Acta Crystallogr D Biol Crystallogr *66*, 12-21.

Christensen, D.E., Brzovic, P.S., and Klevit, R.E. (2007). E2-BRCA1 RING interactions dictate synthesis of mono- or specific polyubiquitin chain linkages. Nat Struct Mol Biol *14*, 941-948.

DaRosa, P.A., Wang, Z., Jiang, X., Pruneda, J.N., Cong, F., Klevit, R.E., and Xu, W. (2015). Allosteric activation of the RNF146 ubiquitin ligase by a poly(ADP-ribosyl)ation signal. Nature *517*, 223-226.

Das, R., Mariano, J., Tsai, Y.C., Kalathur, R.C., Kostova, Z., Li, J., Tarasov, S.G., McFeeters, R.L., Altieri, A.S., Ji, X.*, et al.* (2009). Allosteric activation of E2-RING finger-mediated ubiquitylation by a structurally defined specific E2-binding region of gp78. Mol Cell *34*, 674-685.

Delaglio, F., Grzesiek, S., Vuister, G.W., Zhu, G., Pfeifer, J., and Bax, A. (1995). NMRPipe: a multidimensional spectral processing system based on UNIX pipes. J Biomol NMR *6*, 277-293.

Dou, H., Buetow, L., Sibbet, G.J., Cameron, K., and Huang, D.T. (2012). BIRC7-E2 ubiquitin conjugate structure reveals the mechanism of ubiquitin transfer by a RING dimer. Nat Struct Mol Biol *19*, 876-883.

Dou, H., Buetow, L., Sibbet, G.J., Cameron, K., and Huang, D.T. (2013). Essentiality of a non-RING element in priming donor ubiquitin for catalysis by a monomeric E3. Nat Struct Mol Biol *20*, 982-986.

Dove, K.K., Stieglitz, B., Duncan, E.D., Rittinger, K., and Klevit, R.E. (2016). Molecular insights into RBR E3 ligase ubiquitin transfer mechanisms. EMBO Rep *17*, 1221-1235.

Duda, D.M., Olszewski, J.L., Schuermann, J.P., Kurinov, I., Miller, D.J., Nourse, A., Alpi, A.F., and Schulman, B.A. (2013). Structure of HHARI, a RING-IBR-RING ubiquitin ligase: autoinhibition of an Ariadne-family E3 and insights into ligation mechanism. Structure *21*, 1030-1041.

Emsley, P., Lohkamp, B., Scott, W.G., and Cowtan, K. (2010). Features and development of Coot. Acta Crystallogr D Biol Crystallogr *66*, 486-501.

Johnson, B.A., and Blevins, R.A. (1994). NMR View: A computer program for the visualization and analysis of NMR data. J Biomol NMR *4*, 603-614.

Kabsch, W. (2010). Xds. Acta Crystallogr D Biol Crystallogr *66*, 125-132.

Kamadurai, H.B., Souphron, J., Scott, D.C., Duda, D.M., Miller, D.J., Stringer, D., Piper, R.C., and Schulman, B.A. (2009). Insights into ubiquitin transfer cascades from a structure of a UbcH5B approximately ubiquitin-HECT(NEDD4L) complex. Mol Cell *36*, 1095-1102.

Kelsall, I.R., Duda, D.M., Olszewski, J.L., Hofmann, K., Knebel, A., Langevin, F., Wood, N., Wightman, M., Schulman, B.A., and Alpi, A.F. (2013). TRIAD1 and HHARI bind to and are activated by distinct neddylated Cullin-RING ligase complexes. EMBO J *32*, 2848-2860.

Kim, H.C., and Huibregtse, J.M. (2009). Polyubiquitination by HECT E3s and the determinants of chain type specificity. Mol Cell Biol *29*, 3307-3318.

Kim, H.T., Kim, K.P., Lledias, F., Kisselev, A.F., Scaglione, K.M., Skowyra, D., Gygi, S.P., and Goldberg, A.L. (2007). Certain pairs of ubiquitin-conjugating enzymes (E2s) and ubiquitin-protein ligases (E3s) synthesize nondegradable forked ubiquitin chains containing all possible isopeptide linkages. J Biol Chem *282*, 17375-17386.

Koliopoulos, M.G., Esposito, D., Christodoulou, E., Taylor, I.A., and Rittinger, K. (2016). Functional role of TRIM E3 ligase oligomerization and regulation of catalytic activity. EMBO J *35*, 1204-1218.

Kumar, A., Aguirre, J.D., Condos, T.E., Martinez-Torres, R.J., Chaugule, V.K., Toth, R., Sundaramoorthy, R., Mercier, P., Knebel, A., Spratt, D.E*., et al.* (2015). Disruption of the autoinhibited state primes the E3 ligase parkin for activation and catalysis. EMBO J *34*, 2506-2521.

Lechtenberg, B.C., Rajput, A., Sanishvili, R., Dobaczewska, M.K., Ware, C.F., Mace, P.D., and Riedl, S.J. (2016). Structure of a HOIP/E2~ubiquitin complex reveals RBR E3 ligase mechanism and regulation. Nature *529*, 546-550.

Li, S., Liang, Y.H., Mariano, J., Metzger, M.B., Stringer, D.K., Hristova, V.A., Li, J., Randazzo, P.A., Tsai, Y.C., Ji, X.*, et al.* (2015). Insights into Ubiquitination from the Unique Clamp-like Binding of the RING E3 AO7 to the E2 UbcH5B. J Biol Chem *290*, 30225-30239.

Metzger, M.B., Pruneda, J.N., Klevit, R.E., and Weissman, A.M. (2014). RING-type E3 ligases: master manipulators of E2 ubiquitin-conjugating enzymes and ubiquitination. Biochim Biophys Acta *1843*, 47-60.

Miyamoto, K., Saito, K., Koshiba, S., Inoue, M., Kigawa, T., Yokoyama, S., RIKEN Structural Genomics/Proteomics Initiative. (2004). Solution Structure of the RING finger Domain of the human UbcM4-interacting Protein 4.

Murshudov, G.N., Vagin, A.A., and Dodson, E.J. (1997). Refinement of macromolecular structures by the maximum-likelihood method. Acta Crystallogr D Biol Crystallogr *53*, 240-255.
Ness, S.R., de Graaff, R.A., Abrahams, J.P., and Pannu, N.S. (2004). CRANK: new methods for automated macromolecular crystal structure solution. Structure *12*, 1753-1761.

Plechanovova, A., Jaffray, E.G., Tatham, M.H., Naismith, J.H., and Hay, R.T. (2012). Structure of a RING E3 ligase and ubiquitin-loaded E2 primed for catalysis. Nature *489*, 115-120.

Pruneda, J.N., Littlefield, P.J., Soss, S.E., Nordquist, K.A., Chazin, W.J., Brzovic, P.S., and Klevit, R.E. (2012). Structure of an E3:E2~Ub complex reveals an allosteric mechanism shared among RING/U-box ligases. Mol Cell *47*, 933-942.
Pruneda, J.N., Stoll, K.E., Bolton, L.J., Brzovic, P.S., and Klevit, R.E. (2011). Ubiquitin in motion: structural studies of the ubiquitin-conjugating enzyme approximately ubiquitin conjugate. Biochemistry *50*, 1624-1633.
Riley, B.E., Lougheed, J.C., Callaway, K., Velasquez, M., Brecht, E., Nguyen, L., Shaler, T., Walker, D., Yang, Y., Regnstrom, K.*, et al.* (2013). Structure and function of Parkin E3 ubiquitin ligase reveals aspects of RING and HECT ligases. Nat Commun *4*, 1982.

Rodrigo-Brenni, M.C., and Morgan, D.O. (2007). Sequential E2s drive polyubiquitin chain assembly on APC targets. Cell *130*, 127-139.

Sauve, V., Lilov, A., Seirafi, M., Vranas, M., Rasool, S., Kozlov, G., Sprules, T., Wang, J., Trempe, J.F., and Gehring, K. (2015). A Ubl/ubiquitin switch in the activation of Parkin. EMBO J *34*, 2492-2505.

Schroder, G.F., Levitt, M., and Brunger, A.T. (2010). Super-resolution biomolecular crystallography with low-resolution data. Nature *464*, 1218-1222.

Schrödinger, L. (2002). The PyMOL Molecular Graphics System, Version 1.8.2.0.

Scott, D.C., Rhee, D.Y., Duda, D.M., Kelsall, I.R., Olszewski, J.L., Paulo, J.A., de Jong, A., Ovaa, H., Alpi, A.F., Harper, J.W*., et al.* (2016). Two Distinct Types of E3 Ligases Work in Unison to Regulate Substrate Ubiquitylation. Cell *166*, 1198-1214 e1124.

Scott, D.C., Sviderskiy, V.O., Monda, J.K., Lydeard, J.R., Cho, S.E., Harper, J.W., and Schulman, B.A. (2014). Structure of a RING E3 trapped in action reveals ligation mechanism for the ubiquitin-like protein NEDD8. Cell *157*, 1671-1684.

Sheldrick, G.M. (2010). Experimental phasing with SHELXC/D/E: combining chain tracing with density modification. Acta Crystallogr D Biol Crystallogr *66*, 479-485.

Sheu, S.Y., Yang, D.Y., Selzle, H.L., and Schlag, E.W. (2003). Energetics of hydrogen bonds in peptides. Proc Natl Acad Sci U S A *100*, 12683-12687.

Smit, J.J., Monteferrario, D., Noordermeer, S.M., van Dijk, W.J., van der Reijden, B.A., and Sixma, T.K. (2012). The E3 ligase HOIP specifies linear ubiquitin chain assembly through its RING-IBR-RING domain and the unique LDD extension. EMBO J *31*, 3833-3844.

Spratt, D.E., Walden, H., and Shaw, G.S. (2014). RBR E3 ubiquitin ligases: new structures, new insights, new questions. Biochem J *458*, 421-437.

Stieglitz, B., Morris-Davies, A.C., Koliopoulos, M.G., Christodoulou, E., and Rittinger, K. (2012). LUBAC synthesizes linear ubiquitin chains via a thioester intermediate. EMBO Rep *13*, 840-846.

Stieglitz, B., Rana, R.R., Koliopoulos, M.G., Morris-Davies, A.C., Schaeffer, V., Christodoulou, E., Howell, S., Brown, N.R., Dikic, I., and Rittinger, K. (2013). Structural basis for ligase-specific conjugation of linear ubiquitin chains by HOIP. Nature *503*, 422-426.

Trempe, J.F., Sauve, V., Grenier, K., Seirafi, M., Tang, M.Y., Menade, M., Al-Abdul-Wahid, S., Krett, J., Wong, K., Kozlov, G*., et al.* (2013). Structure of parkin reveals mechanisms for ubiquitin ligase activation. Science *340*, 1451-1455.

Wang, M., Cheng, D., Peng, J., and Pickart, C.M. (2006). Molecular determinants of polyubiquitin linkage selection by an HECT ubiquitin ligase. EMBO J *25*, 1710-1719.

Wang, M., and Pickart, C.M. (2005). Different HECT domain ubiquitin ligases employ distinct mechanisms of polyubiquitin chain synthesis. EMBO J *24*, 4324-4333.

Wauer, T., and Komander, D. (2013). Structure of the human Parkin ligase domain in an autoinhibited state. EMBO J *32*, 2099-2112.

Wauer, T., Simicek, M., Schubert, A., and Komander, D. (2015). Mechanism of phospho-ubiquitin-induced PARKIN activation. Nature *524*, 370-374.

Wenzel, D.M., Lissounov, A., Brzovic, P.S., and Klevit, R.E. (2011). UBCH7 reactivity profile reveals parkin and HHARI to be RING/HECT hybrids. Nature *474*, 105-108.

Xu, Z., Kohli, E., Devlin, K.I., Bold, M., Nix, J.C., and Misra, S. (2008). Interactions between the quality control ubiquitin ligase CHIP and ubiquitin conjugating enzymes. BMC Struct Biol *8*, 26.

Zhang, W., Wu, K.P., Sartori, M.A., Kamadurai, H.B., Ordureau, A., Jiang, C., Mercredi, P.Y., Murchie, R., Hu, J., Persaud, A.*, et al.* (2016). System-Wide Modulation of HECT E3 Ligases with Selective Ubiquitin Variant Probes. Mol Cell *62*, 121-136.

Zheng, N., Wang, P., Jeffrey, P.D., and Pavletich, N.P. (2000). Structure of a c-Cbl-UbcH7 complex: RING domain function in ubiquitin-protein ligases. Cell *102*, 533-539.

Chapter IV: Two functionally distinct E2/E3 pairs coordinate sequential ubiquitination of a common substrate in *C. elegans* development

The following manuscript is currently under revision at the journal ***PNAS.***

Katja K. Dove‡, Hilary A. Kemp‡, Luke J. Milburn, David Camacho, Dana L. Miller*, Rachel E. Klevit*

Department of Biochemistry, University of Washington School of Medicine, Seattle, WA 98195

‡ equal contribution

*Corresponding authors:
REK: email, klevit@uw.edu
DLM: email, dlm16@uw.edu

Author contributions

K.K.D., H.K., D.L.M. and R.E.K. conceived the experiments and wrote the manuscript. K.K.D. performed biochemical assays. H.K. and D.C. performed genetic screens. K.K.D., H.K., D.L.M. and R.E.K. analyzed data. L.J.M. executed yeast two-hybrid experiments.

Introduction

Protein ubiquitination is a posttranslational modification that regulates virtually every aspect of cellular function in eukaryotes. Covalent attachment of the small protein ubiquitin (Ub) to other cellular proteins can lead to myriad outcomes, including proteasomal degradation of the substrate, change of cellular localization, or effects on enzymatic activity and protein-protein interactions (1). Protein ubiquitination is accomplished via a trio of enzymes: a ubiquitin-activating enzyme (E1), a Ub-conjugating enzyme (E2), and a Ub ligase (E3). The E1 activates the C-terminus of Ub and transfers the activated Ub onto an E2 active site cysteine (Cys) to generate a E2~Ub ("~" denotes a thioester bond) which interacts with an E3 Ub ligase to coordinate substrate ubiquitination. A given organism has 1-2 E1s, dozens of E2s, and hundreds of E3s.

Three classes of eukaryotic E3s utilize distinct Ub-transfer mechanisms. The largest class, the RING (Really Interesting New Gene) E3s, do not contain an active site; they bind E2~Ub to activate Ub transfer directly onto a substrate. RBR (RING-in-between-RING) and HECT (Homologous to E6AP C-Terminus) E3s contain an active site Cys residue to which Ub is transferred from the E2~Ub to generate a covalent E3~Ub thioester that transfers Ub to a substrate amino group, often a lysine (Lys) residue. Most E2s can transfer Ub either onto Cys residues (transthiolation) when bound to RBR- and HECT-type E3 or Lys residues (aminolysis) when bound to RING-type E3s. The E2 UbcH7 is unique in that it can only perform transthiolation reactions and is therefore a dedicated E2 for RBR and HECT E3s(2).

Relatively little is known about the biological role of UBCH7. Lacking a homologue in yeast, UBCH7 is highly conserved in worms and flies. The *C.elegans* homolog, UBC-18, is implicated in developmental processes via its cooperation with the RBR E3 ARI-1(3). In human

cell culture, UBCH7 has been shown to regulate S-phase transition of the cell cycle (4). To date, it is mainly the multi-subunit RING-type E3s known as Cullin-RING Ligases (CRL) that are associated with substrate ubiquitination during the cell cycle (5-7). However, as UbcH7 is unable to work with RING E3s, how it performs its role during the cell cycle is unclear.

UBC-18 displays the same biochemical properties as its human counterpart and is only able to work with RBR and HECT E3s, but not RING E3s (2). Although a *ubc-18* loss of function allele is viable, worms carrying this allele show a reduced growth rate and reduction in brood size (8). Furthermore, in combination with loss-of-function in the Retinoblastoma ortholog *lin-35*, *ubc-18* mutants arrest as first stage larvae with a lethal defect in formation of the pharynx, the anterior most portion of the worm gastro-intestinal tract (8).

To deepen our understanding of the biological role of UbcH7, we conducted an RNAi screen to identify genes that interact genetically with *ubc-18* in *C. elegans*. Our screen revealed that the *C. elegans* ortholog of the conserved E2 *CDC34*, *ubc-3*, acts with *ubc-18* in pharyngeal development. *CDC34* is considered a dedicated E2 for Skp/Cullin/Fbox (SCF)-type E3s, a sub-class of CRLs. We further uncovered synthetic genetic relationships between *ubc-18* and other components of SCF-type RING E3s. As UBC-18 is incapable of working with RING E3s and UBC-3 is a dedicated E2 for CRL E3s, these two E2s cannot be functionally redundant. Our data support a model in which UBC-18 and UBC-3 work either in parallel or coordinately. Recent studies in mammalian cell culture suggested that RBR and CRL E3 complexes can work together (9). Here we show that the E3/E3 pairs UBC-18/ARI-1 and UBC-3/CUL-1 work cooperatively to ubiquitinate the Skp1-like protein SUP-36. Our work provides the first biological evidence for the existence of cross-talk between two different types of E3s, RING-and RBR-type E3s, and their respective, dedicated E2s in an organism.

Results

ubc-18 and ubc-3 are redundantly required for pharyngeal development

To identify genes that interact synthetically with *ubc-18*, we performed a synthetic lethal RNAi screen using *ubc-18(ku354)* mutant worms. The *ku354* allele contains a substitution that changes a Glu at the E1 binding interface of UBC-18 to Lys, resulting in a loss-of-function likely due to reduced charging of UBC-18 with Ub (8). Despite a reduction in brood size and a slower growth rate, *ubc-18(ku354)* mutant worms are viable (8). In our primary screen, first larval stage (L1) worms were grown to adulthood on bacteria expressing gene-specific dsRNA clones from the Ahringer library (10). A total of 12,982 clones from the genome-wide Arhinger library were screened, representing 67% of total predicted genes in the *C. elegans* genome (10). We screened only clones from the somatic chromosomes (a total of 14,400 library clones), and a fraction of these (9.8%) failed to grow. Our primary screen identified 213 genes that caused a stronger phenotype when depleted in *ubc-18(ku354)* mutant animals compared to wild-type controls. Bacterial clones that caused a phenotype in the *ubc-18(ku354)* mutant strain but not in wild-type animals were re-tested three times to find those with robust synthetic interactions. RNAi clones that showed identical phenotypes in both wild-type and *ubc-18* mutants were excluded from further analysis. Of 12,982 clones from the Arhinger library screened, 213 were selected for secondary screening, of which sixteen robustly and reproducibly exhibited synthetic phenotypes with *ubc-18* upon rescreening (Table 1). Among these candidates was *lin-35*, previously shown to be synthetically lethal with *ubc-18*, validating our screening method (Fig. 1A, (8)).

To our surprise we found that depletion of *ubc-3,* an E2 Ub-conjugating enzyme homologous to mammalian *CDC34*, was lethal for *ubc-18* mutant animals (Fig. 1A). Of the remaining fifteen genes identified, twelve are synthetically lethal and three synthetically sterile

with *ubc-18* (Table 1). The products of those genes include components of the ubiquitination machinery, metabolic enzymes, and nuclear proteins involved in transcription or splicing. We were especially interested in the interaction of *ubc-18* with *ubc-3*. Based on known properties of the mammalian homologues, it is highly unlikely that *ubc-3* and *ubc-18* act redundantly with the same E3. The UBC-3 homologue in humans, CDC34, is a dedicated E2 for CRLs, the multi-subunit RING-type E3s that target cellular substrates for proteasomal degradation (7, 11). The mammalian homologue of UBC-18, UbcH7, is biochemically restricted to function only with RBR and HECT E3s and cannot function with CRLs (2). A synthetic interaction between these two E2s implied a cooperation between an RBR E3 and a RING-type CRL.

To validate the synthetic interaction observed between *ubc-18* and *ubc-3*, we tested another allele of *ubc-18*, *tm5426*. The *tm5426* allele is a 308 bp deletion beginning in the second exon and extending into the third intron, and is a predicted molecular null. We found that *ubc-18(tm5426)* animals arrested as L1 when grown on *ubc-3(RNAi)* (Fig. S1), similar to *ubc-18(ku354)* mutant animals (Fig. 1A). We conclude that the synthetic lethal interaction between *ubc-18* and *ubc-3* is robust and statistically significant.

We noted that *ubc-18* mutant animals grown on *ubc-3(RNAi)* arrest as L1, reminiscent of the reported synthetic phenotype between *ubc-18* and *lin-35*, in which simultaneous inactivation of *ubc-18* and *lin-35* results in the Pharynx unattached (Pun) phenotype (8). Pun animals have a defect in pharyngeal morphogenesis in which the anterior end of the pharynx does not attach properly to the buccal cavity. As a result, Pun animals are unable to feed, arrest as L1, and subsequently die (8). We considered the possibility that the synthetic interaction between *ubc-18* and *ubc-3* also results in a Pun phenotype. Indeed, examination of *ubc-18; ubc-3(RNAi)* animals revealed a significant fraction of Pun L1 (Fig. 1B,C & S2). We scored the frequency of the Pun

phenotype only in hatched larvae, so animals that died during embryogenesis were not included. While there was variability in the penetrance of this phenotype among experiments, we never observed the Pun phenotype in wild-type animals, consistent with previous reports (Fig. 1C & S2; (8, 12)). Although we did measure low frequency Pun larvae (1-2%) for *ubc-18(ku354)* mutant animals grown on the control RNAi food, the penetrance was much greater in the *ubc-3(RNAi)* animals (Fig. 1C). These data suggest that *ubc-3* also acts in the genetic network controlling pharyngeal morphogenesis.

We used additional genetic tools to test the hypothesis that *ubc-3* acts with *ubc-18* in pharyngeal morphogenesis. To address this possibility, we asked if *ubc-3* was synthetically lethal with *pha-1*, a novel gene that acts redundantly with class B SunMuv genes to regulate pharyngeal development (12). We found a high penetrance of the Pun phenotype in *pha-1(e2123ts)* mutant animals grown on *ubc-3* RNAi food at the permissive temperature of 15°C (Fig. 1C & S2) similar to what has been seen in *ubc-18(RNAi); pha-1(e2123ts)* animals (12). We also found that disruption of *sup-35*, *sup-36*, or *sup-37*, genetic suppressors of the *ubc-18*; *lin-35* synthetic interaction (3, 8), also suppressed the *ubc-18*; *ubc-3* synthetic interaction (Table 2). Altogether, the data show that *ubc-3* is a novel factor with *ubc-18*, *lin-35*, and *pha-1* in the previously described genetic network that regulates pharyngeal development.

Synthetic interactions between ubc-18 and genes of SCF E3 ubiquitination machinery

The genetic interaction between *ubc-18* and *ubc-3* suggests that a CRL E3 complex and RBR E3 cooperate in pharyngeal development. A subclass of CRLs, SCF (Skp1-Cullin1-FBox) E3 complexes are composed of a scaffold protein, Cullin-1, substrate-binding Fbox proteins, and the adaptor protein SKP1 that connects Fboxes to the CUL1 scaffold (13). Consistent with this

notion, our genome-wide RNAi screen also identified the Skp1-like CRL components *skr-1* and *skr-2*[1] as synthetically lethal with *ubc-18* (Table 1) which further strengthens our hypothesis that a CRL E3 complex and RBR E3 cooperate in the same pathway. However, our initial unbiased screen did not recover genes coding for CUL1 or FBOX proteins. To assess the role of other SCF components or other CRLs, we individually tested a set of CRL components for genetic interactions with *ubc-18* by RNAi. The *C. elegans* genome includes over twenty SKP1-related genes, six Cullin-RING E3s, and more than three hundred Fbox genes (14-17). We tested a set of candidate genes that included five Cullins (*cul-1, -2, -4, -5, -6*) and candidate SKP1-related (skr) and Fbox genes chosen based on published genetic and physical interactions with members of the pharyngeal attachment pathway (18-21).

Consistent with previous reports, we found only 25% of wild-type animals grown on *cul-1*(*RNAi)* survive to adulthood (22), which excluded it from our primary screen. However, lethality was significantly more penetrant for *ubc-18* mutant animals grown on *cul-1(RNAi)* food (Fig. 2A). Genetic interactions were not observed between *ubc-18* and *cul-4*, *-5*, or *-6*. To test for genetic interactions with *cul-2*, we used a temperature-sensitive *cul-2(or209)* allele(23). Although *ubc-3(RNAi)* was synthetically lethal with *cul-2(or209)* even at the permissive temperature, no synthetic phenotype was observed with either *lin-35* or *ubc-18* (Fig. 2B). This result suggests that while UBC-3 can function as an E2 for CUL-2 ligases in worms, this function is unrelated to the function of UBC-3 with UBC-18. Of the six SKP1-related genes tested, only *skr-1/2* was synthetically lethal with *ubc-18* (Fig. 2A). Neither *skr-10* nor *skr-17* led to lethality in *ubc-18* mutant animals, though these genes were reported to have synthetic genetic

[1] The *skr-2* gene is very similar to *skr-1*, and it is likely that both genes are targeted by either RNAi construct (14). We therefore refer to these as *skr-2/1* or *skr-1/2* RNAi in the remainder of this report (the intended target of the RNAi is noted first).

interactions with *lin-35* that result in larval lethality (21). We also did not observe genetic interactions with *skr-8* or *skr-9*, which suppress the synthetic lethality of *ubc-18; lin-35* animals (19). We conclude from these results that *ubc-3* works with *cul-1* and *skr-1/2* in pharyngeal development.

Due to the large number of Fbox proteins in worms, we considered it unlikely that we would find a single Fbox to recapitulate the loss-of-function of UBC-3, which works with many different SKR/CUL1/FBOX combinations. Instead, we used RNAi against *cand-1* to perturb FBOX function on a wider scale. CAND-1 is required for the exchange of SKP1/FBOX modules (and their substrates) on and off a SCF complex (24-26) and its depletion impacts known downstream outputs of SCF E3s in worms (27). We found that RNAi depletion of *cand-1* in wild type animals had no phenotype, but significantly reduced survival in *ubc-18* mutant animals (Fig. 2A). Moreover, while *cand-1* deletion mutants are viable, the additional knockdown of *lin-35* or *skr-1/2* is lethal (Fig. 2C). In sum, the data are consistent with a model in which the RBR/HECT-specific E2 *ubc-18* works coordinately with the E2 *ubc-3* and SCF-type E3s in pharyngeal development in worms.

sup-36 rescues synthetic lethality between ubc-18 and SCF components

We observed that the synthetic interactions between *ubc-18* and SCF components such as *ubc-3, skr-1/2,* and *cand-1* were suppressed by disruption of *sup-36* (Fig. 3A, Table 2), similar to genetic interactions of *ubc-18* and components of pharynx development (19). This further supports our assertion that *ubc-3* acts in same genetic pathway as *ubc-18*. Based on sequence similarity *sup-36* is predicted to encode a SKP1-like protein (19). Humans contain a single *SKP-1* gene and its protein product binds simultaneously to SCF subunits CUL1 and FBOX proteins.

SUP-36 was found to bind to several FBOX proteins (FBXC-20, FBXC-32, and FBXC-53) in yeast two-hybrid experiments (18-20), supporting the notion that it has SKP-like properties. To further test the assignment of SUP-36 as a SKP-like protein, we tested for interactions by a yeast two-hybrid assay. We observed a physical interaction between SUP-36 and CUL1 (Fig. 3B). Thus, SUP-36 can bind to both CUL1 and FBOX proteins, consistent with it being part of an SCF complex. The fact that *sup-36* suppresses the synthetic phenotype of *ubc-3* and *ubc-18* indicates that it acts to oppose the function(s) of the E2 enzymes. On this basis, we conclude that SUP-36 is a component of a SCF complex and functions to oppose that of UBC-3 and UBC-18.

UBC-18/ARI-1 and UBC-3/CUL-1 work together to ubiquitinate SUP-36

The E2/RBR E3 pair UBC-18/ARI-1 regulates protein levels of SUP-36(19), implying that SUP-36 may be a substrate of UBC-18/ARI-1. However, the human homologue of ARI-1, HHARI, cannot build the poly-Ub chains that are required for a substrate to be sent to the proteasome (Fig. S4A, (9)). In contrast, the human ortholog of UBC-3, CDC34, binds to CUL1 and is capable of generating poly-Ub chains that lead to substrate degradation (28-30). A physical interaction between human HHARI and neddylated CUL1, 2, 3 & 4A has been reported (31), and our genetic data here implies a functional interaction, in which the E2 for *ari-1*, *ubc-18,* works together with *cul-1* and *ubc-3* in pharyngeal development. Furthermore, as the genetic interaction between *ubc-18* and *ubc-3* is suppressed by a *sup-36* null allele (Table 3, Fig. 3A), we hypothesized that SUP-36 might be a common substrate of UBC-18/ARI-1 and UBC-3/CUL-1.

We used biochemical assays to assess the interplay between UBC-18 and UBC-3. We used human homologs for UBC-18 (UBCH7), UBC-3 (CDC34), ARI-1 (HHARI) and CUL1/RBX1 as they have high sequence similarity and we have previously demonstrated that

combined recombinant worm/human enzymes recapitulate biochemical activity (2). In reactions containing neddylated CUL1 (N8-CUL1/RBX1), UBCH7, and HHARI, we observe mono-ubiquitination of SUP-36 (Fig. 4A, lane 5). No Ub-modified SUP-36 product is detected when CDC34 is the only E2 in the reaction (Fig. 4A, lane 6), confirming that UBCH7, and not CDC34, works with HHARI to ubiquitinate SUP-36. Although UBCH7 can only transfer Ub via the RBR E3 HHARI, and not the RING E3 CUL1, CUL1 is required for mono-ubiquitination of SUP-36 by HHARI/UBCH7 (Fig. 4A lanes 2-5). This confirms previous studies suggesting that HHARI ligase activity is activated by N8-CUL1 (31). Furthermore, although CUL1 binds directly to SUP-36 in our yeast two-hybrid assay (Fig. 3B), no ubiquitination of SUP-36 was observed in reactions containing CDC34/CUL1/HHARI without UBCH7 (Fig. 4A, lane 6). Thus, binding to CUL1 is not sufficient for N8-CUL1/CDC34 to transfer Ub directly to SUP-36 without the function of UBCH7. Together the data support the notion that HHARI/UBCH7 carries out mono-ubiquitination of SUP-36 in a CUL1 dependent manner *in vitro*.

When all components (UBCH7/HHARI and CDC34/N8-CUL1) are present we observed higher molecular weight bands corresponding to poly-Ub chain formation on SUP-36 (Fig. 4A, lane 7). To confirm that the higher molecular weight bands correspond to poly-Ub chains, and not multiple mono-Ub, we repeated the assay using a Lys-less Ub mutant unable to form Ub-chains. With this mutant Ub we no longer observed higher molecular weight bands of SUP-36 (Fig. 4B), confirming that higher molecular weight species of SUP-36 in Fig. 4A, lane 7, contain Ub chains. This assay also reveals that the second modified SUP-36 band seen in Fig. 4A (lane 5) corresponds to addition of two mono-Ubs. We conclude that transfer of mono-Ub onto SUP-36 by HHARI/UBCH7 is required for chains to be built by N8-CUL1/CDC34. The results demonstrate that the two E2s and their respective E3s act in concert to generate poly-

ubiquitinated product(s). Considering the previously reported physical interaction between the Cullin-RING E3 and HHARI (31), it is tempting to speculate that the two E3s form a large multi-subunit, multi-functional E3 that requires two E2s, namely UBC-18 and UBC-3 in worms and by analogy, UBCH7 and CDC34 in humans.

Discussion

Here we present genetic and biochemical evidence to show that two different types of E3s, the RBR E3 HHARI/ARI-1 and the RING-type E3 CUL1, along with their dedicated E2s, UBCH7/UBC-18 and CDC34/UBC3, work cooperatively to ubiquitinate a common substrate, SUP-36. Proteasomal degradation of SUP-36 is likely a significant biological role of ARI-1/UBC-18 and CUL1/UBC-3 in pharyngeal morphogenesis, as RNAi against either UBC-18 or ARI-1 increases SUP-36 protein levels (19) and a SUP-36 null-allele rescues the synthetic lethal phenotype of *ubc-18;ubc-3* (Fig. 3A). We propose a model in which SUP-36 inhibits pharyngeal morphogenesis and its ubiquitination by ARI-1/UBC-18 and CUL-1/UBC-3 and subsequent proteasomal degradation is required for proper development of a pharynx (Fig. 5A). Modification of SUP-36 with Ub requires a minimum of three enzymes: HHARI/ARI-1, UBCH7/UBC-18, and N8-CUL1 (Fig. 4A, lanes 8-10). The E2 UBCH7 is unable to modify Lys residues and can only work with RBR/HECT-type E3s such as HHARI/ARI-1, but not with RING-type E3s such as CUL1 (2). Therefore, UBCH7's sole role in this complex is to transfer Ub to the active site of HHARI/ARI-1 which subsequently transfers Ub to SUP-36. As HHARI/ARI-1 cannot build Ub-chains (Fig. S4A, (9)), the sole product is mono-Ub-SUP-36 (Fig. 4A, lane 5).

Unexpectedly, we found that the presence of N8-CUL1 is required for SUP-36 ubiquitination by HHARI/UBCH7. This can be explained by two separate observations. First, we show here that CUL1 binds to SUP-36 by yeast two-hybrid, suggesting that CUL1 acts as a substrate-binding domain for HHARI (Fig. 3B). Second, formation of a complex between HHARI and N8-CUL1 has been shown to activate ligase activity of HHARI while recombinant HHARI is auto-inhibited on its own (31, 32). A fourth enzyme, CDC34/UBC-3, is required to build poly-Ub chains on SUP-36 that has been primed with a first Ub by HHARI/UBCH7 (Fig. 4A, lane 7). CDC34 is well known as a K48-linked Ub chain building E2, thereby marking substrates for proteasomal degradation (33). Altogether the observations lead to a model in which CUL1 binds to both SUP-36 and HHARI. The dedicated HHARI E2 UBCH7 (UBC-18) first transfers Ub to the active site of HHARI (Fig. 5B, Step1) which subsequently primes SUP-36 with one Ub (Fig. 5B, Step2). Following the mono-ubiquitination of SUP-36 by HHARI, CDC34/UBC-3 can build poly-Ub chains on SUP-36 (Fig. 5B, Step3) to mark it for proteasomal degradation.

Although the precise function of *sup-36* is still unknown, previous evidence indicates that *sup-36* inhibits pharyngeal development along with two other proteins *sup-35* and *sup-37*, possibly through the function of a large macromolecular complex (19). Consistent with that notion, both *sup-35* and *sup-37* mutant alleles also rescue the *ubc-18;ubc-3* synthetic phenotype (Table 2). A reduction of any component of the ubiquitination complex, ARI-1/UBC-18/CUL-1/UBC-3, likely increases SUP-36 protein levels. However, a complete loss of UBC-18 or a reduction of UBC-3 alone does not lead to a frequent Pun phenotype--a knockdown of both UBC-18 and UBC-3 is needed to observe a penetrant phenotype. This result implies that another E2 is able to perform a redundant role. We speculate that the redundant E2 could be the homolog

to human UbcH5, UBC-2. UbcH5 is a promiscuous E2 that is active with a variety of E3s, including HHARI and CUL-1 (2, 34). Independent of its identity, it is clear that the ability of the redundant E2 is limited because *ubc-18;ubc-3* double knockdown causes a synthetic phenotype. Due to the lack of a loss-of-function allele for *ubc-3* we could not ascertain whether its deletion alone would cause a Pun phenotype. Therefore, it is possible that one E2 can substitute for either UBC-18 or UBC-3, but not for both simultaneously. *ubc-2(RNAi*) is embryonic lethal, precluding us from testing for a synthetic interaction wit *ubc-18* or *ubc-3* RNAi.

Initially, twenty-one Skp1-related (skr) genes were predicted in *C. elegans* (15). Not originally identified as a skr gene, *sup-36* was later suggested to have Skp1-like properties based on its ability to bind FBOX proteins (18-20). Here we show by yeast two-hybrid that SUP-36 also binds to CUL-1 (Fig. 3B), strengthening the notion that SUP-36 has Skp1-related functions. There is only one human Skp1 gene and its only documented function is to act as an adaptor that connects FBOX proteins to CUL1. However, while SUP-36 can bind both to FBOX proteins and CUL1, our genetic and biochemical evidence suggests that it acts as a substrate for, rather than a component of the CUL1 complex during pharyngeal morphogenesis. We therefore propose that SUP-36 performs a skr-independent role in pharyngeal morphogenesis and that its ability to bind to CUL-1 allows for its HHARI/CUL1-dependent degradation. Notably, SUP-36 has been shown to bind to a microtubule-associated protein PTL-1 and SUP-35 has been shown to bind directly to microtubules (19). Null alleles of either *sup-36* and *sup-35* rescue the *ubc-18;ubc-3* lethal phenotype (Fig. 3A&S3). Altogether the data suggest that SUP-35 and SUP-36 work together in pharyngeal morphogenesis and that the role of SUP-36 is likely independent of its skr function. It is worth noting here that the single skp-like gene in yeast, SKP-1, is known to perform both SCF-dependent and SCF-independent functions, the latter as part of the kinetochore, from which

it got its name, "S-phase Kinase-associated Protein-1" (35, 36). Whether human SKP-1 has lost its non-SCF functions or these remain to be discovered is unknown.

Coordination between multiple E3s such as the RBR/CRL complexes characterized here are an emerging theme for tight regulation of protein ubiquitination. In addition to CUL-1, HHARI can also form complexes with CUL2, 3, and 4A (9, 31). Furthermore, a study published while ours was in preparation demonstrated that HHARI knockdown in cell culture leads to accumulation of known CRL substrates and that some CRL substrate are primed with Ub by HHARI/UBCH7 *in vitro* followed by poly-ub chain formation by CDC34/CRL (9). Our genetic evidence presented here complements and expands those findings by showing that an RBR E3 (ARI-1) and its E2 (UBC-18) work together with a CRL- E3 (CUL-1) and its E2 (UBC-3) in the same biological pathway to ubiquitinate a common substrate *in vivo* and that the ability of the E2/E3 pairs to work coordinately is absolutely critical to a biological process. Our findings help explain previously puzzling results such as the reported increase in Chk1 protein levels, a known SCF substrate, on knockdown of the HECT/RBR E2 UbcH7 (37). We believe it is likely that UBCH7/HHARI act as the priming E2/E3 pair for many CRL substrates. However, which substrates are common among the RBR E2/E3 and CRL E2/E3 pairs, how they are selected, and the biological importance of the coordinated modification all remain to be elucidated in the future.

Acknowledgements

We thank N. Zheng for his generous gift of recombinant neddylated-Cul-1/Rbx-1, Cdc34 and Skp1/Fbox$_{Skp2}$, and R. Gardner for plasmids and assistance with yeast two-hybrid experiments. We thank M. Stewart and K. Reiter for discussions and reading of the manuscript.

Some strains were provided by the CGC, which is funded by NIH Office of Research Infrastructure Programs (P40 OD010440). This work was supported by National Institute of General Medical Sciences grant R01 GM088055 (REK), UW Hurd Fellowship Fund, and PHS NRSA 5T32 GM007270 (KKD), and R01 AG044378 (DLM). DLM is a New Scholar in Aging of the Ellison Medical Foundation.

Conflict of Interest

The authors declare that they have no conflict of interest.

Experimental Procedures

strains and maintenance

Worms were cultured according to standard methods on nematode growth media (NGM) plates seeded with OP50 bacteria at 20C, except temperature-sensitive strains which were maintained at 15°C (38). Strains used in this study are listed in Table S1. Double mutant strains were constructed by standard techniques, and alleles were genotyped by PCR using primer sequences shown in Table S2.

RNAi knockdown and screening

RNAi knockdown of target genes was performed as described (10). All RNAi clones were in HT115 bacteria, from the Ahringer library. The empty vector pL4440 was used as a negative control in these experiments. *lin-35(RNAi)* was used as a positive control for synthetic lethality with *ubc-18(ku354)* mutant animals. The *ku354* allele encodes a non-conservative missense mutation (E10K) in the E1-binding surface and acts as a strong loss of function allele

(8). *unc-45* and *pos-1*, which generate strong unc/ste and emb phenotypes respectively, were used to gauge the strength of the RNAi effect in a given experiment. For double RNAi experiments with *sup-35* RNAi, animals were fed a 1:1 mixture of fresh, saturated overnight cultures of both RNAi strains.

For the primary screen, 10 P0 were grown on each indicated RNAi clone from L1 in 24 well plates. In each well, 15uL of saturated bacterial culture was seeded onto solid agar. After five days, the F1 progeny were examined for sterile (ste), embryonic lethal (emb), or larval arrest (lva) phenotypes. Bacterial clones that caused a phenotype in the *ubc-18(ku354)* mutant strain but not in wild-type animals were re-tested three times to find those with robust synthetic interactions. If both wild-type and *ubc-18* mutants showed identical phenotypes, these RNAi were excluded from further analysis. Of 12,982 clones from the Arhinger library screened, 213 were selected for secondary screening. To quantitate RNAi phenotypes and for the secondary screen, timed egg lay assays were performed. Synchronized populations of L1 larvae were grown to gravid adult on RNAi, then 10 RNAi-fed adults were transferred to fresh RNAi plates and allowed to lay eggs for up to four hours. The adults were removed and progeny scored within the next 72h.

To quantitate synthetic phenotypes, the fraction of embryos that developed to fertile adults was calculated. Embryos were counted immediately after the egg-lay period, and the number of adults counted after three days or when control animals on L4440 RNAi food had developed to gravid adults. To quantitate the synthetic Pun phenotype, animals were rinsed off plates 48 h after the timed egg-lay, allowed to settle by gravity, and then resuspended in M9 with

25mM sodium azide. The fraction of Pun L1 larvae was assessed by counting worm samples on a compound microscope equipped with a 40x oil objective.

Statistical significance in quantitative analyses of synthetic lethality (Figure 1A and S1) was assessed using a two-way ANOVA with a Bonferroni posttest on data from three separate biological replicates, each consisting of three technical replicates. Statistical significance of synthetic Pun phenotypes (Figure 1C) was assessed similarly with a two-way ANOVA on data from at least two separate biological replicates each consisting of at least two technical replicates. For all experiments, data were graphically plotted and statistical analyses performed with GraphPad Prism5.

Yeast Two-hybrid

To construct yeast two-hybrid (Y2H) fusion constructs the full coding sequence of each gene was amplified by PCR from cDNA (primer sequences are in Supplemental Table 1). To generate cDNA, mRNA was isolated from mixed-stage *C.elegans* using Trizol (Thermo Fisher scientific) following the manufacturer's recommended protocol and cDNA was synthesized from 5ug total RNA using Superscript III Reverse Transcriptase (Invitrogen). PCR Primers were designed to include restriction enzyme sites, and the PCR product was digested with the appropriate restriction enzyme (New England Biolabs) and ligated into plasmids to generate protein fusions with the Gal4-activation domain (GAD) or Gal4 DNA binding domain (GBD). Plasmids used for this study are pGAD-C1 (skr-1 and sup-36) and pGBD-C1 (cul-1 and cul-6) (39). Final plasmids were sequenced to verify that the fusion constructs were correct.
Two hybrid assays were performed as described (40). Serial dilutions of yeast cells expressing fusions with GAD and GBD fusions were spotted onto selective media (–His –Leu – Trp) to

assess interactions and onto nonselective media (-Leu, -Trp) with histidine to control for spotting efficiency.

Recombinant proteins used for in vitro ubiquitination assays

The following constructs were used in this study. If not otherwise indicated, the constructs coded for full-length and human proteins: E1, wheat E1, HA-Ub-wt, HA-Ub-K0 (lysine-less), UbcH7, Cdc34, neddylated-Cul-1$^{13\text{-}776}$/Rbx-$^{116\text{-}108}$, His_6-T7-SUP-36, SKP1$^{1\text{-}147, \Delta 38\text{-}43, \Delta 71\text{-}82}$ /$FBOX_{skp2}$$^{101\text{-}153.}$ HHARI full-length, GST-HHARI-RBR$^{177\text{-}395}$.

Expression and purification of recombinant proteins

Proteins were expressed and purified as previously described (2, 13, 32, 41, 42).

Ubiquitination assays

E3 auto-ubiquitination assays: 0.5μM wheat E1, 20μM Ub, 2μM UbcH7, 2μM GST-$HHARI_{RBR}$, were incubated at 37°C in 25mM $NaPO_4$, 150mM NaCl, pH 7.0. Reactions were initiated by addition of 10mM ATP and quenched with SDS-page reducing buffer. Time points were run on SDS-page gel and visualized by western blotting for GST (HHARI).

Sup-36 ubiquitination assays: 0.5μM human E1, 20μM Ub, 0.5μM UbcH7, 0.5μM Cdc34 0.5μM HHARI, 0.5μM neddylated-Cul-/Rbx-1, 2μM His_6-T7-SUP-36 were incubated as indicated in each assay at 37°C in 25mM $NaPO_4$, 150mM NaCl, pH 7.0. Reactions were initiated by addition of 10mM ATP and quenched with SDS-page reducing buffer. Time points were run on SDS-page gel and visualized by western blotting for T7 (SUP-36).

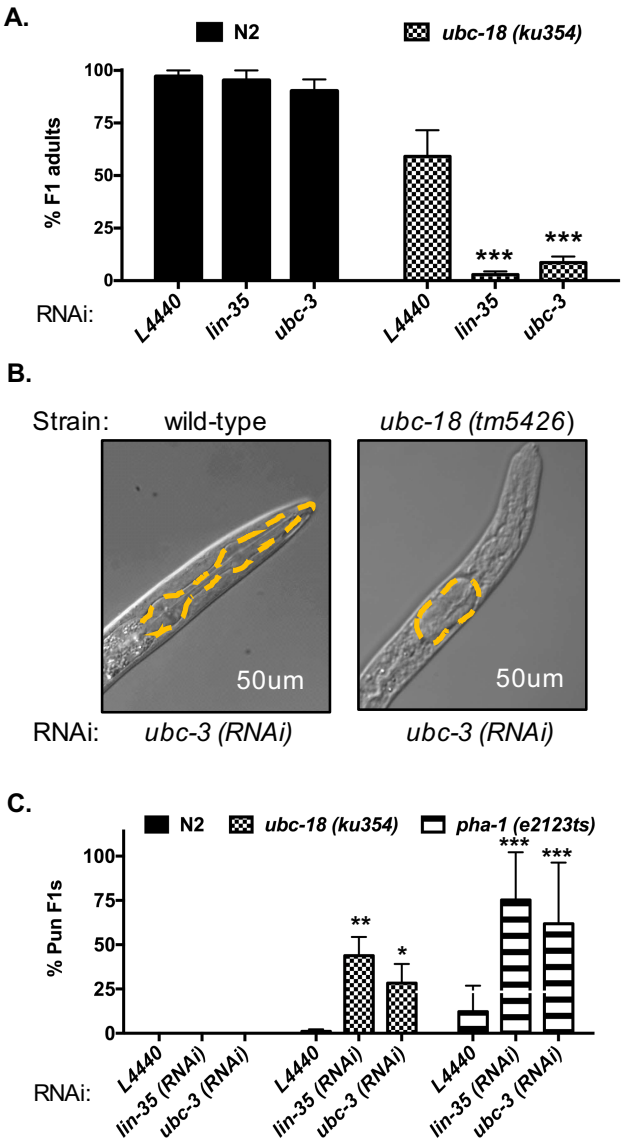

Figure 1. RNA1 screen identified a synthetic genetic interaction between *ubc-18* and *ubc-3*. A) Quantitation of synthetic interaction between *ubc-3* and *ubc-18*, measured as percent survival to adulthood. The pL4440 empty vector is included as the negative control, and *lin-35* is a positive control (8). A list of other synthetic interactions identified in the RNAi screen is in Table 1. Error bars indicate the standard deviation of at least three independent experiments. B) Synthetic lethality between *ubc-18(ku354)* and *ubc-3* is associated with a Pharynx unattached (Pun) phenotype. In each image, the pharynx basement membrane is traced with the yellow dashed line. Left: wild-type L1 grown on *ubc-3* RNAi food; right: *ubc-18(tm5426)* L1 grown on *ubc-3* RNAi food C) Quantification of synthetic Pun phenotype. The percent Pun L1 from animals grown on the indicated RNAi for *ubc-18* (checkered bars) and *pha-1* mutants (striped bars) is shown. The wild-type control (N2, black bars) does not produce Pun progeny under any of the experimental conditions. Error bars indicate the standard deviation of at least three independent experiments. *, $p<0.05$ and **, $p<0.01$, ***, $p<0.001$ relative to L4440 controls. Absence of stars implies no significant difference relative to L4440 controls.

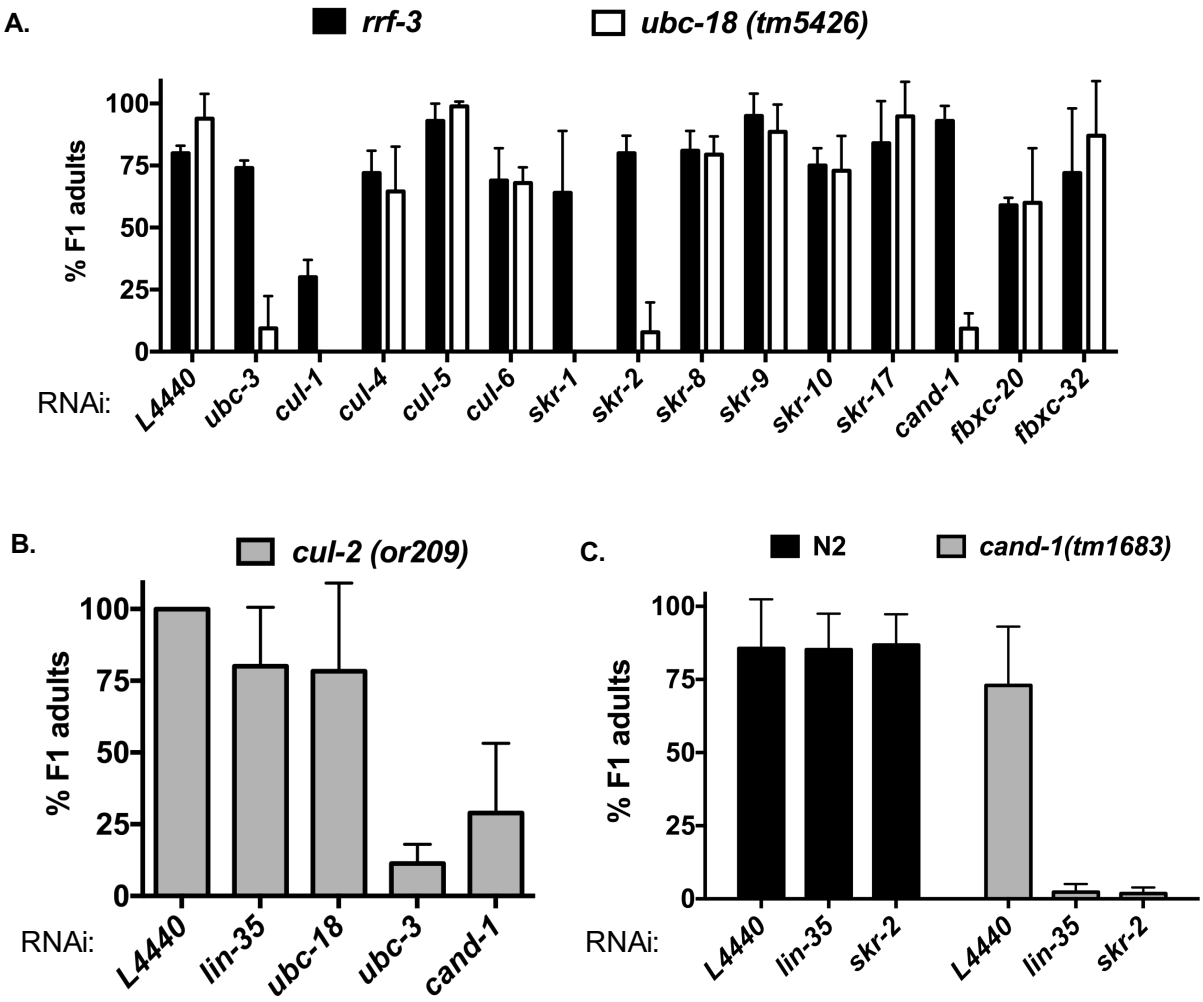

Figure 2. *ubc-18* interacts synthetically with genes encoding SCF E3 ubiquitination machinery. A) Quantification of synthetic lethal interactions with *ubc-18*. Percent F1 progeny of RNAi-fed animals that survive to adulthood is shown for *rrf-3(pk1426)* and *ubc-18 (tm5426)* strains (black and white bars, respectively). The *rrf-3* mutant is wild type at the *ubc-18* locus and reported to be RNAi-sensitive (43). Error bars are the standard deviation between technical replicates in one representative experiment. The candidate screen was performed only once for genes that were not affected. Synthetic interactions with *skr-1/2, cul-1* and *cand-1* were observed in at least three independent experiments. B) *ubc-18* does not genetically interact with *cul-2(or209ts)*. Percent F1 progeny of RNAi-fed animals that survive to adulthood is shown for *cul-2(or209ts)*. Error bars are the standard deviation between two independent experiments. C) *cand-1* genetically interacts with *lin-35* and *skr-2/1*. Percent F1 progeny viable to adulthood is shown for N2, wild-type (black bars) or *cand-1(tm1683)* mutant (grey bars) animals grown on each indicated RNAi. Error bars indicate the standard deviation of at least three independent experiments.

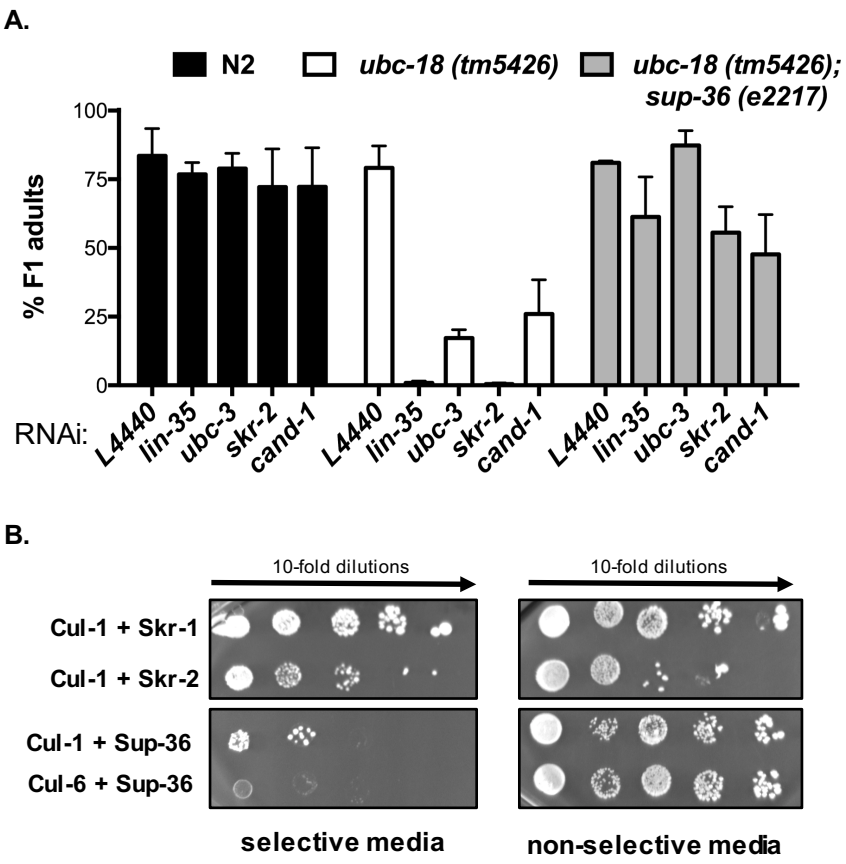

Figure 3. Sup-36 is an SCF component. A) The *Sup-36(e2217)* null allele rescues genetic interactions between *ubc-18 and SCF components*. B) Yeast Two-hybrid experiments with either *cul-1* or *cul-6* fused to Gal4 DNA binding domain and either *skr-1/2* or *sup-36* fused to the Gal4 DNA activating domain. Growth on selective media (-His - Leu –Trp) indicates interactions of the two proteins tested (left). As previously shown, CUL-1 binds to both SKR-1 and SKR-2. SUP-36 binds to CUL-1 (top), but not CUL-6 (bottom). Yeast were also spotted on non-selective media (- Leu –Trp) to control for growth rate (right).

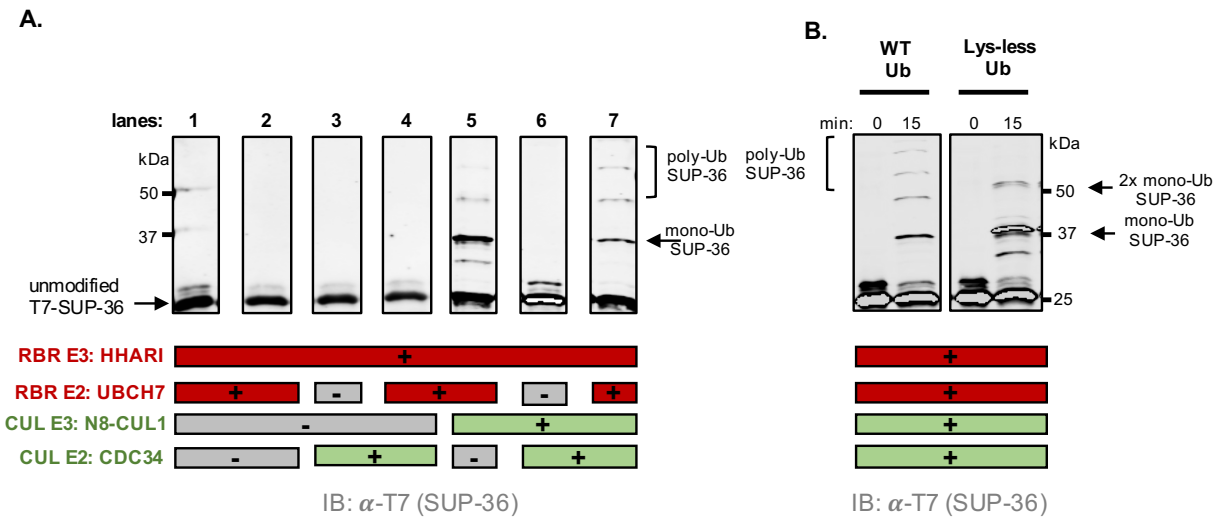

Figure 4. SUP-36 is ubiquitinated by UbcH7/HHARI and CDC-34/Cul-1. A) *In vitro* ubiquitination of T7-SUP-36. Each reaction contained T7-SUP-36 and other reaction components as indicated with bars below gel. Reactions were incubated for 30 min after addition of ATP, except lane 1, in which the reaction was immediately quenched (0 min). B) The in vitro T7-SUP-36 ubiquitination assay was performed using either WT Ub (left) or Lys-less Ub (right) that is unable to form chains. In both panels, T7-SUP-36 was visualized by Western blot. Unmodified SUP-36 runs at an apparent molecular weight of ~ 25kDa, and is indicated by an arrow on the left. Mono- and double-Ub T7-SUP-36 are indicated by arrows on the right of the gels, and poly-Ub T7-SUP-36 is noted by brackets.

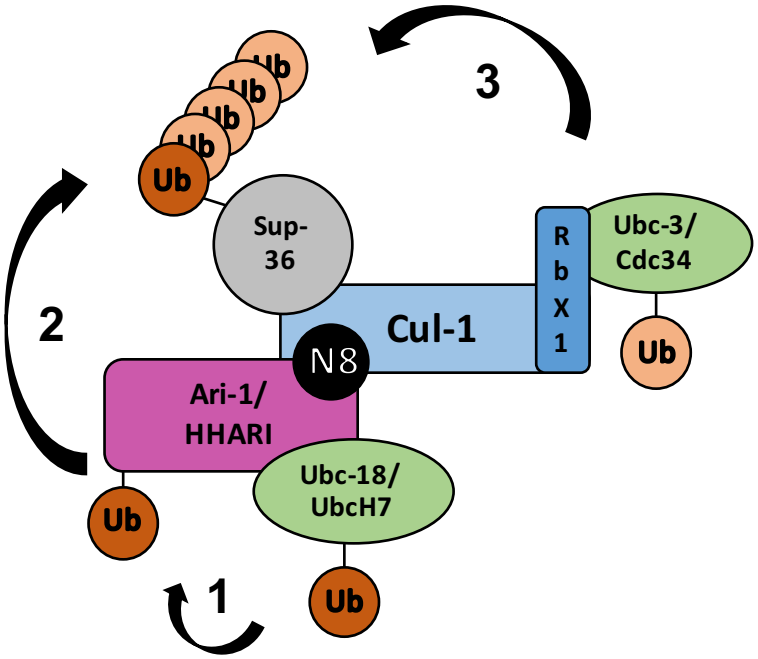

Figure 5. Proposed model for UBC-18/UBC-3-dependent ubiquitination of SUP-36. SUP-36 inhibits pharyngeal morphogenesis; its ubiquitination by UBC-18/ARI-1 and UBC-3/CUL-1 and subsequent proteasomal degradation is required for proper development of the pharynx. CUL-1 and HHARI coordinate ubiquitination of SUP-36 through a multi-component E3 complex. CUL-1 binds to both SUP-36 and HHARI. The dedicated HHARI E2 UBCH7 (UBC-18) transfers Ub to the active site of HHARI (Step1) which subsequently primes SUP-36 with a single mono-Ub (Step2). Following the mono-ubiquitination of SUP-36 by HHARI, CDC34/UBC-3 can build poly-Ub chains on SUP-36 (Step3) to mark SUP-36 for proteasomal degradation

Gene	synthetic phenotype	process	function/homology
ubc-3	let	ubiquitination	E2 specific to SCF type E3; regs G1 and G2 in cell cycle
skr-2	let	ubiquitination	Skp1-related component of SCF type E3 ubiquitin ligase complex
skr-1	let	ubiquitination	Skp1-related component of SCF type E3 ubiquitin ligase complex
egl-27	let	chromatin regulation	MTA (human metastasis) homolog - nucleosome remodeling
lin-54	let	nucleic acid regulation	DNA binding protein
Y65B4A.1	let	nucleic acid regulation	Nucleotide binding
smu-2	let	nucleic acid regulation	RNA splicing
emb-4	let	nucleic acid regulation	ortholog to human spliceosome
dpy-10	let	body morphology and movement	cuticle collagen protein
prx-13	let	proteolysis	human PEX13 homolog (endopeptidase); human Zellweger syndrome
ptc-1	let	cytokinesis	sugar modification; eggshell development
B0035.1	let	UNKNOWN	ZNF207/BUGZ ortholog
T09A5.9	let	UNKNOWN	PPP1R7 homolog (protein phosphatase)
fbf-2	ste	nucleic acid regulation	RNA binding
mrpl-10	ste	mitochondrial translation	mitochondrial ribosomal protein, large subunit
trr-1	ste	chromatin regulation	homolog of protein kinase in chromatin remodeling complex; Syn Muv

Table 1. Genetic interactions with *ubc-18* identified from RNAi screen. Validated hits from RNAi screen using *ubc-18(ku354) loss-of-function allele*. let - lethal; ste - sterile. Process and function/homology are from Wormbase build WS254 (www.wormbase.org).

Genotype	% viable (n)
ubc-18 (tm5426)	92 (470)
ubc-18 ; lin-35 (RNAi)	5 (603)
ubc-18; ubc-3 (RNAi)	6 (853)
ubc-18; sup-35 (RNAi) ubc-3 (RNAi)	96 (161)
ubc-18; sup-36; ubc-3 (RNAi)	100 (171)
ubc-18; sup-37; ubc-3 (RNAi)	100 (263)
pha-1(e2123ts)	75 (135)
pha-1(e2123ts); lin-35 (RNAi)	0.8 (69)
pha-1(e2123ts); ubc-3 (RNAi)	0 (69)
pha-1(e2123ts); sup-35; ubc-3 (RNAi)	99.7 (696)
pha-1(e2123ts); sup-36; ubc-3 (RNAi)	87.9 (555)
pha-1(e2123ts); sup-37; ubc-3 (RNAi)	97.3 (802)

Table 2. Viability of animals to adulthood was measured for each genotype. Temperature sensitive *pha-1* strains were assayed at the permissive temperature (15°C). Data are aggregated from three independent experiments.

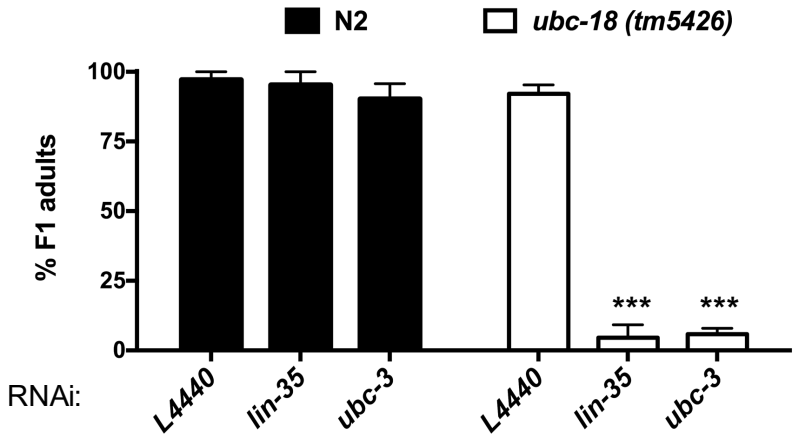

Supplemental Figure 1. Synthetic genetic interactions between *ubc-18(tm5426)*, and *ubc-3(RNAi)*, as in Fig. 1B (white bars). The *tm5426* allele is predicted to be a molecular null as it contains a deletion of the second and partially the third exon. N2 wild-type control is in black bars. Error bars indicate the standard deviation of at least three independent experiments. ***, $p<0.001$ relative to L4440 controls. Absence of stars implies no significant difference relative to L4440 controls

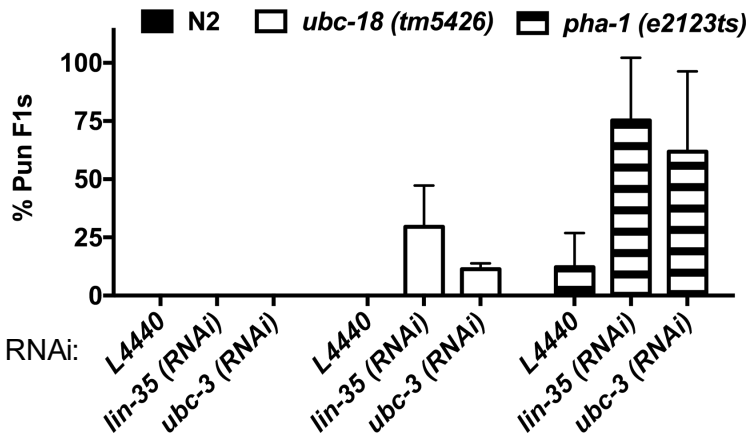

Supplemental Figure 2. Fraction of Pun L1, as in Fig. 1C. The percent Pun F1 progeny from animals grown on the indicated RNAi for *ubc-18(tm5426)* (white bars) and *pha-1(e2123ts)* (striped bars) is shown. Experiments with *pha-1(e2123ts)* were done at 16C. The isogenic wild type control (N2, black bars) does not form Pun progeny under any of the experimental conditions. Error bars indicate the standard deviation of at least three independent experiments.

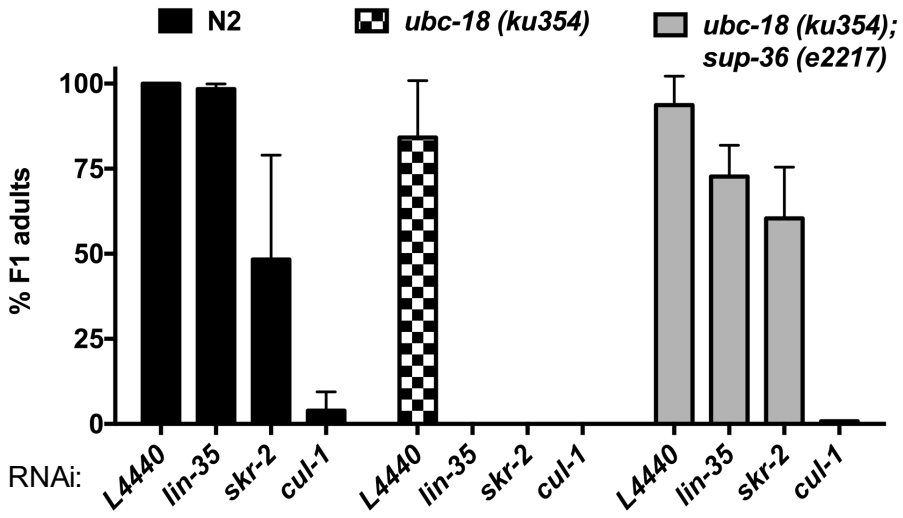

Supplemental Figure 3. Synthetic genetic interactions between *ubc-18(ku354); lin-35(RNAi)* and *ubc-18(ku354);skr-2* are rescued by *sup36(e2217).*

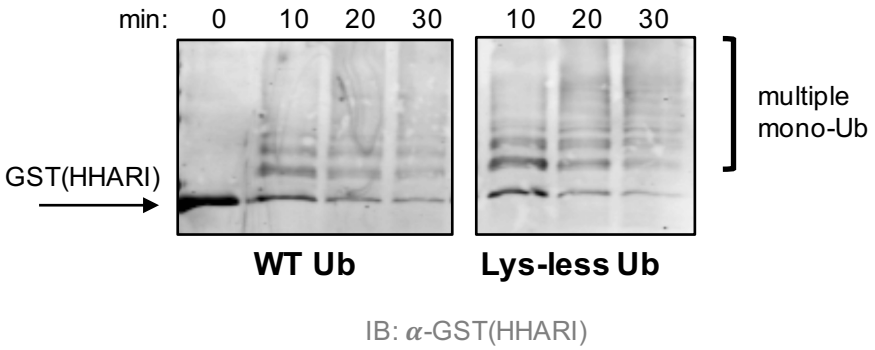

Supplemental Figure 4. $HHARI_{RBR}$ does not form poly-Ub chains. Auto-ubiquitination assays in which the E3 (HHARI) serves as a proxy substrate were performed with either WT Ub (left) or Lys-less Ub (right). The construct used, $HHARI_{RBR}$, lacks the Ariadne domain and is therefore constitutively active (32). Lys-less Ub is unable to form Ub-chains, therefore the higher molecular weight bands observed are multiple mono-Ub modifications. Products were visualized by western blotting against the GST-tag on HHARI.

Strain	Genotype	Source
N2	wild type	Bristol isolate, from CGC
WY34	*ubc-18(ku354)*	CGC
DLM37	*ubc-18(tm5426)*	National Bioresource Project (NBRP) strain, outcross to N2
GE24	*pha-1(e2123)*	CGC
DLM70	*ubc-18(tm5426); sup-35(e2223)*	DLM37 crossed to GE346
MT14541	*sup-36(e2217)*	David Fay, U Wyoming
DLM72	*ubc-18(tm5426); sup-36(e2217)*	DLM37 crossed to MT14541
DLM74	*ubc-18(tm5426); sup-37(e2215)*	DLM37 crossed to GE347
GE346	*pha-1(e2123); sup-35(e2223); dpy-18 (e499)*	CGC
DLM71	*pha-1(e2123); sup-36(e2217)*	GE24 crossed to MT14541
GE337	*pha-1(e2123); sup-37(e2215); dpy-18 (e499)*	CGC
DLM76	*cand-1 (tm1683)*	National Bioresource Project (NBRP) strain outcrosse to N2
EU640	*cul-2(or209)*	CGC

Table S1. *C.elegans s*trains used in this study.

Gene (allele)	Forward	Reverse	PCR product
ubc-18 (ku354)	cagaaggtgagaaaatcatg	ggctccttatcctgaaaatt	200bp, *ku354* allele introduces Hpy188I site
ubc-18 (tm5426)	cgagaatgttgagtgcgagg	agtgacagcaaggccatcat	430bp (wt), 120bp (mutant)
pha1 (e2123)	gctttctctgctgaaacc	gcgcactactgaatcagagt	900bp , *e2123* intoduces AccI site
sup-35 (e2223)	atgctctttggcctcttctg	acgtctccaaagcaaaagcg	480bp, *e2223* removes BseI site
sup-36 (e2217)	cgcgcaatactcatagagtttc	aatccatccgtcttcctctg	750bp (wt) or no band (mutant)
sup-37(e2215)	gaaagcccatggcagaattcatccagatatgatggag	gggtgagagcgcagatgcgagtattc	105bp, allele removes DpnI site
cand-1 (tm1683)	cgcatcatgtcagtaatcgg	caaaaaaggctcatttgggc	875bp (wt) or 250bp (mutant)

Table S2. Genotyping primers

References

1. Schnell JD & Hicke L (2003) Non-traditional functions of ubiquitin and ubiquitin-binding proteins. *J Biol Chem* 278(38):35857-35860.

2. Wenzel DM, Lissounov A, Brzovic PS, & Klevit RE (2011) UBCH7 reactivity profile reveals parkin and HHARI to be RING/HECT hybrids. *Nature* 474(7349):105-108.

3. Mani K & Fay DS (2009) A mechanistic basis for the coordinated regulation of pharyngeal morphogenesis in Caenorhabditis elegans by LIN-35/Rb and UBC-18-ARI-1. *PLoS Genet* 5(6):e1000510.

4. Whitcomb EA & Taylor A (2009) Ubiquitin control of S phase: a new role for the ubiquitin conjugating enzyme, UbcH7. *Cell Div* 4:17.

5. Chaugule VK & Walden H (2016) Specificity and disease in the ubiquitin system. *Biochem Soc Trans* 44(1):212-227.

6. Zheng N, Wang Z, & Wei W (2016) Ubiquitination-mediated degradation of cell cycle-related proteins by F-box proteins. *Int J Biochem Cell Biol* 73:99-110.

7. Willems AR, Schwab M, & Tyers M (2004) A hitchhiker's guide to the cullin ubiquitin ligases: SCF and its kin. *Biochim Biophys Acta* 1695(1-3):133-170.

8. Fay DS, Large E, Han M, & Darland M (2003) lin-35/Rb and ubc-18, an E2 ubiquitin-conjugating enzyme, function redundantly to control pharyngeal morphogenesis in C. elegans. *Development* 130(14):3319-3330.

9. Scott DC*, et al.* (2016) Two Distinct Types of E3 Ligases Work in Unison to Regulate Substrate Ubiquitylation. *Cell* 166(5):1198-1214 e1124.

10. Kamath RS*, et al.* (2003) Systematic functional analysis of the Caenorhabditis elegans genome using RNAi. *Nature* 421(6920):231-237.

11. Schwob E, Bohm T, Mendenhall MD, & Nasmyth K (1994) The B-type cyclin kinase inhibitor p40SIC1 controls the G1 to S transition in S. cerevisiae. *Cell* 79(2):233-244.

12. Fay DS*, et al.* (2004) The coordinate regulation of pharyngeal development in C. elegans by lin-35/Rb, pha-1, and ubc-18. *Dev Biol* 271(1):11-25.

13. Zheng N*, et al.* (2002) Structure of the Cul1-Rbx1-Skp1-F boxSkp2 SCF ubiquitin ligase complex. *Nature* 416(6882):703-709.

14. Kipreos ET & Pagano M (2000) The F-box protein family. *Genome Biol* 1(5):REVIEWS3002.

15. Nayak S, *et al.* (2002) The Caenorhabditis elegans Skp1-related gene family: diverse functions in cell proliferation, morphogenesis, and meiosis. *Curr Biol* 12(4):277-287.

16. Kipreos ET, Lander LE, Wing JP, He WW, & Hedgecock EM (1996) cul-1 is required for cell cycle exit in C. elegans and identifies a novel gene family. *Cell* 85(6):829-839.

17. Sarikas A, Hartmann T, & Pan ZQ (2011) The cullin protein family. *Genome Biol* 12(4):220.

18. Li S, *et al.* (2004) A map of the interactome network of the metazoan C. elegans. *Science* 303(5657):540-543.

19. Polley SR, *et al.* (2014) Implicating SCF complexes in organogenesis in Caenorhabditis elegans. *Genetics* 196(1):211-223.

20. Simonis N, *et al.* (2009) Empirically controlled mapping of the Caenorhabditis elegans protein-protein interactome network. *Nat Methods* 6(1):47-54.

21. Ceron J, *et al.* (2007) Large-scale RNAi screens identify novel genes that interact with the C. elegans retinoblastoma pathway as well as splicing-related components with synMuv B activity. *BMC Dev Biol* 7:30.

22. Yamanaka A, *et al.* (2002) Multiple Skp1-related proteins in Caenorhabditis elegans: diverse patterns of interaction with Cullins and F-box proteins. *Curr Biol* 12(4):267-275.

23. Merlet J & Pintard L (2013) Role of the CRL2(LRR-1) E3 ubiquitin-ligase in the development of the germline in C. elegans. *Worm* 2(3):e25716.

24. Zheng J, *et al.* (2002) CAND1 binds to unneddylated CUL1 and regulates the formation of SCF ubiquitin E3 ligase complex. *Mol Cell* 10(6):1519-1526.

25. Wu S, *et al.* (2013) CAND1 controls in vivo dynamics of the cullin 1-RING ubiquitin ligase repertoire. *Nat Commun* 4:1642.

26. Pierce NW, *et al.* (2013) Cand1 promotes assembly of new SCF complexes through dynamic exchange of F box proteins. *Cell* 153(1):206-215.

27. Bosu DR, *et al.* (2010) C. elegans CAND-1 regulates cullin neddylation, cell proliferation and morphogenesis in specific tissues. *Dev Biol* 346(1):113-126.

28. Hodge A & Mendenhall M (1999) The cyclin-dependent kinase inhibitory domain of the yeast Sic1 protein is contained within the C-terminal 70 amino acids. *Mol Gen Genet* 262(1):55-64.

29. Petroski MD & Deshaies RJ (2003) Context of multiubiquitin chain attachment influences the rate of Sic1 degradation. *Mol Cell* 11(6):1435-1444.

30. Feldman RM, Correll CC, Kaplan KB, & Deshaies RJ (1997) A complex of Cdc4p, Skp1p, and Cdc53p/cullin catalyzes ubiquitination of the phosphorylated CDK inhibitor Sic1p. *Cell* 91(2):221-230.

31. Kelsall IR*, et al.* (2013) TRIAD1 and HHARI bind to and are activated by distinct neddylated Cullin-RING ligase complexes. *EMBO J* 32(21):2848-2860.

32. Duda DM*, et al.* (2013) Structure of HHARI, a RING-IBR-RING ubiquitin ligase: autoinhibition of an Ariadne-family E3 and insights into ligation mechanism. *Structure* 21(6):1030-1041.

33. Chau V*, et al.* (1989) A multiubiquitin chain is confined to specific lysine in a targeted short-lived protein. *Science* 243(4898):1576-1583.

34. Wu K, Kovacev J, & Pan ZQ (2010) Priming and extending: a UbcH5/Cdc34 E2 handoff mechanism for polyubiquitination on a SCF substrate. *Mol Cell* 37(6):784-796.

35. Connelly C & Hieter P (1996) Budding yeast SKP1 encodes an evolutionarily conserved kinetochore protein required for cell cycle progression. *Cell* 86(2):275-285.

36. Bai C*, et al.* (1996) SKP1 connects cell cycle regulators to the ubiquitin proteolysis machinery through a novel motif, the F-box. *Cell* 86(2):263-274.

37. Zhang YW*, et al.* (2009) The F box protein Fbx6 regulates Chk1 stability and cellular sensitivity to replication stress. *Mol Cell* 35(4):442-453.

38. Brenner S (1974) The genetics of Caenorhabditis elegans. *Genetics* 77(1):71-94.

39. James P, Halladay J, & Craig EA (1996) Genomic libraries and a host strain designed for highly efficient two-hybrid selection in yeast. *Genetics* 144(4):1425-1436.

40. Rosenbaum JC*, et al.* (2011) Disorder targets misorder in nuclear quality control degradation: a disordered ubiquitin ligase directly recognizes its misfolded substrates. *Mol Cell* 41(1):93-106.

41. Dove KK, Stieglitz B, Duncan ED, Rittinger K, & Klevit RE (2016) Molecular insights into RBR E3 ligase ubiquitin transfer mechanisms. *EMBO Rep* 17(8):1221-1235.

42. Duda DM*, et al.* (2008) Structural insights into NEDD8 activation of cullin-RING ligases: conformational control of conjugation. *Cell* 134(6):995-1006.

43. Simmer F*, et al.* (2002) Loss of the putative RNA-directed RNA polymerase RRF-3 makes C. elegans hypersensitive to RNAi. *Curr Biol* 12(15):1317-1319.

Chapter V: Concluding Remarks

It was only six years ago that a landmark study discovered that RBR E3s are indeed not RING-type E3s as had been assumed for many years. Instead *Wenzel et al.* (2011) showed that the RBR E3s HHARI and Parkin contain an active site Cys, indispensable for ligase activity. The combination of an E2 binding RING1 domain (similar to RING-type E3s) and an active site Cys (reminiscent of HECT-type E3s) resulted in the RBR nickname "RING/HECT-hybrids". Since then the requirement of an active site Cys for ligase activity has also been shown for other RBR E3s including HOIP, HOIL-1L, TRIAD1, and RNF144 [1-4]. All RBR E3s contain a conserved Cys at an analogous position and it is therefore reasonable to assume that all RBR E3s function via a RING/HECT-hybrid mechanism.

In 2011, when I began my studies, very little was known about how RBR E3s function. In fact, RBR E3 were originally termed RING-type E3s based on their primary sequence analysis of RING1 and RING2. At first glance those reveal a similar patter or Zinc-coordinating residues. Today there are several structures of RBR E3s (HHARI, HOIP and Parkin) and from those we know that RING2 does not even remotely resemble a RING domain [5-10]. However, RING1 domains are structurally very similar to canonical RING domains and a RING1 domain NMR structure of the RBR RNF144 released in 2004 supported the initial hypothesis that RBR E3s are RING-type E3s.

Very shortly after RBR E3s were identified to be RING/HECT-hybrids, it was shown that canonical RING-type E3s are not only scaffolds that bind substrate and the E2~Ub, but canonical RING domains actually *activate* E2~Ub for aminolysis reactions (Ub transfer onto Lys residues) by promoting closed E2~Ub conformations [11-15]. This provides a rationale as for RING-type catalyzed Ub transfer mechanisms for which it is the E2 that modifies substrate Lys residues

with Ub. Therefore, that RINGs promote increased Lys reactivity of E2~Ub is functionally relevant. On the contrary, E2~Ub bound to RING1 domains of RBR E2 ***must*** transfer Ub onto the active site Cys but not to Lys residues that might be within proximity. This is important, because in all cases known to date, it is the enzyme that carries out the *final* aminolysis reaction that determines the type of Ub modification on a given substrate. In the case of RING-type E3s it is the E2 that determines whether poly-Ub chains are built as well as the chain topology (for example K48- vs. K63-linked Ub chains). But in the case of E3s that utilize an E3~Ub intermediate, the E3 controls the final Ub product formation. For example, the E2 E2-25K possesses intrinsic ability to build K48-linked Ub chains in the absence of an E3, but this preference is suppressed when paired with the linear chain building complex that contains HOIL-1L/HOIP known to build linear Ub chains [16]. In such reactions the E2~Ub acts as a supplier of Ub for the E3, but must not modify substrates directly. The remarkable similarity of canonical RING domains and RING1 domains does not provide an obvious explanation for how RBR E3s ensure Ub transfer from the E2 to the active site Cys and not Lys residues.

In my graduate work I addressed this question and I demonstrate that RING1 domains perform opposing functions to canonical RING domains: not only do they fail to induce *closed* E2~Ub conformations, but instead RING1s actively favor *open* E2~Ub conformations (Chapter II, [17]. This strategy ensures that the transfer of Ub proceeds via the active site Cys on RING2 and therefore that the type of product generated (e.g., mono- or a specific poly-Ub chain) is determined by the RBR E3 and not by the E2. This unique feature of RBR RING1 domains allows RBR E3s to accept Ub from a variety of E2~Ubs including E2s that are able to transfer Ub onto either Lys or Cys, while ensuring that Ub transfer occurs through the active site Cys on RING2.

That RBR RING1 domains have opposing functions to canonical RING domains can be explained functionally, yet a structural explanation for this observation is not easily apparent. Despite their common function, it is remarkable that there are only a few conserved residues among RING1 domains, most of which are Zinc-coordinating Cys and His residues.

A highly conserved position in canonical RINGs, called the linchpin residue, is largely responsible for the ability to promote closed E2~Ubs by forming hydrogen bonds to both E2 and Ub [14]. In RINGs, the linchpin is most often a basic residue (Arg or Lys) and is occasionally a neutral H-bonding residues such as Asn. HHARI contains an Asp residue in the structurally analogous position to the linchpin, and RBRs in general do not share a common residue that could fulfill the function of a hydrogen-bonding linchpin. This provides one possible explanation for why RBR RING1's *fail* to induce closed states of E2~Ub yet it does not explain how RBR RING1 domain actively promote open E2~Ubs.

Instead, I found that a two-residue extension of the second Zn^{2+}-loop of HHARI RING1 is largely responsible for disrupting closed E2~Ub conjugate. The last two Zn^{2+}-coordinating Cys in canonical RING domains are consistently separated by *exactly* two residues in canonical RINGs (C_{7th}-X-X-C_{8th}), but the same loop contains up to four residues in RING1s (C_{7th}-X-X-X-X-C_{8th}). Deletion of the two extra residues in the HHARI Zn^{2+}-loop II to create a two-residue loop as found in canonical RING-type E3s generates a RING1 that has diminished ability to disrupt closed UbcH7~Ub. In particular, I show that the loop length rather than a specific side chain leads to the opening activity; which explains why there is no obvious conservation among the four-residue loops among RBR RING1s. Parkin has a three-residue loop and two other RBRs, including HOIP, have two-residue loops similar to canonical RINGs. A notable difference between HHARI and Parkin is that auto-inhibited HHARI can bind an E2~Ub with high affinity

whereas auto-inhibited Parkin cannot due to its E2-binding site being partly occluded by the inhibitory element known as the REP (repressor element) [8]. It may therefore be less important for Parkin to actively disfavor closed E2~Ub states than it is for HHARI, as Parkin may only be able to bind an E2~Ub once it is in its fully activated conformation.

While I was conducting my research, two crystal structures of RBR E3s bound to E2~Ub were solved by other labs; one complex includes HOIP:UbcH5~Ub and the other one HHARI:UbcH7~Ub ([5] and Chapter III). Both structures confirm that the E2~Ub occupies an open conformation while bound to RBR E3s. Furthermore, HOIP is one of four human RBRs that contains a short Zn^{2+}-loop II comprised of only two spacer residues between the Zinc-coordinating Cys as seen with canonical RINGs. Yet, the crystal structure reveals and open conformation of UbcH5~Ub suggesting another mechanism by which UbcH5~Ub is kept open. In this structure, the Ub moiety of UbcH5~Ub makes non-covalent contacts to several other domains of HOIP possibly explaining the open state of UbcH5~Ub. Interestingly, Ub contacts RING2 at a site similar to the one I had shown to be a Ub:RING2 contact site for HHARI. However, unlike the structure of HHARI:UbcH7~Ub which is still auto-inhibited, HOIP bound to UbcH5~Ub Ub is presumed to be in a more activated form. Therefore, it is not clear whether the Ub:RING2 contact site is the cause or the result of an open UbcH5~Ub. It is possible that additional Ub contacts with other domains, as seen in the crystal structure, are aiding in keeping the E2~Ub in an open state while bound to HOIP. However, it should be noted that a structure of HOIP:UbcH5~Ub representing one complex actually
involve multiple copies of HOIP, UbcH5, and Ub due to domain swapping by HOIP (shown to not be a true dimer in solution, [5]. Therefore, it is unlikely that this structure represents an accurate complex found in solution.

During the course of my studies regarding the Ub transfer mechanism by RBR E2s, I also identified two different Ub binding sites on HHARI. The first Ub binding site is located on HHARI RING2. This binding site serves to recruit RING2 to the RING1:E2~Ub complex and despite its weak affinity it is crucial for HHARI ligase activity. In structures of auto-inhibited RBR E3s, RING1 and RING2 are far from each other and a large domain rearrangement is required to bring the RING2 active site close to the E2~Ub active site bound to RING1 [6-9, 18, 19]. Consistent with this notion, mutations in either Ub or RING2 at the Ub:RING2 interface substantially reduce Ub transfer from E2~Ub to RING2. Furthermore, I was able to show that this mechanism is utilized by a variety of RBR E3s, indicating its generality for this important class of enzymes.

The second Ub binding site on HHARI is located on its UBA-L domain which was proposed to bind Nedd8 [6]. My NMR studies show that the HHARI UBA-L is able to bind to Ub and Nedd8 in solution. An analysis of the binding interface reveals that Ub residues involved in binding to UBA-L are conserved among Nedd8 explaining why the UBA-L is able to bind to both. There is currently no evidence that a UBA-L:Ub interaction has functional biological significance and it is possible that the observed weak interaction could be a consequence of the high similarity between Ub and Nedd8. On the contrary, HHARI has been shown to bind to neddylated Cullins *in vitro* and human cell lines and that this event leads to activating of HHARI ligase activity, suggesting that Nedd8 binding to the UBA-L of HHARI might be biologically relevant.

Three years ago, an initial study proposed that is HHARI able to bind to neddylated cullins (N8-CUL) and as a result activation of the normally auto-inhibited full-length HHARI

occurs. At the time, the biological significance of this complex formation was perplexing. Cullin-type E3s already form large, multi-subunit complexes, therefore it was surprising that an additional set of proteins, HHARI and its E2 UbcH7, might join those large cullin complexes. Three years later two separate studies, *Scott et al*. (2016) and *Dove et al.* (2016; and Chapter IV), build on this initial observation to show that a large complex comprised of the RBR E3/E2 pair HHARI/UbcH7 works together with Cullin-type E3 ligase complexes to ubiquitinate common substrates.

The RBR E3 ARI-1 and its E2 UBC-18, homologs of HHARI and UbcH7, had been shown to work together during *C.elegans* development [20]. We took advantage of this relationship and a suitable *ubc-18* allele to perform a genome-wide RNAi screen to look for genes that synthetically interact with *ubc-18* (and by extension *ari-1*). However, biochemically, UBC-18/UBCH7 are unable to work with SCF complexes and therefore the genetic results cannot be explained bases on the redundancy principle [21]. Several observations led to the hypothesis that the RBR complex UBCH7/HHARI might work together with the CDC34/SCF complex: 1) a previous study showed that ARI-1/UBC-18 regulate levels of a putative substrate (SUP-36) yet our studies of ARI-1/HHARI show its inability to form poly-Ub chains required for degradation and 2) HHARI was shown to bind to CUL1 [3, 22]. We verified our hypothesis by performing assays with reconstituted CDC34/SCF and UBCH7/HHARI complexes in the presence the putative substrate SUP-36. Our experiments led us to propose a model in which the RBR pair UBCH7/HHARI primes the substrate with Ub (mono-Ub-substrate). This priming step requires the presence to CUL1 confirming that CUL1 activate HHARI ligase activity as previously suggested [3,23]. Following the addition of the first Ub by UBCH7/HHARI, the the CDC34/SCF complex is then able to build poly-Ub chains on the substrate. While we were

completing our studies, a large team of researchers led by Drs. Brenda Schulman and Wade Harper published a paper demonstrating physical and functional interactions between HHARI and SCF [23]. Our work supports this work and in addition provides the missing biological, genetic link and suggests that the cooperative action of the two distinct E2/E3 pairs is a conserved feature from worm to humans.

Six years ago, the ubiquitin field was surprised to realize that RBR E3s are actually RING-HECT-hybrids. Since then, additional surprising discoveries were made. Today, we know that RBR E3s are not true RING-HECT-hybrids in that RING1 domains actually *oppose* the function of canonical RINGs. Furthermore, RBRs are auto-inhibited – a unique feature among eukaryotic E3s. Some light has been shed on how auto-inhibition is released for a few RBRs; future studies are needed to fully understand the role and release of auto-inhibition among the RBR E3s. Another fascinating breakthrough revealed that the RBR HHARI works together with Cullin E3 complexes to sequentially ubiquitinate common substrates. Although RBR E3s comprise a small class with only 12-14 members, the few, most-studied RBRs to date, HHARI, Parkin, HOIP & HOIL-1L, perform important biological roles yet details regarding binding partners and substrates are still unknown. It will be quite fascinating to discover what roles other members of this unique class might play in biological processes.

References

1. Stieglitz B, Morris-Davies AC, Koliopoulos MG, Christodoulou E, Rittinger K (2012) LUBAC synthesizes linear ubiquitin chains via a thioester intermediate. *EMBO Rep* **13**: 840-6

2. Smit JJ, Monteferrario D, Noordermeer SM, van Dijk WJ, van der Reijden BA, Sixma TK (2012) The E3 ligase HOIP specifies linear ubiquitin chain assembly through its RING-IBR-RING domain and the unique LDD extension. *EMBO J* **31**: 3833-44

3. Kelsall IR, Duda DM, Olszewski JL, Hofmann K, Knebel A, Langevin F, Wood N, Wightman M, Schulman BA, Alpi AF (2013) TRIAD1 and HHARI bind to and are activated by distinct neddylated Cullin-RING ligase complexes. *EMBO J* **32**: 2848-60

4. Ho SR, Mahanic CS, Lee YJ, Lin WC (2014) RNF144A, an E3 ubiquitin ligase for DNA-PKcs, promotes apoptosis during DNA damage. *Proc Natl Acad Sci U S A* **111**: E2646-55

5. Lechtenberg BC, Rajput A, Sanishvili R, Dobaczewska MK, Ware CF, Mace PD, Riedl SJ (2016) Structure of a HOIP/E2~ubiquitin complex reveals RBR E3 ligase mechanism and regulation. *Nature* **529**: 546-50

6. Duda DM, Olszewski JL, Schuermann JP, Kurinov I, Miller DJ, Nourse A, Alpi AF, Schulman BA (2013) Structure of HHARI, a RING-IBR-RING ubiquitin ligase: autoinhibition of an Ariadne-family E3 and insights into ligation mechanism. *Structure* **21**: 1030-41

7. Wauer T, Komander D (2013) Structure of the human Parkin ligase domain in an autoinhibited state. *EMBO J* **32**: 2099-112

8. Trempe JF, Sauve V, Grenier K, Seirafi M, Tang MY, Menade M, Al-Abdul-Wahid S, Krett J, Wong K, Kozlov G*, et al.* (2013) Structure of parkin reveals mechanisms for ubiquitin ligase activation. *Science* **340**: 1451-5

9. Riley BE, Lougheed JC, Callaway K, Velasquez M, Brecht E, Nguyen L, Shaler T, Walker D, Yang Y, Regnstrom K*, et al.* (2013) Structure and function of Parkin E3 ubiquitin ligase reveals aspects of RING and HECT ligases. *Nat Commun* **4**: 1982

10. Spratt DE, Mercier P, Shaw GS (2013) Structure of the HHARI catalytic domain shows glimpses of a HECT E3 ligase. *PLoS One* **8**: e74047

11. Branigan E, Plechanovova A, Jaffray EG, Naismith JH, Hay RT (2015) Structural basis for the RING-catalyzed synthesis of K63-linked ubiquitin chains. *Nat Struct Mol Biol* **22**: 597-602

12. Plechanovova A, Jaffray EG, Tatham MH, Naismith JH, Hay RT (2012) Structure of a RING E3 ligase and ubiquitin-loaded E2 primed for catalysis. *Nature* **489**: 115-20

13. Saha A, Lewis S, Kleiger G, Kuhlman B, Deshaies RJ (2011) Essential role for ubiquitin-ubiquitin-conjugating enzyme interaction in ubiquitin discharge from Cdc34 to substrate. *Mol Cell* **42**: 75-83

14. Pruneda JN, Littlefield PJ, Soss SE, Nordquist KA, Chazin WJ, Brzovic PS, Klevit RE (2012) Structure of an E3:E2~Ub complex reveals an allosteric mechanism shared among RING/U-box ligases. *Mol Cell* **47**: 933-42

15. Dou H, Buetow L, Sibbet GJ, Cameron K, Huang DT (2012) BIRC7-E2 ubiquitin conjugate structure reveals the mechanism of ubiquitin transfer by a RING dimer. *Nat Struct Mol Biol* **19**: 876-83

16. Kirisako T, Kamei K, Murata S, Kato M, Fukumoto H, Kanie M, Sano S, Tokunaga F, Tanaka K, Iwai K (2006) A ubiquitin ligase complex assembles linear polyubiquitin chains. *EMBO J* **25**: 4877-87

17. Dove KK, Stieglitz B, Duncan ED, Rittinger K, Klevit RE (2016) Molecular insights into RBR E3 ligase ubiquitin transfer mechanisms. *EMBO Rep* **17**: 1221-35

18. Kumar A, Aguirre JD, Condos TE, Martinez-Torres RJ, Chaugule VK, Toth R, Sundaramoorthy R, Mercier P, Knebel A, Spratt DE*, et al.* (2015) Disruption of the autoinhibited state primes the E3 ligase parkin for activation and catalysis. *EMBO J* **34**: 2506-21

19. Sauve V, Lilov A, Seirafi M, Vranas M, Rasool S, Kozlov G, Sprules T, Wang J, Trempe JF, Gehring K (2015) A Ubl/ubiquitin switch in the activation of Parkin. *EMBO J* **34**: 2492-505

20. Mani K, Fay DS (2009) A mechanistic basis for the coordinated regulation of pharyngeal morphogenesis in Caenorhabditis elegans by LIN-35/Rb and UBC-18-ARI-1. *PLoS Genet* **5**: e1000510

21. Wenzel DM, Lissounov A, Brzovic PS, Klevit RE (2011) UBCH7 reactivity profile reveals parkin and HHARI to be RING/HECT hybrids. *Nature* **474**: 105-8

22. Polley SR, Kuzmanov A, Kuang J, Karpel J, Lazetic V, Karina EI, Veo BL, Fay DS (2014) Implicating SCF complexes in organogenesis in Caenorhabditis elegans. *Genetics* **196**: 211-23

23. Scott DC, Rhee DY, Duda DM, Kelsall IR, Olszewski JL, Paulo JA, de Jong A, Ovaa H, Alpi AF, Harper JW*, et al.* (2016) Two Distinct Types of E3 Ligases Work in Unison to Regulate Substrate Ubiquitylation. *Cell* **166**: 1198-1214 e24